

Editor-in-Chief B.E.Paton

EDITORIAL BOARD

Yu.S. Borisov,
B.V. Khitrovskaya (*exec. secretary*),
V.F. Khorunov, I.V. Krivtsun,
S.I. Kuchuk-Yatsenko (*vice-chief editor*),
V.I. Kyrian, Yu.N. Lankin,
V.N. Lipodaev (*vice-chief editor*),
L.M. Lobanov, A.A. Mazur,
O.K. Nazarenko, I.K. Pokhodnya,
V.D. Poznyakov, I.A. Ryabtsev,
K.A. Yushchenko,
A.T. Zelnichenko (*exec. director*)
(*Editorial Board Includes PWI Scientists*)

**INTERNATIONAL EDITORIAL
COUNCIL**

N.P. Alyoshin
N.E. Bauman MSTU, Moscow, Russia
V.G. Fartushny
Welding Society of Ukraine, Kiev, Ukraine
Guan Qiao
Beijing Aeronautical Institute, China
V.I. Lysak
Volgograd State Technical University, Russia
B.E. Paton
PWI, Kiev, Ukraine
Ya. Pilarczyk
Weiding Institute, Gliwice, Poland
U. Reisgen
Welding and Joining Institute, Aachen, Germany
O.I. Steklov
Welding Society, Moscow, Russia
G.A. Turichin
St.-Petersburg State Polytechn. Univ., Russia
M. Zinigrad
College of Judea & Samaria, Ariel, Israel
A.S. Zubchenko
OKB «Gidropress», Podolsk, Russia

Founders

E.O. Paton Electric Welding Institute
of the NAS of Ukraine,
International Association «Welding»

Publisher

International Association «Welding»

Translators

A.A. Fomin, O.S. Kurochko,
I.N. Kutianova
Editor
N.A. Dmitrieva
Electron galley
D.I. Sereda, T.Yu. Snegiryova

Address

E.O. Paton Electric Welding Institute,
International Association «Welding»
11, Bozhenko Str., 03680, Kyiv, Ukraine
Tel.: (38044) 200 60 16, 200 82 77
Fax: (38044) 200 82 77, 200 81 45
E-mail: journal@paton.kiev.ua
www.patonpublishinghouse.com

State Registration Certificate
KV 4790 of 09.01.2001
ISSN 0957-798X

Subscriptions

\$348, 12 issues per year,
air postage and packaging included.
Back issues available.

All rights reserved.

This publication and each of the articles contained
herein are protected by copyright.
Permission to reproduce material contained in this
journal must be obtained in writing from the
Publisher.

CONTENTS

SCIENTIFIC AND TECHNICAL

- Torop V.M., Garf E.F., Yakimkin A.V. and Gopkalo E.E.*
Determination of the causes for crack initiation in structural
elements of the tower of new ventilation pipe at Chernobyl
NPP 2
- Gajvoronsky A.A., Zhukov V.V., Vasiliev V.G., Zuber T.A. and
Shishkevich A.S.* Structural changes in overheating zone of
haz metal of railway wheels in arc surfacing 13
- Sukhovaya E.V.* Quasi-crystalline alloys-fillers for composite
layers produced using method of furnace surfacing 20
- Pismenny A.A.* Improvement of power efficiency of machines
for resistance spot welding by longitudinal compensation of
reactive power 25
- Makhlin N.M. and Korotynsky A.E.* Analysis and procedure of
calculation of series connection electronic devices for
contactless arc excitation 30

INDUSTRIAL

- Lobanov L.M., Garf E.F., Kopylov L.N. and Sineok A.G.* Welded
structure of Kiev TV-tower is 40 years old 41
- Chvertko P.N., Moltasov A.V. and Samotryasov S.M.*
Calculation of upsetting force in flash butt welding of
closed-shape products 46
- Akhonin S.V., Belous V.Yu., Antonyuk S.L., Petrichenko I.K.
and Selin R.V.* Properties of fusion-welded joints on
high-strength titanium alloy T110 51
- Majdanchuk T.B.* Electrode and filler materials for surfacing
and welding of cast tin bronzes (Review) 55

NEWS

- International Conference «Welding and Related Technolo-
gies — Present and Future» 61

INFORMATION

- 20 years in the world of flux-cored wires 63

«The Paton Welding Journal» abstracted and indexed in Ukrainian refereed
journal «Source», RJ VINITI «Welding» (Russia), INSPEC, «Welding
Abstracts», ProQuest (UK), EBSCO Research Database, CSA Materials
Research Database with METADEX (USA), Questel Orbit Inc. Weldasearch
Select (France); presented in Russian Science Citation Index & «Google
Scholar»; abstracted in «Welding Institute Bulletin» (Poland) & «Rivista Italiana
della Saldatura» (Italy); covered in the review of the Japanese journals
«Journal of Light Metal Welding», «Journal of the Japan Welding Society»,
«Quarterly Journal of the Japan Welding Society», «Journal of Japan Institute
of Metals», «Welding Technology».



DETERMINATION OF THE CAUSES FOR CRACK INITIATION IN STRUCTURAL ELEMENTS OF THE TOWER OF NEW VENTILATION PIPE AT CHERNOBYL NPP

V.M. TOROP¹, E.F. GARF¹, A.V. YAKIMKIN¹ and E.E. GOPKALO²

¹E.O. Paton Electric Welding Institute, NASU

11 Bozhenko Str., 03680, Kiev, Ukraine. E-mail: office@paton.kiev.ua

²G.S. Pisarenko Institute for Problems of Strength, NASU

2 Timiryazevskaya Str., 01014, Kiev, Ukraine. E-mail: office@ipp.kiev.ua

Analysis of design and service documentation, as well as correspondence of actual loads and service modes of the new ventilation pipe (NVP) to this documentation requirements, has been performed. Results of non-destructive testing of base metal and welded connections of structural elements on the NVP at ChNPP have been analyzed. Cracks in tower nodes of ChNPP NVP are of systematic nature. They formed in the zones of node welded connections of tower three upper tiers, in which the lattice elements are made of pipes of 193.7 × 6 mm cross-section. At present cracks were detected in 17 nodes of slotted gusset of the post and in 17 nodes of brace attachment to straining sill. Templates were cut out, which are crack-containing fragments of gussets, i.e. structural elements of ChNPP NVP, samples were prepared and experimental investigations of the composition, microhardness, mechanical properties and structure of base metal, HAZ and weld metal have been performed. Causes for and mechanisms of cracking in structural elements of the NVP have been determined during performance of materials science investigations in two cut-out templates. Fractographic studies revealed the fatigue nature of surface crack initiation and propagation in gussets. Aerodynamic and strength analyses of the construction and its individual elements have convincingly demonstrated that the cause of cracking are resonance vibrations of braces in the upper three sections of the tower, directed out of face plane and inducing alternating bending stresses in the nodes. Vibration frequencies and forces transferred to the nodes have been determined. Stress fields caused by periodic forces in the braces, confirm the existence of the zone of fracture initiation and development, and maximum stress levels greatly exceed welded connection fatigue limits. A conclusion was made that the tower was designed using out-dated design concepts for nodes, characterized by numerous zones of high stress concentration, low fatigue and corrosion resistance. 12 Ref., 1 Table, 20 Figures.

Keywords: *welded connections, welded nodes, fatigue, resonance, fatigue life, fractography, metallographic investigations, fatigue crack, strength analysis, new ventilation pipe, Chernobyl NPP*

Analysis of design documentation showed that construction of new ventilation pipe (NVP) was performed over premise 7001 of block C of the main building of second stage of Chernobyl NPP (ChNPP) between D1-Zh/36-37 axes. The main building of ChNPP second stage is a complex construction, including 3rd power generating unit, destroyed 4th power generating unit («Ukritie» structure) and block C common for both power generating units. The currently operating ventilation pipe VT-2 is located between axes I-N/36-40.

NVP is a tower in the form of a load-carrying steel frame accommodating a gas flue of 6 m diameter. Load-carrying frame of NVP tower is a tetrahedral latticed structure of 8.05 × 8.05 m

dimensions (in the axes) in plan view and 50 m height. Inside the tower horizontal diaphragms with 7.2 m step are envisaged which are combined with foot platforms. Vertical trestle ladders provide access to the platforms. NVP tower is resting against a metal support contour at 71.65 m mark. Tower posts, main ties and lattices between the posts are made of cylindrical electric-welded pipes.

Gas flue of 6 m diameter with four vertical stiffeners is supported by a metal contour at 71.65 m mark. Top mark of the gas flue is 125 m. Gas flue is tied every 7.2 m along its height to tower diaphragms in the horizontal direction. Gas flue butts are joined by flanged connections using bolts. Dismantling of ceramsite concrete plates of the roofing at 71 m mark on D1-Zh/36-37 axes is envisaged for connection of the gas flue to premise 7001 of block C.

Metal support contour is a system of beams, attached by horizontal ties. NVP tower posts are fixed on two main beams of support contour,



Figure 1. Cases of crack propagation in tower brace nodes (for *a* and *b* see the text)

located along axes D1 and Zh. Support contour main beams are attached to the existing concrete structures of block C in four points at 70.7 m mark along axes D1-Zh/36-37. Supporting nodes of main beam fastening are designed to accommodate vertical (including tearing) and horizontal loads from NVP.

Braces of NVP tower lower tiers are pipes of 245 mm diameter with 8 mm wall thickness for BC1 braces. For BC2 braces 1219 × 6 mm pipe was specified. BC3 braces, mounted at 100.36–121.96 m mark, are made from 193.7 × 6 mm pipe. Flexibility λ of BC3 braces is 170. Flexibility of BC1 and BC2 braces is 130 and 150, respectively, negative influence of vibrations being less pronounced for these elements. It should be also taken into account that in the lower tiers gussets are made from rolled sheets of greater thickness than gussets in fastening nodes of BC3 braces, the thickness of which is 12 mm. According to the data given in [1], a potentially hazardous area of development of self-excited oscillations of round steel rods in latticed structures are elements with λ from 100 up to 350.

Examination of NVP tower node connections performed by PWI specialists and the thus revealed crack-like defects [2], materials science investigations of metal in the cracking zone and detailed analysis of fracture surface [3], enabled applying a weighted and substantiated approach to establishing the causes for crack initiation in NVP nodes.

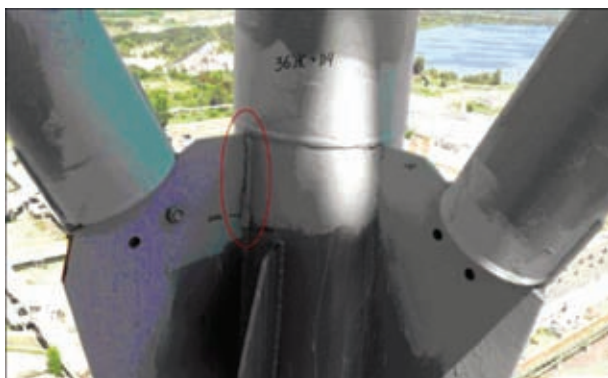


Figure 2. Crack-like defects in the node of brace abutment to tower post



Figure 3. Node of brace abutment to tower post after cutting out template #1

Examination of metal structures of NVP load-carrying frame on the level of upper tiers of tower frame at 114.92, 107.72 and 100.52 m marks [2] revealed the following drawbacks:

- absence of assembling bolts, because of misalignment of holes in connecting gussets (caused by violation of geometrical accuracy during frame assembly);
- presence of cracks in the upper part of vertical gussets of posts in points of brace abutment.

Note the fact that location of detected cracks is of systematic nature. All the cracks were found in three upper sections of the tower. A common feature for these sections is the fact that the lattice elements are made of cylindrical pipes of 193.7 × 6 mm cross-section, and gussets have 12 mm wall thickness. In these sections cracks were found in 17 out of 24 nodes connecting the brace to slotted gusset of tower post, and out of the 24 nodes connecting the brace to straining sill cracks were detected in 17 of them (Figure 1). It should be noted that specialists conducted examination under the conditions of a high radiation background and were limited in time. Therefore, there is strong probability that not all the crack were detected.

Cracks are of different length. They initiate from the edge in the upper part of node gusset



Figure 4. Schematic of cutting out template #2 (cracked fragment of gusset with complete weld structure up to the end of detected crack)



Metal composition, wt.%

Data source	C	Si	Mn	P	S	Cr	Mo	Ni	Cu	Al	Co
Q2 ION spectrometer	0.146–0.158	0.134–0.170	0.60–0.62	<0.03	<0.01	0.026–0.032	<0.01	<0.01	0.005	<0.047	0.016
GOST 27772–88 (S255)	≤0.22	0.15–0.30	≤0.65	≤0.04	≤0.05	≤0.30	–	≤0.30	≤0.30	–	–
GOST 380–94 (St3Gps) (semikilled)	0.14–0.22	≤0.15	0.8–1.1	≤0.04	≤0.05	≤0.30	–	≤0.30	≤0.30	–	–
GOST 380–94 (St3Gsp) (killed)	0.14–0.20	0.15–0.30	0.8–1.1	≤0.04	≤0.05	≤0.30	–	≤0.30	≤0.30	–	–

(node of lattice elements abutment to tower post) and develop downwards along the gusset and in-depth (Figure 1, *a*). In the node of braces abutment to the straining sill cracks are found in the connection of the stiffener and brace pipe through a thin plug sealing the brace inner space (Figure 1, *b*).

Another specific feature: in tower post nodes cracks form from two sides of the gusset, propagating in-depth and moving towards each other. Cracks propagate along the boundary of transition from fillet weld joining the tower post to slotted gusset, to gusset base metal. In those cases, when fillet welds from one and the other side of the gusset have different legs, cracks propagate with the appropriate shifting.

The characteristic appearance of crack-like defects detected by NDT is given in Figure 2.

Metallographic and fractographic investigations were performed to establish the causes for initiation of crack-like defects in NVP metal structures. Templates of gussets with anticipated cracks were cut out at 36Zh + 114 (cutting out area is shown in Figure 3) – template #1 and 36D1 + 107 marks (cutting out schematic is shown in Figure 4) – template #2, respectively.

According to documentation, gusset metal (12 mm sheet) is low-carbon structural steel of S255 class.

To identify the gusset material, composition of gusset base metal was analyzed (optico-emission spectrometer Q2 ION based on CCD detectors) and the results are given in the Table.

By chemical composition (manganese content) the specified gusset metal did not meet the requirements of GOST 380–94 to steels of St3Gps and St3Gsp grades (S255 steel analogs), although it meets the requirements for steel S255, according to GOST 27772–88 (see the Table). In addition, mechanical testing was performed for accurate identification of gusset steel grade, the results of which confirmed their correspondence to steel S255 (according to the requirements of GOST 1497–84). Mechanical testing of standard smooth samples conducted at 20 °C showed mean values of tensile strength of 453 MPa, yield point of 285 MPa, relative elongation of 31.7 and reduction in area of 54.4.

To analyze (establish) the causes for and mechanisms of formation of crack-like defects in the structure, comprehensive investigations of

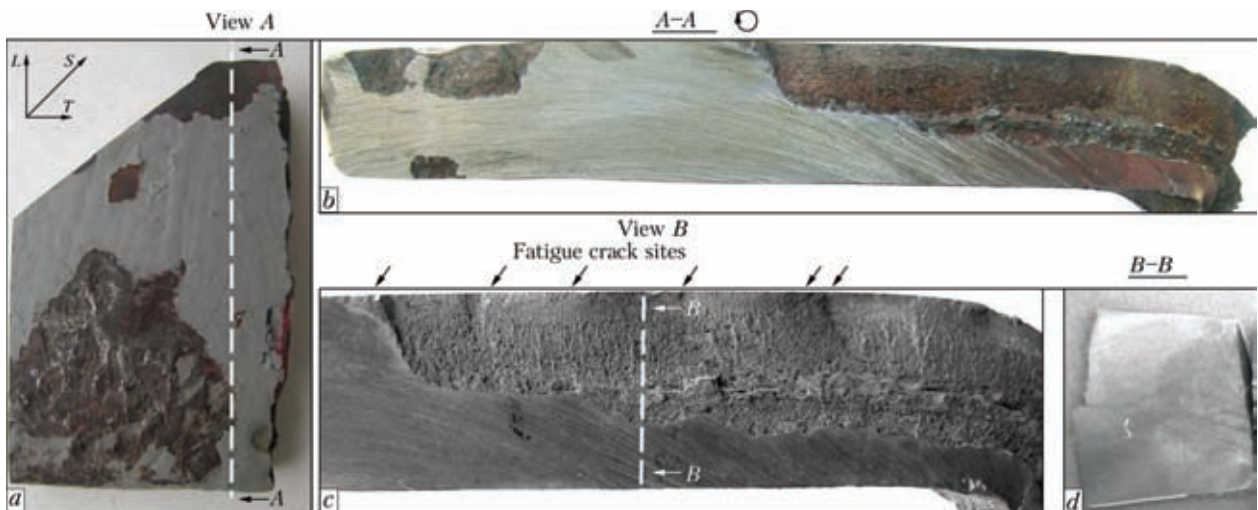


Figure 5. Template #1 with open crack: *a* – template appearance; *b*, *c* – fragment of gusset in crack plane *L-S* before and after crack surface cleaning to remove corrosion products, respectively (gusset section *A-A*); *d* – microsection plane in plane *S-T* (gusset section *B-B*)



the presented templates in the vicinity of welded connections, including visual examination, metallographic analysis in optical inverted microscope AXIOVERT 40-MAT and fractographic analysis in an upgraded scanning electron microscope REM-100U were performed.

Samples for metallographic examination were cut out in the plane of S - T cross-section of the gussets normal to sheet rolling plane L - T (where L is the rolling direction coinciding with longitudinal direction of the weld; T is the direction in the rolling plane; S is the direction normal to rolling plane).

Template #1 in as-delivered condition along one of the sides was cut out in crack plane L - S along the fillet weld normal to gusset sheet rolling plane L - T (Figure 5). Crack surface in cut plane is covered by corrosion products, and that is why ultrasonic cleaning of the surfaces from corrosion products was performed in ultrasonic disperser UZDH before fractographic investigation, using 2 % alcohol solution of oxalic acid and then pure ethyl alcohol. Figure 5, *c* shows a gusset fragment in crack plane L - S after removal of the protective layer from the sheet outer surfaces and crack surface cleaning from corrosion products.

Fractographic investigations of opened crack surfaces in the cut plane revealed crack initiation sites and propagation mechanisms in welded connection of template #1, although the weld zone proper is not in the template. Proceeding from fractographic studies cracks are identified as fatigue, initiating on surface defects. Fatigue crack sites are marked by arrows in Figure 5, *c*. Figure 6 shows a characteristic fragment of fractogram of a gusset with fatigue crack (with initiation site, characteristic fracture relief and traces of fatigue crack front arresting). The main crack formed as a result of coalescence of several fatigue cracks, which initiated from different sites on the gusset outer surface and grew in-depth of the sample to 5 to 6 mm (approximately to half of gusset sheet thickness). In some fracture areas coarse globular non-metallic inclusions are observed, which are commensurate with ferrite of gusset base metal (crack might have crossed the fusion zone in such areas).

As shown by metallographic investigations of crack profile fragments in plane S - T of one of the cross-sections, the crack initiated on gusset outer surface in HAZ coarse-grain zone.

Here fine secondary delamination microcracks several micrometers long oriented along the rolling texture are observed along the primary crack profile line (in welded connection cross-section), and at about 5 mm distance from the outer surface already an extended secondary delamination crack of about 450–500 μm length formed (Fi-

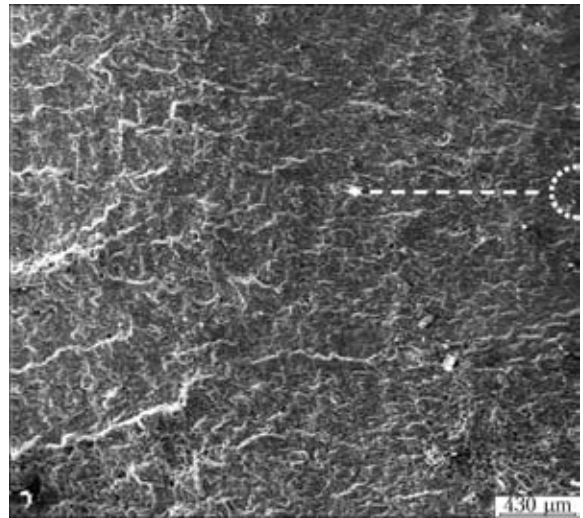


Figure 6. Fractogram of gusset (template #1) in plane L - S with fatigue crack (white contour marks fatigue crack site, arrow shows direction of crack front)

gure 7), which was also due to rolling texture. It propagated along extended pearlite colonies and sulphide inclusions, which are observed in the studied template section (see enlarged fragment in Figure 7).

Figure 8 shows a fragment of template #2 of a welded connection in plane S - T after etching in 4 % solution of nitric acid in ethyl alcohol with marking of zones of weld, HAZ and BM.

Microstructure of gusset BM is a ferrite-pearlite mixture of polyhedral ferrite with a small amount of fine-grained pearlite. With general diversity of ferrite grains (14–30 μm) average size of ferrite grains was 20–25 μm . A high density of finely dispersed carbide was observed in ferrite grains. Gusset BM is characterized by striated rolled pattern. Measurement of microhardness at 0.5 N load was conducted in T-Durascan-20 microhardness meter according to GOST 9450–84. Microhardness of ferrite grains in BM, depending on density of finely dispersed carbide in them,

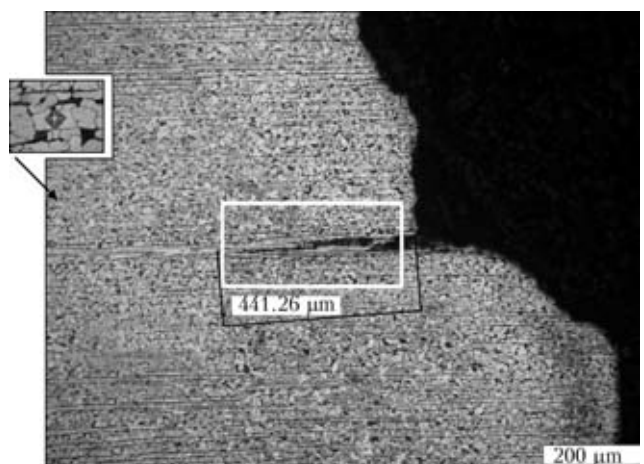


Figure 7. Fractogram of secondary crack of gusset delamination

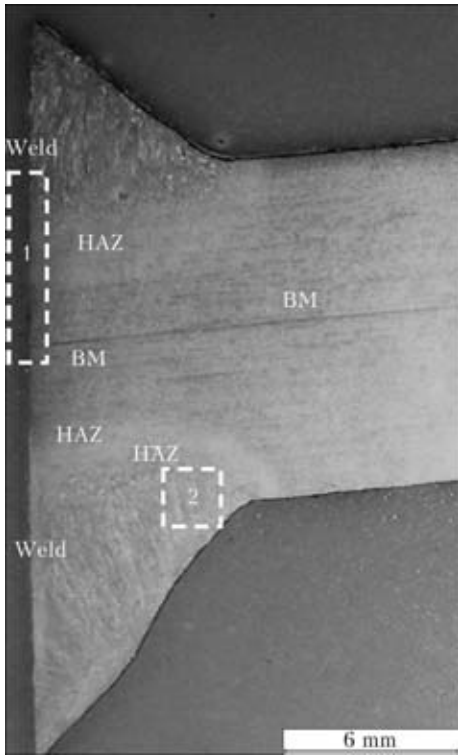


Figure 8. Fragment of welded joint microsection (template #2) in plane *S-T*

varies in the range of *HV* 1500–1670, and that of pearlite is of about *HV* 1770–1930 MPa.

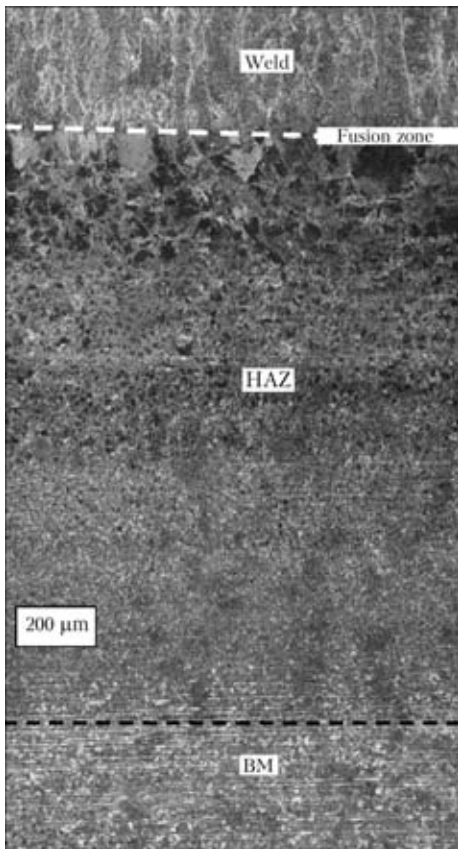


Figure 9. Panoramic view of microstructure fragment (template #2) of section 1 in Figure 8

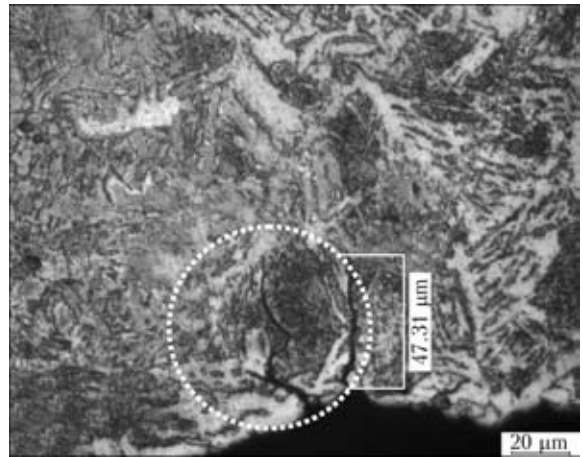


Figure 10. Microstructure fragment (template #2) of section 2 in Figure 8 (dot contour marks microcrack area)

In weld zones no defects in the form of microcracks were found. Weld metal microstructure are columnar crystallites with characteristic directed orientation, indicating direction of solidification from the liquid state. Microhardness of columnar crystallites at 1 N load was of about *HV* 2350 MPa on average.

Panoramic view of a fragment of microstructure in zone 1 (see Figure 8) including the structure of the weld, fusion zone, HAZ and gusset BM is shown in Figure 9. Overheating zone («coarse-grain» zone of about 400–600 μm width) is located near the fusion zone in the HAZ. Its grains are characterized by Widmanstaetten structure with lower mechanical properties. Total HAZ width is within 900–2900 μm.

Detailed investigation of welded connection microstructure in plane *S-T* of the microsection near the fusion zone revealed two microcracks of 50–60 μm size, initiating on the stress raiser in the form of a defect of template outer surface in the area of HAZ coarse grain (Figure 10). Such fine cracks could hardly be detected by other methods, in view of outer surface roughness, and presence of a layer of scale on it. As shown by investigations, thickness of scale layer on gusset surface reaches 30 μm in individual locations,

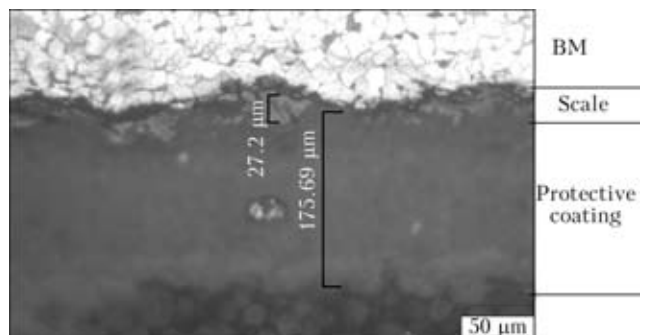


Figure 11. Fragment of gusset section with scale and protective coating



and protective coating thickness is 180 μm (Figure 11).

The above data lead to the conclusion that forces in tower braces are responsible for crack initiation and propagation, as exactly the forces in braces in slotted gussets induce stresses, the nature of distribution of which is in complete agreement with the regularities of crack propagation in tower nodes. However, if we assume that only longitudinal forces are found in tower braces, caused by loads applied during the construction service, then stresses induced by them could not in any way lead to detected damage. Initiation and propagation of cracks from two sides of slotted gussets in tower post nodes and crack formation in the nodes of brace connection to the sill, are indicative of the fact that bending stresses are present in these nodes, which can be caused only by the respective forces in braces.

The fact that in the post gussets cracks initiate and propagate along the boundary of transition from welded joint to base metal, and across metal thickness cracks develop normal to its surface, as well as the difference in crack dimensions in different nodes, are indicative of their fatigue origin. This is convincingly confirmed also by the above-described fractographic investigations, in particular, characteristic fracture surface, presence of crack initiation sites, striations characteristic for crack arresting and initiation (see Figures 5 and 6).

Therefore, it terms of welded structure strength there is no doubt that the cracks detected in NVP tower nodes are of fatigue nature and are caused by bending stresses, developing at brace vibration out of tower panel plane. Here periodical forces should arise in the crack zone, causing cyclic stresses sufficient for fatigue crack initiation and propagation. Note that it took less than seven months for the cracks to initiate. That is why, crack formation is possible only in the case if the braces start resonating at certain real wind velocities, and the forces and stresses arising here are capable of causing fatigue fractures in the nodes. Another argument in favour of exactly this cause for damage initiation consists in that brace flexibility is the highest in the three upper tiers of the tower. This also accounts for the fact that cracks were detected exactly in these tiers.

On the other hand, we cannot ignore the opinion on the considered problem expressed by specialists of Bechtel Company, USA, who conducted an independent investigation of NVP elements, containing defects [4]. Two specialists in the field of metallurgy and one specialist on welding technology and NDT participated in investi-

gations. At the very beginning of their investigations the authors conclude that the «design is ruled out as a possible cause for defect initiation», substantiating it by the fact that the construction was not exposed to design loads since the moment building was over and up to crack detection. By doing that the investigation authors essentially limited the area of searching for the causes for crack initiation in the tower nodes. If the design factor is eliminated a priori, then simply nothing else, but the technological factor, is left to account for the fracture causes.

During investigation it was established that steel of S345 class was used in 12 mm gusset cut out together with the fillet weld from a node at 100 m mark, while the project envisaged class S255 steel. It is not of any fundamental importance in itself, but higher hardness (HV up to 3985 MPa) and a «small amount of martensite in the near-weld zone» were found in the weld and HAZ that may be indicative of an increased rate of welded joint cooling. The above was used as a basis to make the conclusion that «the most probable cause of crack initiation is hydrogen cracking». The authors realize that increased hardness and martensite presence in the HAZ proper cannot cause cold cracks, so an assumption is made that in the manufacturing plant welding was performed under the conditions of «rain, snow, high humidity or strong wind».

Certainly, it is difficult to accept such a conclusion, although the authors do express it cautiously enough. First, the conditions of welding must have been the same along the entire length of the gusset, and cracks in all the cases are found in those points where the force is transferred from the brace, i.e. in the gusset upper part. Secondly, cold cracks are located predominantly in the HAZ, i.e. along the weld fusion zone, and the considered cracks propagate normal to gusset surface, and, finally, none of the studies revealed presence of cold cracks either in the weld, or in the HAZ. In addition, cracks are found both in gussets made from steel of S345 class, and in gussets made from steel S255, although the authors of the analyzed investigation are convinced that no cracks will be present in steel of S255 class.

To determine the conditions of development of brace resonance vibrations, their frequency characteristics, as well as levels of induced cyclic stresses, a complex analysis of braces for wind load was performed, which was treated as disturbing factor, causing resonance vibrations.

Note that the above data, based on the results of examination and fractographic investigations of fracture surface, are quite sufficient to make

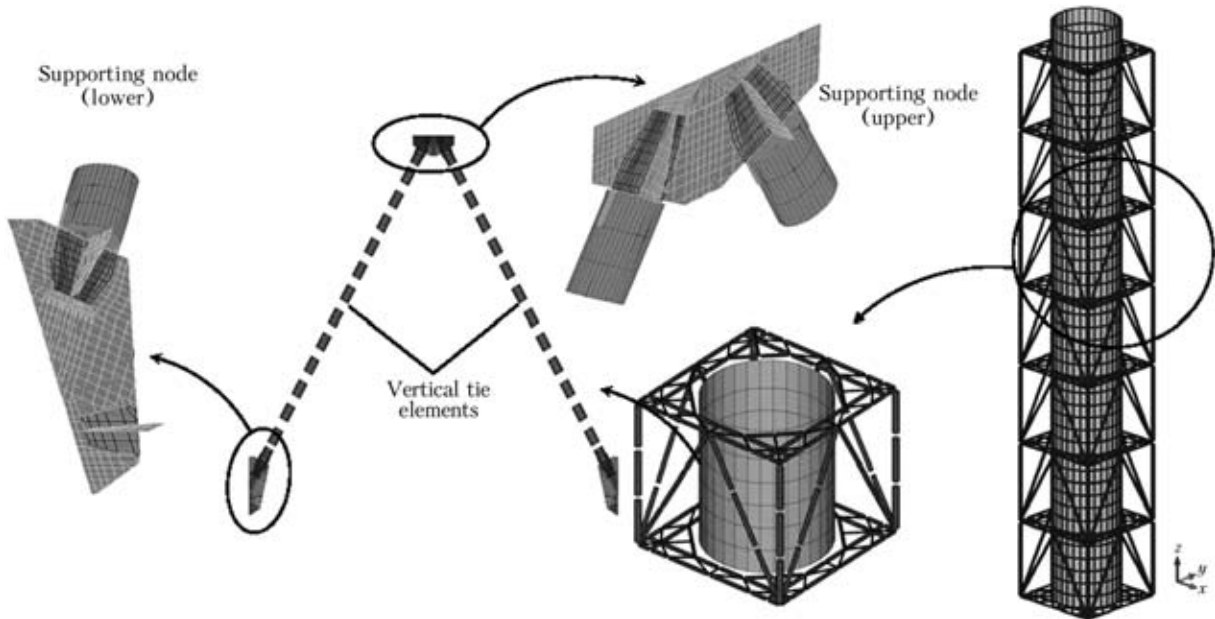


Figure 12. NVP FEM models

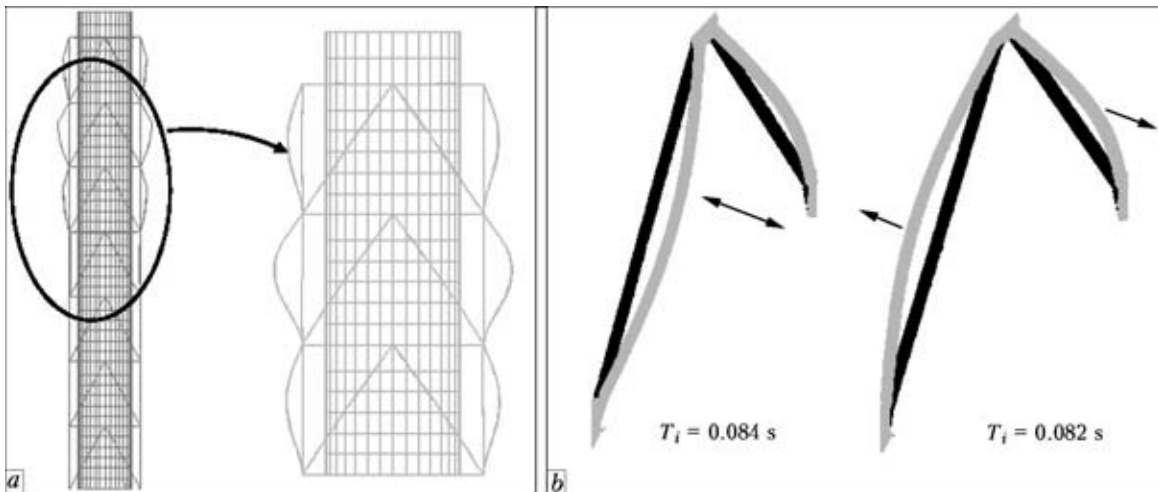


Figure 13. Forms of natural vibrations (for a and b see the text)

an unambiguous conclusion about the causes for and nature of initiating cracks.

Calculation given below is just a tool, explaining facts quite obvious for specialists, and it can only be regarded as an independent criterion for taking a critical decision, if one is absolutely sure of its correctness. Authors have to draw attention to this fact as insufficiently cor-

rectly performed calculation leads to erroneous conclusions.

Main stages and sequence of calculation performance. According to the above-given results of metallographic analysis of gusset fragments it is established that the mechanism, which caused crack initiation and propagation, is of fatigue nature.

Analysis of initial data allowed ignoring some kinds of loads (taken into account in NVP design), namely: class 3 tornado, 5 and 6 point earthquake, snow load and temperature impact. As during NVP operation (since the moment of its commissioning and up to crack initiation in gussets) some of the above loads were completely absent, others did not exceed their design values, while their repeatability was insignificant, they could not cause cracking.

Considering that for high-rise constructions it is exactly the wind load as a dynamic disturbing

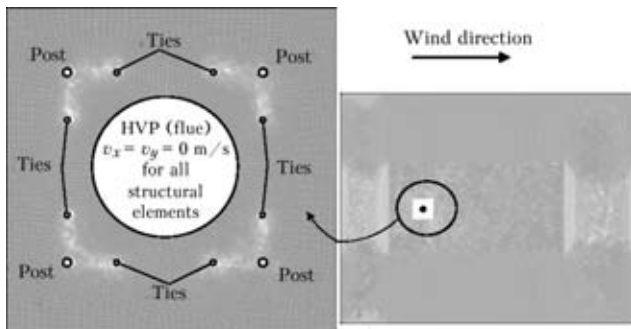


Figure 14. Aerodynamic model: general view, loads and boundary conditions ($v_x = 12$, $v_y = 0$ m/s, $P = 0$ Pa)

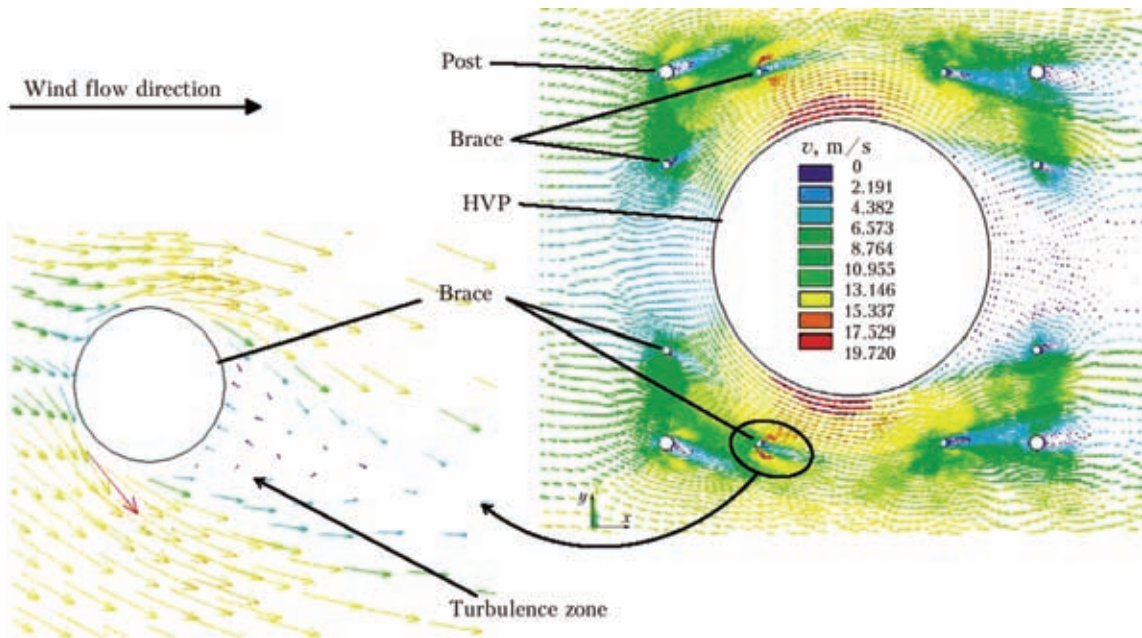


Figure 15. Direction of wind flow velocity vectors

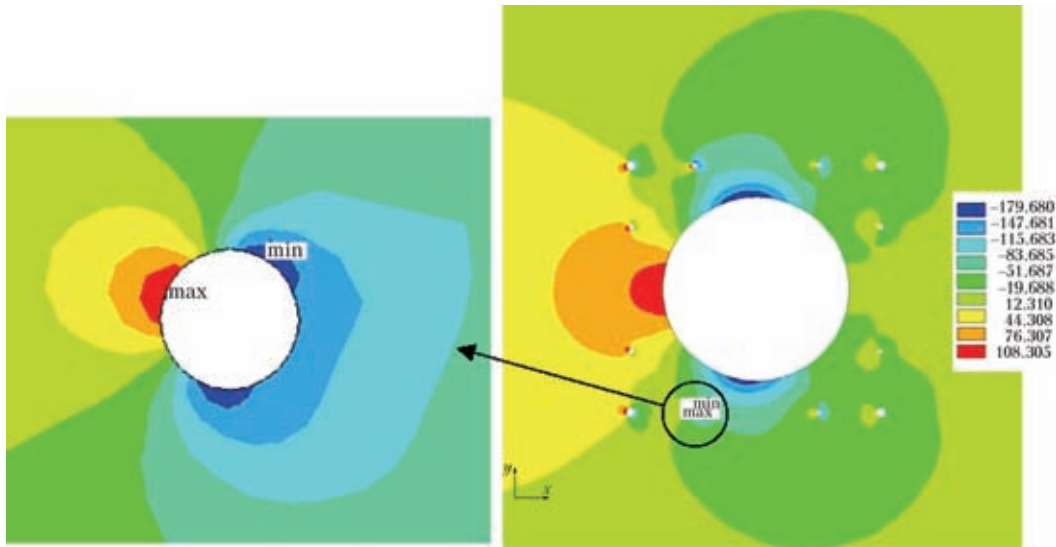


Figure 16. Wind pressure isofields

factor that is the main one, the influence of wind flow on stress-strain state of NVP and its individual structural elements is analyzed.

Problem was solved in several stages, using aerodynamic and strength numerical models. This is due to a rather complicated nature of interaction of the wind flow and building structures — cross-effect of adjacent structural elements on distribution of velocity and force of winds, etc.

As a result of calculation of shell-rod 3D FEM models (Figure 12) forms and periods of system natural vibrations were determined.

Detailed analysis of the derived results revealed that in a number of cases the forms of NVP natural vibrations are created by group deformation of braces of three upper sections (Figure 13, a). Brace vibrations are characterized by their buckling out of panel plane. Charac-

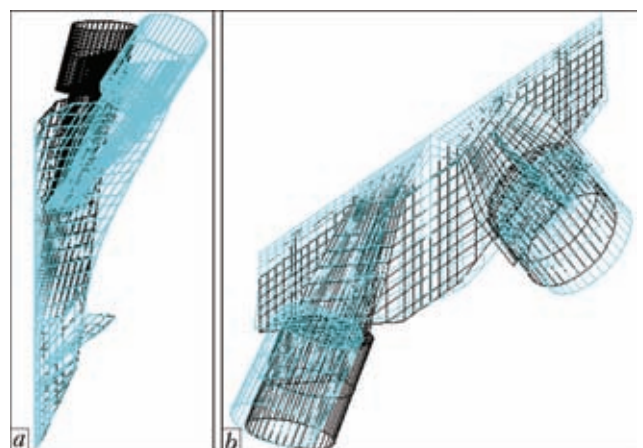


Figure 17. Schematics of supporting gusset deformation: a – lower; b – upper gussets

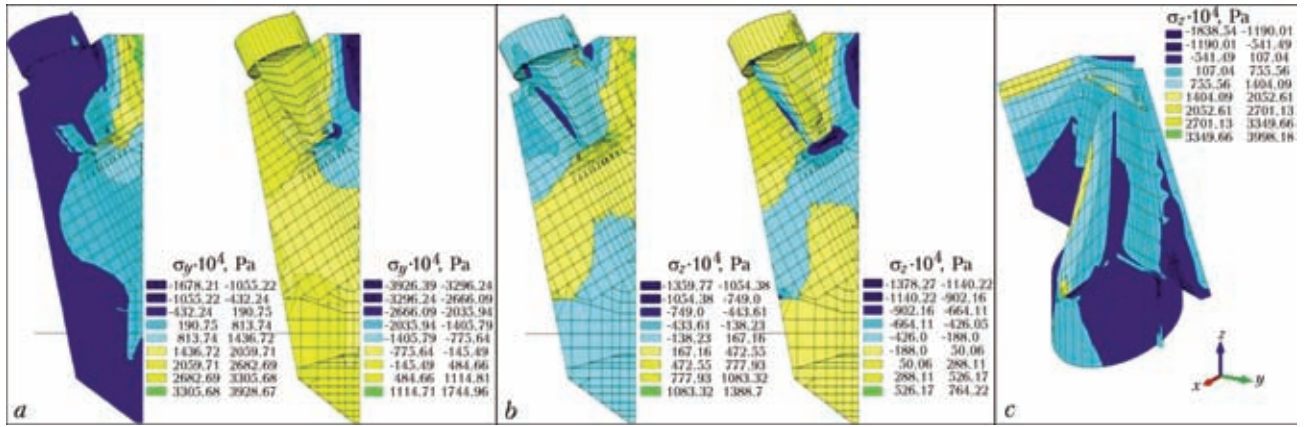


Figure 18. Isofields of stresses on faces of lower (a, b) and upper (c) supporting nodes

teristic forms of brace vibrations and respective magnitudes of natural vibration periods are given in Figure 13, b.

To determine the critical velocity of wind flow v_{cr} , capable of causing wind resonance in the brace, we will use formulas given in [5]. In the first approximation we will assume that critical wind velocity, caused by resonance vibrations in the direction normal to wind flow, is equal to

$$v_{cr} = \frac{d}{T_i \text{Sh}} = \frac{0.194}{0.084 \cdot 0.2} = 11.6 \text{ m/s} \approx 12 \text{ m/s},$$

where $T_i = 0.082 \text{ s}$ is the period of brace natural vibrations by i -th form; $\text{Sh} = 0.2$ is the Strouhal number for round section; $d = 0.194 \text{ m}$ is the diameter of tie element ($193.7 \times 6 \text{ mm}$ pipe) in three upper levels of the tower.

Using the value of critical velocity $v_{cr} = 12 \text{ m/s}$ of wind flow as initial data, the aerodynamic model (Figure 14) was applied to determine the nature of distribution of wind flow and pressure over the surface of NVP structural elements.

Performed calculations showed that structural elements of NVP tower and flue affect the parameters of wind flow distribution around the

tower flue and elements of vertical ties. Increase of wind flow velocity along the flue side surface (Figure 15) leads to the braces located in this zone becoming exposed to higher magnitudes of wind pressure (Figure 16).

In addition, cross-effect of structural elements of NVP tower leads to the fact that wakes arising behind the braces (vertical ties) penetrate into the wake jets of flows formed by tower corner posts. As a result the wakes of vertical ties are subjected to turbulization practically immediately after the flow separation, and a turbulent wake forms between layers located at a certain distance from each other with a shift.

Studies [1, 6] note that the most hazardous are vibrations of a non-insulated cylinder, i.e. cylinder located in the wake jet of another one or in parallel to other cylinders. Here brace vibration arises much easier — at lower velocity of the flow and can be maintained in a wide range of velocities, and not in a certain range, that is why it is more dangerous. According to [1], aerodynamic forces applied to the construction vary by the harmonic law. In this connection, harmonic analysis of the structure was performed in order to determine the extent of wind flow influence on strength properties of support elements of vertical ties.

Results, derived at solving the aerodynamic problem, were used as initial data at determination of the magnitude of disturbing force (intensity amplitude), applied to vertical tie elements.

As a result of calculation of a precised model of harmonic force action (intensity amplitude F_0) simulating the dynamic impact of wind load, values of stresses and strains were determined in supporting gussets and other structural elements of the considered fragment of the construction.

Analysis of the derived results showed that the applied forces cause out-of-plane deflection of supporting gussets. Figure 17 gives the deformation diagrams of supporting gussets.



Figure 19. General view of NVP tower structure



Bending of lower supporting gussets leads to formation on their faces of stresses reaching values $\sigma_y = \pm 38.56$ MPa. Regions of highest stresses are located in upper zone of supporting gussets, in the area of their abutment to tower posts. In addition stress increase is observed in areas of variable rigidity, namely in zones of connection of supporting gussets to brace gussets. Isofields of stresses σ_y and σ_z in supporting nodes are given in Figure 18.

A zone with a pronounced stress raiser is found in the brace upper node, in the area of stiffener abutment to end plug. Schematic of deformation and isofields of stresses σ_z on the faces in the zone of upper supporting node are given in Figure 18, *c*. In these sections stresses reach the magnitudes of $\sigma_z = 39.9$ MPa.

Additional investigations and calculations. Additional investigations revealed the following facts.

1. Considering that coefficient of transverse force C_y , used at determination of disturbing force, is the theoretically minimum possible value and reaches greater values in practice, calculation of precised model for $C_y = 0.3$ was performed.

Performed calculations showed that the nature of stress distribution in structural elements remained similar to earlier obtained analogous isofields. Here stress values on face surfaces of lower supporting gussets increased by 25 % (up to 49 MPa). Increase of stress values was also noted in the upper supporting node.

2. Design solutions of supporting nodes are identical in all the sections of NVP tower, therefore evaluation check of supporting nodes of lower lying sections was performed.

Calculations showed that for vertical ties made of round 219×6 mm pipe, the period of the first form of natural vibrations $T_i = 0.07$ s, and critical velocity $v_{cr} = 15.5\text{--}16.0$ m/s. Stress amplitude modulo in supporting gussets, depending on the value of dynamic coefficient C_y , can change from 31 to 39 MPa.

For vertical tie elements made of round 245×8 mm pipe, $T_i = 0.06$ s, $v_{cr} = 20.5\text{--}21.0$ m/s.

Obtained values of critical velocities of wind flow are not mentioned in statistical data on wind velocities recorded in Chernobyl weather station over the elapsed period. The provided information on wind velocities was given as hourly measurements that introduces a certain averaging parameter. In [7] it is noted that the mean velocity of wind averaging depends on averaging time. At shortening of averaging interval maximum value of mean velocity, corresponding to this interval, becomes higher. For instance, the difference between the mean hourly velocity and mean veloc-

ity over 20 s period can differ two times. Thus, for sections of the third-fourth level, the wind flow velocity $v = 15\text{--}16$ m/s is probable.

3. Considering that the Strouhal number is of a tentative nature and can vary for different cross-sectional shapes within a certain range (for cylinders it is assumed that $Sh = 0.2$, although in practice $Sh = 0.185\text{--}0.220$), external loads can change their values in an even greater range that, in its turn, leads to an even greater increase of stresses in supporting elements of NVP tower frame.

Analysis of stresses in slotted gusset induced by resonance vibration of braces. Calculated values of cyclic stresses arising in a slotted gusset at the boundary of a fillet weld connecting the gusset to post pipe are considered for compliance to norms in force in Ukraine [8], and IIW Recommendations [9].

According to [8], fatigue limit R_p for 5th group of elements, into which the connection of a slotted gusset to the post can be included, $R_{\sigma_{-1}} = 16.83$ MPa at residual stresses of not more than $0.5\sigma_y$ in the cracking zone for a symmetrical loading cycle. Note that according to norms [8], fatigue limit is determined on the base of 10^7 loading cycles.

As in the gusset cyclic stresses under the conditions of resonance vibrations of the brace are equal to ± 39 MPa, crack initiation can be anticipated at fatigue life of $8.04 \cdot 10^5$ loading cycles. Allowing for brace vibration frequency under resonance conditions (12.2 Hz), 20 h of operation are sufficient for fatigue cracks to form.

According to IIW procedure, limit values of stress ranges on the base of $2 \cdot 10^6$ loading cycles are given for characteristic types of welded connections. For a connection close to the one found in NVP tower, limit value of stress range is 45 MPa.

As in the gusset stress range value is equal to 78 MPa, fatigue life, at which fatigue cracks can be anticipated, is equal to $384 \cdot 10^3$ loading cycles, according to this procedure.

The given data once more confirm the fatigue nature of crack initiation in NVP tower nodes.

Analyzing the causes for crack initiation in the nodes of NVP tower, we cannot avoid assessment of the taken design solutions. The load-carrying frame of NVP tower is made of cylindrical pipes (Figure 19).

Selection of this type of pipe sections for tower structural elements is quite justified, as it allows lowering wind loads on the construction, increasing design length of elements, and, therefore, reducing construction weight and its cost. In addition, tubular elements have an increased cor-

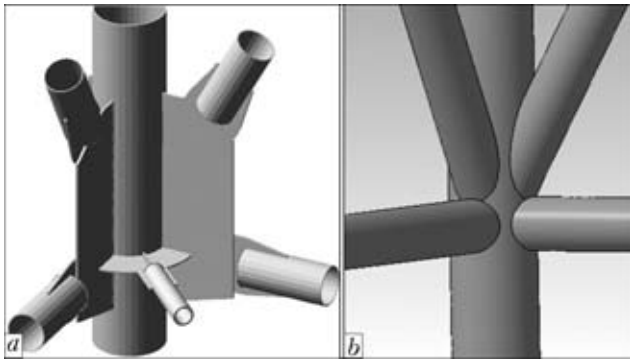


Figure 20. Schematics of node connection of NVP tower structural elements with the post: *a* – with slotted gussets; *b* – with direct abutment

rosion resistance owing to good air blowing and small surface area. These advantages, however, can be realized in full only at a rational design of node connections. It is known that in tubular structures node connections in a number of cases predetermine the strength and reliability of the entire construction [10].

Over the recent decades, in connection with application of cylindrical pipes as load-carrying elements of stationary off-shore platforms and other critical constructions, a large volume of investigations has been performed, which are aimed at development of optimum node design solutions, and methods of assessment of their strength under static and cyclic loading. It is shown that the most rational solution is direct abutment of lattice elements to the post. The structure has a high strength, low stress concentration, small number of welded connections, and high corrosion resistance. For such nodes normative documents for their strength analysis [11, 12, etc.] at static and cyclic loading have been developed. For comparison let us give the node of NVP tower and a node, corresponding to modern concepts of tubular structure design (Figure 20). If the design of NVP tower was made on an up-to-date level, many drawbacks could have been avoided.

Conclusions

1. Cracks in ChNPP NVP tower nodes are of a systematic nature. They formed in the zones of node welded connections of tower three upper tiers with lattice elements from 193.7×6 mm pipes. Cracks were detected in 17 nodes of post slotted gusset and in 17 nodes of brace attachment to straining sill.

2. There is no doubt that cracking is caused by cyclic forces acting in braces. This is confirmed by characteristic locations of their formation and presence of cracks from both ends of braces.

3. Cracks are of fatigue origin, initiate in post gussets on the outer surface from two sides, and propagate along the weld boundary from gusset upper edge and in-depth. Fractographic studies of fracture surfaces revealed initiation sites, characteristic relief of fatigue fracture and traces of fatigue crack arresting. In sill nodes the cracks also have characteristic features of fatigue fracture.

4. Aerodynamic and strength analyses of the construction and its individual elements have convincingly demonstrated that cracking is caused by resonance vibrations of braces in the tower three upper sections, directed out of face plane and inducing alternating bending stresses in the nodes. Vibration frequencies and forces transferred to nodes have been determined.

5. Fields of stresses caused by periodic forces in the braces confirm the presence of a zone of fatigue fracture initiation and propagation, and maximum stress levels greatly exceed welded connection fatigue limits.

6. Calculation showed that braces made from 219×6 mm pipes present a hazard in terms of fatigue crack initiation. This should be taken into account in development of NVP tower repair project.

7. The tower was designed using out-dated node design solutions, characterized by numerous zones of high stress concentration, low fatigue and corrosion resistance.

1. Savitsky, G.A. (1972) *Wind loading on constructions*. Moscow: Strojizdat.
2. (2012) *Results of inspection of welded joints of new ventilation pipe frame on «Chernobyl NPP» object*: Report. Kiev: PWI.
3. (2012) *Expertise of causes of crack-type defect initiation in new ventilation pipe*: Report. Kiev: Ukr-Atomenergo.
4. Maclean, D., Campbell, R., Colwell, R. (2012) *Independent examination of structural defects of NVP*: Sci.-Techn. Report. Kiev.
5. (1978) *Guidelines on design of buildings and constructions under wind action*. Moscow: Strojizdat.
6. Vilkerd, D.S., Popov, S.G., Savitsky, G.A. (1951) Oscillations of bodies in aerodynamic wake. *Vestnik MGU*, **12**, 23–25.
7. Simiu, E., Scanlan, R.H. (1984) *Wind effects on buildings and constructions*. Moscow: Strojizdat.
8. *DBN V.2.6-163:2010*: Steel structures. Norms of design, fabrication and assembly. Valid from 01.12.11. Kiev: Minregionbud.
9. Recommendations for fatigue design of welded joints and components. *IIW Doc. XIII-7539-96*.
10. Marshal, P.W. (1984) Connections for welded tubular structures. In: *Proc. of Int. Conf. on Welding of Tubular Structures*. Pergamon Press, 11–17.
11. *VSN 51.4-85*: Departmental building norms. Gussetless connections of structures of offshore oil-field facilities. Procedure of strength analysis. Introd. 03.06.1985. Moscow: Mingazprom.
12. *API Recommended practice for planning, designing and constructing fixed offshore platforms*: Doc. RP2A.

Received 03.09.2013



STRUCTURAL CHANGES IN OVERHEATING ZONE OF HAZ METAL OF RAILWAY WHEELS IN ARC SURFACING

A.A. GAJVORONSKY, V.V. ZHUKOV, V.G. VASILIEV, T.A. ZUBER and A.S. SHISHKEVICH

E.O. Paton Electric Welding Institute, NASU

11 Bozhenko Str., 03680, Kiev, Ukraine. E-mail: office@paton.kiev.ua

The objective of the work is investigation of the parameters of welding thermal cycle (WTC) in arc surfacing, including heating and cooling stages, on formation of metal structure and properties in overheating zone of the HAZ of high-strength wheel steel of grade 2, containing 0.58 % C. Gleeble 3800 complex was used to conduct heat treatment of model samples at heating rate of 25 to 210 °C/s up to the temperature of 1250 °C with subsequent cooling by WTC ($w_{6/5} = 2.5\text{--}64$ °C/s), perform metallographic investigations of the structure and plot diagrams of overcooled austenite transformation. At testing by the Implant method influence of cooling rate and structural state of metal in overheating zone of HAZ on critical stress values at delayed cracking of wheel steel was assessed. It is established that incompleteness of the processes of metal austenite homogenizing in arc surfacing, because of its fast heating and limited time of soaking at the temperature above A_{c3} , has an essential influence on subsequent γ - α transformation in the HAZ metal. This leads to lowering of the critical cooling rate to 20 °C/s, at which not more than 50 % of martensite forms in the structure (w_{50M}). It is shown that the high delayed fracture resistance of HAZ metal on the level of $\sigma_{cr} \geq 0.45\sigma_{0.2}$ can be ensured, provided $w_{6/5} \leq w_{50M}$. Investigation results can be used at specifying the technology of building-up by surfacing of items from high-strength steels. 12 Ref., 4 Tables, 4 Figures.

Keywords: arc surfacing, wheel steel, thermal cycle, HAZ, austenite transformation diagram, structure, martensite, bainite, delayed fracture

Cracking in welded joints of high-strength steels depends on the state of the structure in the HAZ overheating zone, degree of metal quenching during the welding thermal cycle (WTC) and its plastic properties. This determines the quantity and density of dislocations, depth of running of diffusion and relaxation processes in the quenched metal that essentially influences the processes of crack initiation and propagation at loading and, eventually, the performance of welded joints and metal structures as a whole [1–5].

Problems at building-up by surfacing of items from high-strength wheel steels are similar to those arising in welding of alloyed steels. The main of them is prevention of cracking in the HAZ metal. Unlike high-strength alloyed steels, wheel steels do not contain any additional alloying elements, such as chromium, nickel, molybdenum, stabilizing the metal structure under the impact of thermoderformational cycle of welding. The main alloying element in wheel steel is carbon, the content of which is more than 0.50 %. Railway wheels made from such steel have ferrite-pearlite structure. Strength level of wheel

metal exceeds 900 MPa at its comparatively low ductility and toughness [6, 7].

As is known, carbon forms an interstitial solid solution with iron, considerably strengthening the ferrite, and to a much greater extent than alloying elements forming the substitutional solid solution. Carbon solubility in iron is different, depending on the crystalline form, in which iron is present. So, carbon solubility in α -iron (BCC lattice) is equal to less than 0.02 %, and in γ -iron (FCC lattice) it is 100 times greater (up to 2 %) [1, 2]. At heat impact during heating and cooling changes of crystalline lattice will proceed in the metal. At cooling, depending on the degree of overcooling, γ - α transformation of austenite can proceed along two paths. At low cooling rates transformation will be accompanied by diffusion processes with formation of ferrite-pearlite mixture and upper bainite. At high cooling rate γ - α transformation will proceed without diffusion, with formation of hardening structures of lower bainite and martensite.

At the same time it is known that nature of γ - α transformation in the metal at cooling also depends on heating conditions and degree of austenite homogenizing [1, 2, 8, 9]. Shortening of the time of metal soaking at heating above A_{c3} temperature leads to compositional heterogeneity

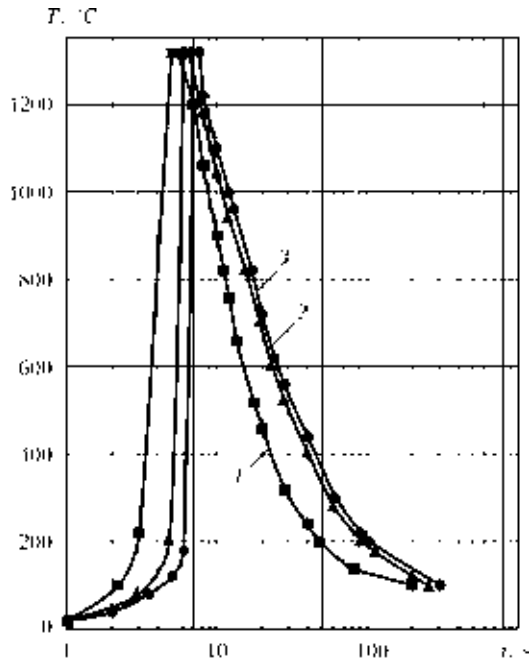


Figure 1. Thermal cycles in HAZ metal in arc surfacing of wheel steel 20 mm thick at heat input of 8.6 (1), 11.5 (2) and 15 (3) kJ/cm

of the structure of austenite forming from ferrite-pearlite mixture. Carbon-enriched austenite forms in the sections, where pearlite was located earlier, and where earlier there was pearlite, γ - α transformation runs at higher temperatures, and austenite contains much less carbon. This leads to metal structure containing austenite with varying carbon content. Presence of such an inhomogeneity in many cases leads to essential changes of austenite transformation kinetics at cooling, of metal structure and its properties. Therefore, the degree of austenite homogenizing in the metal of HAZ overheating zone will have an essential influence on structure formation and properties of railway wheels buildt-up by surfacing. Here, the main WTC parameters, on which metal structure and properties will depend, are not only maximum heating temperature T_{max} and cooling rate in the temperature range of 600–500 °C ($w_{6/5}$), but also heating rate (w_{heat}), as well as the time of metal staying at temperatures above A_{c3} (t_1).

Table 1. Main WTC parameters in HAZ metal in arc surfacing of wheel steel 20 mm thick

Surfacing heat input Q_w , kJ/cm	Thermal cycle parameters ($T_{max} = 1320$ °C)				
	w_{heat} , °C/s	t_1 , s	$w_{6/5}$, °C/s	$t_{8/5}$, s	$t_{8/1}$, s
8.6	260	7	25–30	8	170
11.5	220	10	14–16	14	245
15.0	190	11.5	10–12	19	285

There is one more factor having an essential influence on structure formation in HAZ metal in welding. This is austenite grain growth, which leads to reduction of the area of intergranular boundary, and this, at other conditions being equal, reduces the probability of nucleation of ferrite and pearlite, increases austenite stability and promotes development of bainite and martensite transformation [1–3, 8].

Arc surfacing began to be extensively applied for reconditioning worn flanges of railway wheels of freight cars in repair enterprise of Ukraine and CIS countries comparatively recently. These are processes of single- and twin-arc surfacing under a layer of flux in modes ensuring heat input on the level of 10 to 14 kJ/cm. Mandatory technology elements are application of preheating of wheel treads to temperatures of 150–200 °C, depending on the used process of surfacing and slow cooling of wheels after surfacing in heat chambers. Meeting the requirements made to surfacing technology, guarantees a high quality of the deposited metal and service reliability of wheels. However, the question of the features of arc surfacing WTC parameters influence on the nature of structural changes in the overheating zone of HAZ metal of wheel steel still has not been clarified.

The objective of this work was studying the influence of WTC parameters in railway wheel surfacing, including the stages of heating and cooling, on formation of structure of HAZ metal overheating zone and its properties. Material used for investigations was high-strength wheel steel of grade 2 (GOST 10791) of the following composition, wt.%: 0.58 C; 0.44 Si; 0.77 Mn; 0.10 Ni; 0.05 Cr; 0.012 S; 0.011 P.

Characteristic thermal cycles in the HAZ metal in arc surfacing of wheel steel 20 mm thick, depending on heat input, are shown in Figure 1, and Table 1 gives the main WTC parameters. As is seen from the presented data, at arc surfacing heat input in the range of 8.6–15.0 kJ/cm, the time of metal heating in the HAZ overheating zone up to the temperature of 1320 °C is equal to 5–7 s, that corresponds to heating rate of 190–260 °C/s. Here the time of metal staying above A_{c3} temperature (800 °C) is equal to $t_1 = 6.5$ –11.5 s.

HAZ metal structure at arc surfacing is heterogeneous, and dimensions of its individual zones are extremely small. Therefore, structural changes occurring under the impact of WTC in the metal were studied on model samples. Used for this purpose was research complex Gleeble 3800, fitted with a thermostat and high-speed dilatometer [10], and comparative studies were



performed on cylindrical samples of 6 mm diameter and 80 mm length. In keeping with the testing procedure, they were heated up to the temperature of 1250 °C at the rate of 25 and 210 °C/s (heating time was 50 and 6 s, respectively), and then cooled at different rates in accordance with surfacing thermal cycles. Time of metal staying at temperatures above A_{c3} , depending on the cooling rate, was equal to 23–66 and 7–10 s, respectively. Cooling thermal cycles were selected so that in the temperature range of 600–500 °C, sample cooling rate $w_{6/5}$ varied in the range of 2.5–64 °C/s.

Temperature of the start and end of overcooled austenite transformation was determined by the point of tangent drifting away from the dilatometric curve, while the ratio of phases, formed as a result of transformations, was established by section method [11]. Furtheron, the structure of heat-treated samples was studied by the methods of optical metallography, which was followed by more precise determination of structural components ratio and critical cooling rate at γ - α transformations. Structural studies were performed using Neophot-32 microscope, microhardness of individual structural components and integral hardness of metal were measured in the LECO hardness meter M-400 at the load of 100 g ($HV0.1$) and 1 kg ($HV10$), respectively.

Generalized results of these investigations in the form of diagrams of overcooled austenite transformation in the metal of HAZ overheating zone, depending on heating rate, time of metal staying at temperatures above A_{c3} and cooling rate in keeping with WTC in arc surfacing, are given in Figure 2.

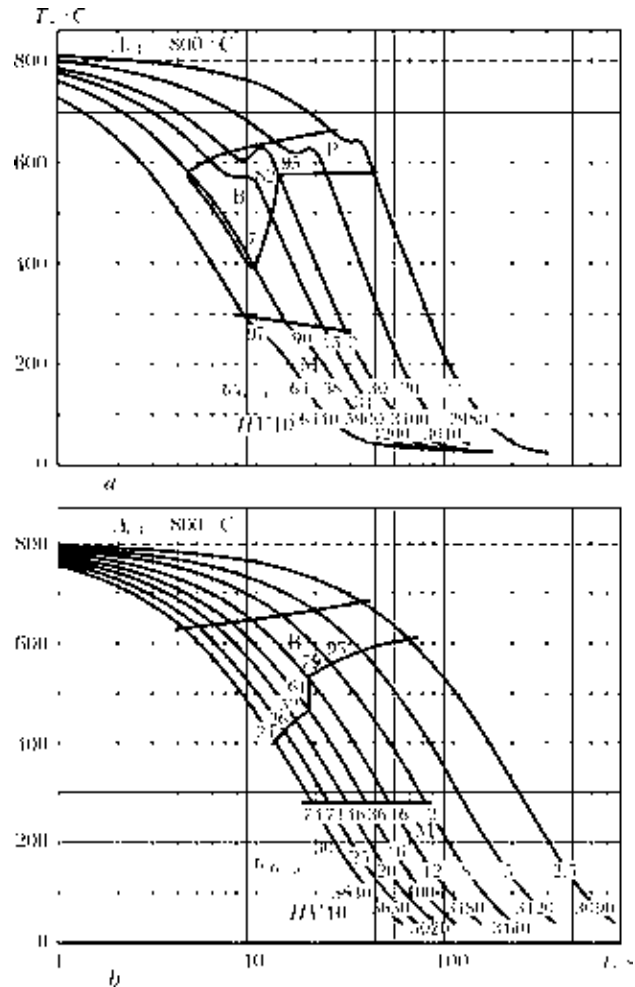


Figure 2. Diagram of overcooled austenite transformation in wheel steel HAZ metal in arc surfacing at $w_{heat} = 25$ °C/s, $t_1 = 23-66$ s (a) and $w_{heat} = 210$ °C/s, $t_1 = 7-10$ s (b)

Figures 3 and 4 show the characteristic microstructure of metal in HAZ overheating zone at different WTC parameters, and Tables 2 and 3 give the main structural parameters.

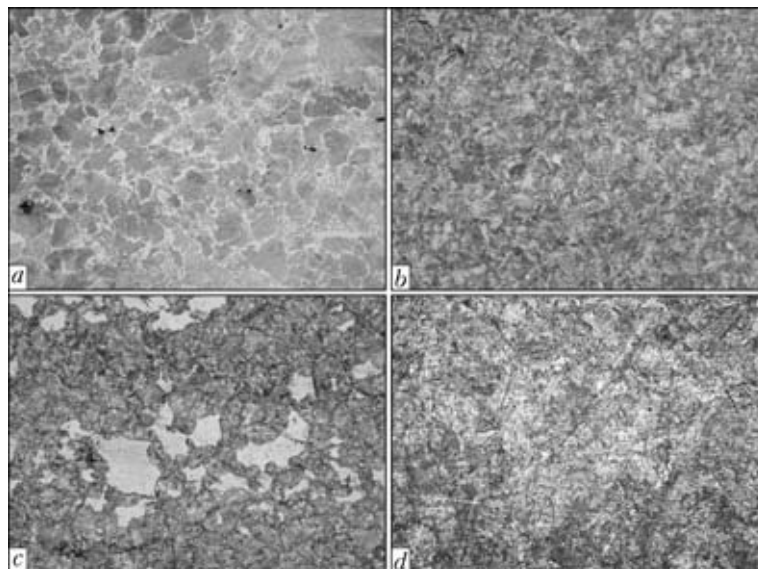


Figure 3. Metal microstructure ($\times 320$, 2 times reduction) in HAZ overheating zone at $w_{heat} = 25$ °C/s, $t_1 = 23-66$ s: a – base metal; b – $w_{6/5} = 20$; c – 30; d – 64 °C/s

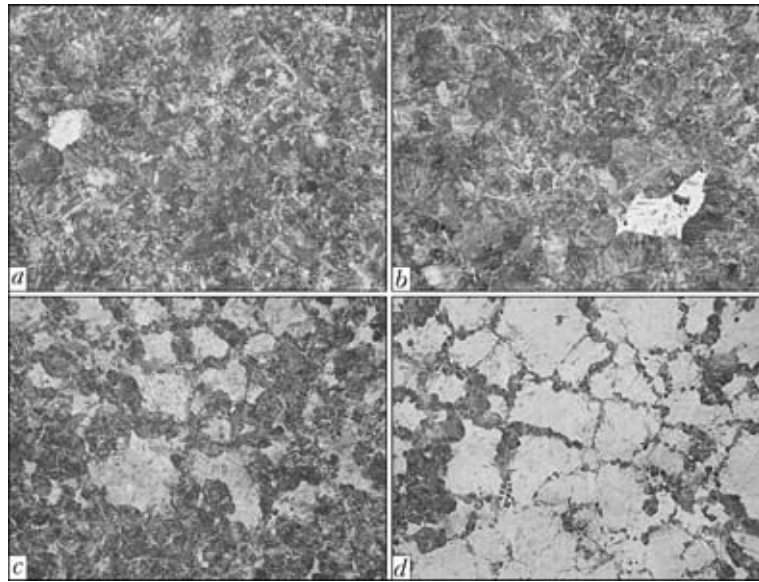


Figure 4. Metal microstructure ($\times 320$, 2 times reduced) in wheel steel HAZ overheating zone at $w_{\text{heat}} = 210 \text{ }^\circ\text{C/s}$, $t_1 = 7\text{--}10 \text{ s}$: *a* – $w_{6/5} = 8$; *b* = 12; *c* = 16; *d* – $25 \text{ }^\circ\text{C/s}$

Structure of grade 2 wheel steel in as-delivered condition is represented by pearlite-ferrite mixture (Figure 3, *a*), grain size is $16\text{--}32 \text{ }\mu\text{m}$ and microhardness of structural components is $HV0.1\text{--}1990\text{--}2450 \text{ MPa}$.

Located along grain boundaries are ferritic fringes of $5\text{--}10 \text{ }\mu\text{m}$ size. Integral hardness of metal was $HV10\text{--}2200 \text{ MPa}$.

At heating at $w_{\text{heat}} = 25 \text{ }^\circ\text{C/s}$ transformation of overcooled austenite with cooling rate $w_{6/5} < 30 \text{ }^\circ\text{C/s}$ ($t_1 = 30\text{--}66 \text{ s}$), runs in the pearlitic-bainitic region (see Figures 2 and 3, *b*, *c*). Temperature range of pearlite transformation, depending on cooling rate, is equal to $660\text{--}630 \text{ }^\circ\text{C}$.

It is practically impossible to accurately determine the start of bainite transformation by dilatometric curves, tentatively it is approximately $630 \text{ }^\circ\text{C}$. Therefore, in the diagram the region of pearlite and bainite formation is shown as a common pearlite-bainite one. Temperature of the end of bainite transformation in this range is equal to $580 \text{ }^\circ\text{C}$. Metallographic investigations of sample microstructure revealed that microhardness of structural components of pearlite and bainite rises from 2450 up to 3220 MPa with increase of cooling rate from 11 up to $30 \text{ }^\circ\text{C/s}$. By the features of structure and microhardness values bainite is identified as upper bainite structure,

Table 2. Structure parameters in overheating zone of HAZ metal in wheel steel (0.58 % C) at $w_{\text{heat}} = 25 \text{ }^\circ\text{C/s}$, $t_1 = 65 \text{ s}$

$w_{6/5}, \text{ }^\circ\text{C/s}$	Metal structure	Structural components, %				Hardness $HV0.1, \text{ MPa}$
		Pearlite	Upper bainite	Lower bainite	Martensite	
BM	Ferrite-pearlite	86	–	–	–	1990–2450
11	Pearlite-bainite	30	65	–	–	2450–2970
20	Pearite-bainite	16	80	–	–	2640–3220
30	Bainite	–	95	–	–	2970–6060
64	Martensite	–	–	–	97	4640–6420

Table 3. Structure parameters in overheating zone of HAZ metal in wheel steel (0.58 % C) at $w_{\text{heat}} = 210 \text{ }^\circ\text{C/s}$, $t_1 = 10 \text{ s}$

$w_{6/5}, \text{ }^\circ\text{C/s}$	Metal structure	Structural components, %			Hardness $HV0.1, \text{ MPa}$
		Upper bainite	Lower bainite	Martensite	
8	Bainite	95	–	2	2900–4420
12	Same	39	43	16	2900–5660
16	Bainite-martensite	–	61	36	3220–6060
25	Martensite-bainite	–	26	71	3360–6060



and its second name — sorbite as can be found in publications. In this range of cooling rates upper bainite content rises from 65 up to 95 %, and that of pearlite decreases from 30 % to 0 (see Table 2). Metal structure also reveals ferrite sections, located along grain boundaries, with total ferrite content not higher than 5 %. Grain size is 63–94 μm , and it is characteristic for metal at all rates of sample cooling.

Cooling rate, at which martensite formation starts, is equal to $w_{6/5} = 30\text{ }^\circ\text{C/s}$. At this cooling rate approximately 2 % of martensite was found in the metal structure, which is arranged as small isolated areas in the grain bulk. Temperature of the start of martensite transformation T_{Ms} is equal to approximately 265 $^\circ\text{C}$, temperature of the end of martensite transformation could not be determined. Martensite microhardness was 5660–6060 MPa, that of upper bainite was 2970–3220 MPa. At cooling rate of 38 $^\circ\text{C/s}$, the amount of martensite in the structure is equal to 90 %, and integral metal hardness rises up to 5900 MPa. When the structure contains 97 % of martensite ($w_{6/5} = 64\text{ }^\circ\text{C/s}$), metal hardness rises up to 6440 MPa (see Figure 3, *d*). Here, martensite formation starts at higher temperatures ($T_{\text{Ms}} = 295\text{ }^\circ\text{C}$). As to its structure, martensite is less homogeneous, its microhardness varying in the range of 4640 to 6420 MPa. Bainite transformation in the range of cooling rates of 30 to 38 $^\circ\text{C/s}$ starts at $T_{\text{Bs}} = 630\text{--}580\text{ }^\circ\text{C}$.

With increase of cooling rates in this temperature range, temperature of bainite transformation completion drops from 580 to 390 $^\circ\text{C}$. It is obvious that at the cooling rate of 30 $^\circ\text{C/s}$ upper bainite structure forms (95 %), and at 34–38 $^\circ\text{C/s}$ — predominantly that of lower bainite, proceeding by diffusionless mechanism at lower temperatures. At cooling rate above 38 $^\circ\text{C/s}$, bainite transformation is absent. In the metal structure, ferrite was also found along grain boundaries, its content not exceeding 3 %.

A metal heating and cooling by arc surfacing cycle ($w_{\text{heat}} = 210\text{ }^\circ\text{C/s}$, $t_1 = 7\text{--}10\text{ s}$), austenite homogenizing proceeds not as completely, as in the previous case. This essentially affects also the structural transformations of overcooled austenite (see Figures 2 and 4, Table 3). Cooling rate, at which formation of martensite begins in the amount of 2 %, decreases to $w_{6/5} = 8\text{ }^\circ\text{C/s}$ (Figure 4, *b*). Martensite microhardness is equal to approximately 4420 MPa. Now, at cooling rate of 30 $^\circ\text{C/s}$, unlike slower heating, a martensite-bainite structure with 74 % of martensite forms in the metal of HAZ overheating zone. Integral hardness of metal here rises from 3140 up to

5830 MPa. Temperature of the start of martensite transformation $T_{\text{Ms}} = 280\text{ }^\circ\text{C}$, and it remains constant in the studied range of cooling rates. At cooling rate of 12–25 $^\circ\text{C/s}$, martensite microhardness is equal to 5660–6060 MPa.

During investigations it is also established that critical cooling rate, at which not more than 50 % of martensite ($w_{50\text{M}}$) forms in the metal structure, is equal to 20 $^\circ\text{C/s}$. Coming back to previous data, obtained at heating with parameters $w_{\text{heat}} = 25\text{ }^\circ\text{C/s}$ and $t_1 = 23\text{--}66\text{ s}$, critical cooling rate is in the range of 34–38 $^\circ\text{C/s}$, when 15 to 90 % of martensite forms. For slow heating we will assume this value to be equal to $w_{50\text{M}} = 35\text{ }^\circ\text{C/s}$.

At heating at a high rate the nature of overcooled austenite transformation in the intermediate region changes accordingly. Temperature range of bainite transformation becomes wider. At $w_{6/5} < 8\text{ }^\circ\text{C/s}$ the main $\gamma\text{-}\alpha$ transformation in the metal at cooling occurs in the pearlite-bainite region in the temperature range of 680–560 $^\circ\text{C}$. By analogy with slow heating (at $w_{6/5} = 11\text{--}30\text{ }^\circ\text{C/s}$) predominantly upper bainite structures form in the HAZ metal at heating by WTC (see Figure 4, *a*). Metal hardness is 3090–3140 MPa, grain size is 47.5–94.0 μm .

$\gamma\text{-}\alpha$ transformation with lower bainite formation starts at the cooling rate of 12 $^\circ\text{C/s}$ and higher. Temperature of the start of formation in the bainite region is $T_{\text{Bs}} = 650\text{--}630\text{ }^\circ\text{C}$, and temperature of the end of bainite transformation drops to 540–400 $^\circ\text{C}$ with increase of the cooling rate. So, at $w_{6/5} = 12\text{ }^\circ\text{C/s}$ the amount of lower bainite in the structure is equal to 43 %, and at 16 $^\circ\text{C/s}$ it is already 61 % (see Table 3). With increase of martensite content in the metal structure, which occurs at increase of cooling rate to $w_{6/5} = 25\text{ }^\circ\text{C/s}$, the amount of lower bainite decreases to 26 % (Figure 4, *d*), while microhardness of structural components rises from 2900–5660 up to 3360–6060 MPa.

The influence of WTC on HAZ metal properties was determined by the method of quantitative assessment of delayed fracture resistance, generally known as Implant method [4, 5]. Surfacing of technological plates with samples-insets was performed by mechanized gas-shielded process with Sv-08G2S wire of 1.2 mm diameter in the following mode: welding current $I_w = 160\text{--}180\text{ A}$, arc voltage $U_a = 26\text{--}28\text{ V}$, surfacing speed $v_w = 14\text{ m/h}$. Heat input was equal to $Q_w = 8.6\text{ kJ/cm}$. Diffusible hydrogen content in the deposited metal, determined by the «pencil» sample method, was $[\text{H}]_{\text{dif}} = 1/3\text{ ml/100 g}$. Welding of Implant samples was performed with preheat-

**Table 4.** WTC parameters, structure and critical stresses at delayed fracture of HAZ metal at testing by Implant method ($Q_w = 8.6 \text{ kJ/cm}$)

$T_{pr}, ^\circ\text{C}$	Thermal cycle parameters			Structure in HAZ metal overheating zone*, %	σ_{cr}, MPa
	$w_{6/5}, ^\circ\text{C/s}$	$t_{8/5}, \text{s}$	$t_{8/1}, ^\circ\text{C}$		
20	25–30	8	170	Bl = 26–24, M = 71–74	100
50	20–25	10	230	Bl = 52–26, M = 46–71	220
70	15–20	11	250	Bl = 61–52, M = 36–46	320
100	12–15	12	450	Bup \leq 39, Bl = 57–61, M = 16–36	>460

*Bup – upper bainite, Bl – lower bainite, M – martensite.

ing at $T_{pr} \leq 100 ^\circ\text{C}$. Cooling rate $w_{6/5}$ was varied in the range of 12–30 $^\circ\text{C/s}$, and in zone of HAZ metal overheating a bainite-martensite structure with different content of structural components formed. Sample loading was performed after their cooling to 50 $^\circ\text{C}$ temperature. During testing maximum loading stresses σ_{cr} were determined, at which no delayed fracture occurs for 24 h. Generalized results of testing samples of grade 2 wheel steel by the Implant method are given in Table 4.

Presented data show that delayed fracture resistance of wheel steel HAZ metal at surfacing without preheating ($T_{pr} = 20 ^\circ\text{C}$) is the lowest, critical stresses being just 0.14 of HAZ metal yield point ($\sigma_{0.2} \sim 715 \text{ MPa}$ [7]), and fracture proceeds in the brittle mode. Under such conditions of surfacing a martensite-bainite structure with higher dislocation density forms in the HAZ metal overheating zone. Amount of martensite in the structure is higher than 71 %, that of lower bainite is not more than 24 %, and the level of dislocation density is up to $\rho = 5\text{--}8 \cdot 10^{10} \text{ cm}^{-2}$ [12]. As a result, the metal has a lower capacity for microplastic flow under loading, stress relaxation in it runs by formation of microcracks, and it fails at quite low stresses.

At application of preheating changes occur in the structure of the metal of HAZ overheating zone and σ_{cr} values rise. So, at $T_{pr} = 50 ^\circ\text{C}$ lower bainite content in the structure is equal to approximately 26–52 %, and volume fraction of martensite decreases accordingly. At preheating up to 70 $^\circ\text{C}$, further change of structural component ratio occurs towards increase of lower bainite up to 61 %. Here critical stresses rise 3 times up to the level of $0.45\sigma_{0.2}$. At preheating up to $T_{pr} = 100 ^\circ\text{C}$, when the cooling rate is equal to 12–15 $^\circ\text{C/s}$ and martensite content in the structure is not higher than 36 %, HAZ metal does not develop delayed fracture at stresses of 450 MPa. Implant sample could not be loaded to higher stress values during testing, as deposit

metal starts flowing. Therefore, at preheating temperature of 100 $^\circ\text{C}$, critical stresses were conditionally taken to be above 460 MPa.

Conducted testing by Implant method showed that in order to ensure an increased delayed cracking resistance of wheel steel HAZ metal at 0.58 % C, $w_{6/5} \geq w_{50M}$ condition has to be fulfilled, which is achieved at application of metal preheating to 100 $^\circ\text{C}$.

It should be further noted that the presented results of investigation of the state of metal structure in the overheating zone of wheel steel HAZ at arc surfacing and testing by the Implant method are logically interconnected. It is practically impossible to explain these data by another method, without using the diagram of overcooled austenite transformation under the real conditions of impact of arc surfacing WTC, given in Figure 2, and investigations of HAZ metal microstructure. Classical diagrams of $\gamma\text{-}\alpha$ transformation plotted under the conditions of isothermal soaking, or at constant slow heating (see Figure 2) do not reflect the real changes in the structure of HAZ metal of welded joints on high-strength carbon steels.

Conclusions

1. It is established that incompleteness of the processes of metal austenite homogenizing in arc surfacing as a result of its fast overheating and limited time of staying at temperature above A_{c3} , essentially affects the subsequent $\gamma\text{-}\alpha$ transformation in the HAZ metal of high-strength wheel steel. This leads to the situation, when in the metal of wheel steel HAZ overheating zone with carbon content of 0.58 %, the critical cooling rate in the range of temperatures of 600–500 $^\circ\text{C}$, at which not more than 50 % of martensite forms in the structure, decreases 1.5 times and is equal to $w_{50M} = 20 ^\circ\text{C/s}$. Here the minimum cooling rate, at which formation of martensite component of the structure starts, is equal to $w_{6/5} = 8 ^\circ\text{C/s}$.



2. At heating and cooling by the thermal cycle of arc surfacing, the nature of overcooled austenite transformation in the intermediate region changes. Temperature range of austenite transformation becomes wider, and upper and lower bainite structures form in the HAZ metal. γ - α transformation with formation of lower bainite starts at $w_{6/5} \geq 12$ °C/s. Its maximum amount corresponds to the cooling rate of 16 °C/s, being equal to 61 %. With increase of cooling rate to 25 °C/s, volume fraction of lower bainite drops to 26 %, and that of martensite rises up to 71 %. Microhardness $HV0.1$ of structural components rises from 2900–5660 up to 3360–6060 MPa, and metal hardness $HV10$ in the HAZ overheating zone — from 3480 to 5660 MPa.

3. High delayed cracking resistance of HAZ metal of wheel steel with 0.58 % C, at the level of $\sigma_{cr} \geq 0.45\sigma_{0.2}$, can be ensured at $w_{6/5} \leq w_{50M}$. Such conditions of cooling in surfacing at heat input of 8.6 kJ/cm correspond to application of preheating to 100 °C.

1. Shorshorov, M.Kh. (1965) *Metals science of welding of steel and titanium alloys*. Moscow: Nauka.
2. Gulyaev, A.P. (1978) *Metals science*. Moscow: Metallurgiya.

3. Grabin, V.F., Denisenko, A.V. (1978) *Metals science of welding of low- and medium-alloyed steels*. Kiev: Naukova Dumka.
4. Makarov, E.L. (1981) *Cold cracks in welding of alloyed steels*. Moscow: Mashinostroenie.
5. Gajvoronsky, A.A. (2013) Influence of diffusible hydrogen on delayed cracking resistance of high-carbon steel welded joints. *The Paton Welding J.*, **5**, 14–20.
6. Sarzhevsky, V.A., Gajvoronsky, A.A., Gordonny, V.G. et al. (1996) Influence of technological factors on structure and properties of HAZ metal in repair-reconditioning hardfacing of flanges of all-rolled train wheels. *Avtomatich. Svarka*, **3**, 22–27, 33.
7. Gajvoronsky, A.A., Poznyakov, V.D., Sarzhevsky, V.A. et al. (2010) Influence of thermodeformational cycle of hardfacing on the structure and properties of high-strength railway wheels in its reconditioning. *The Paton Welding J.*, **5**, 15–18.
8. Astafiev, A.S., Gulyaev, A.P. (1972) About grain growth in near-weld zone. *Svarochn. Proizvodstvo*, **7**, 45–47.
9. Livshits, L.S. (1979) *Metals science for welders*. Moscow: Mashinostroenie.
10. Grigorenko, G.M., Kostin, V.A., Orlovsky, V.Yu. (2008) Current capabilities of simulation of austenite transformations in low-alloyed steel welds. *The Paton Welding J.*, **3**, 22–24.
11. Cherepin, V.T. (1968) *Experimental technique in physical metals science*. Kiev: Tekhnika.
12. Gajvoronsky, A.A., Poznyakov, V.D., Markashova, L.I. et al. (2012) Influence of deposited metal composition on structure and mechanical properties of reconditioned railway wheels. *The Paton Welding J.*, **8**, 16–22.

Received 20.08.2013



QUASI-CRYSTALLINE ALLOYS-FILLERS FOR COMPOSITE LAYERS PRODUCED USING METHOD OF FURNACE SURFACING

E.V. SUKHOVAYA

O. Gonchar Dnepropetrovsk National University
72 Gagarin Ave., 49010, Dnepropetrovsk, Ukraine. E-mail: sukhovaya@ukr.net

Structure and properties of macro-heterogeneous composite layers produced using method of furnace surfacing were investigated. As the fillers the quasi-crystalline alloys Al-Cu-Fe, Al-Co-Cu and Al-Co-Ni were used. As the bonds the alloys based on aluminium and copper were used. It was shown that the method of furnace surfacing allows obtaining the content of quasi-crystalline icosahedral ψ -phase of not less than 30 vol.% in the structure of composite layers strengthened by Al-Cu-Fe alloy-filler, and the content of quasi-crystalline decagonal D-phase of up to 55 vol.% in the structure of composite layers with alloys-fillers Al-Co-Cu and Al-Co-Ni. The regularities of formation of interfaces between filler and bond during surfacing are explained by realization of solution-diffusive mechanism of processes of contact interaction. The primary dissolution of crystalline phases of alloys-fillers was established, which leads to penetration of molten bonds inside the filler along the boundaries of crystals of the quasi-crystalline phase. The increase in intensity of processes of dissolution of filler crystalline phases in use for surfacing of Cu-based bonds results in their complete recrystallization in the process of cooling at retaining not-dissolved inclusions of quasi-crystalline phase in the structure of composite layers. To produce the surfaced layers operating under the conditions of dry friction, the composite material based on tin bronze Br.Ots 10-2 armored by the Al-Co-Ni alloy-filler was recommended. The composite material with bond of brass L62 and alloy-filler Al-Co-Cu has the maximum resistance in oxide media. 11 Ref., 1 Table, 4 Figures.

Keywords: *composite layer, furnace surfacing, quasi-crystalline phase, interphase interaction, dissolution, corrosion resistance in oxide media, tribotechnical properties*

The efficient method to increase the life of parts operating under the conditions of intensive abrasive and gas-abrasive wear is the furnace surfacing which was developed by the associates of the E.O. Paton Electric Welding Institute [1]. It consists in impregnation of preliminary formed powders of refractory alloys-fillers by fusible bond in the process of heating in furnace. The method allows regulating the cooling rate during crystallization, and under the condition of wetting it provides a high quality of surfaced composite layers and bimetal joints. Besides, using this method the service life of such critical parts of metallurgical equipment as valves, small and large cones of charging units of blast furnaces is 3–15 times increased [2]. To perform the process, the special expensive equipment is not required and due to the so-called autovacuum effect the limited access of oxygen to the surfaces of contacting phases during surfacing is provided.

The best operation characteristics are observed in the surfaced composite alloys, where in capacity of alloys-fillers the tungsten carbides [3] in

cast (relite) and baked form and also as cermet alloys with a cobalt bond (of type VK) are used. To manufacture the composite layers without the content of scarce and expensive tungsten carbides, the chromium carbides Cr_3C_2 and chromium carbides with nickel bond KKhN5, KKhN10 and KKhN15 are applied [4]. In the composition of composite layers alongside with the carbides the borides of refractory metals are used, which have a high heat resistance, hardness and abrasive wear resistance, that promotes their sufficiently wide application in industry.

In works [5, 6] the possibility of replacement of W-containing hard alloys, used in manufacture of composite alloys, by the following borides of metals of IVa–VIa subgroups: TiB_2 , ZrB_2 , HfB_2 , FeB_2 , TaB_2 , CrB_2 , Mo_2B_5 , W_2B_5 , was studied. However, among all the studied materials the most prospective, in opinion of the authors of [7], are the surfaced composite layers containing fillers of binary Ti–Cr borides $(\text{Ti}, \text{Cr})\text{B}_2$. This boride alongside with high strength properties has the lower brittleness as compared to pure borides, and as to the wear resistance it is close to hard alloys.

The field of application of the method of furnace surfacing to produce the composite layers can be sufficiently expanded due to application



of quasi-crystalline alloys-fillers in their composition, having high hardness, low friction coefficient, increased corrosion resistance [8]. At the combination of quasi-crystals with ductile metallic matrix it is possible to overcome such their main disadvantage as brittleness, which limits the application of quasi-crystals in the products of modern engineering.

As far as information concerning the use of the method of furnace surfacing to produce surfaced composite layers, strengthened by quasi-crystalline alloys-fillers, is absent, in the present work the results of investigation of structure and properties of this class of surfacing materials, intended to strengthen and restore the parts operating under the conditions of dry friction and oxide environments effect, are given.

Methods of experiment. The alloys-fillers Al-Cu-Fe, Al-Co-Cu and Al-Co-Ni were melted in Tamman furnace from chemically pure elements. The cooling rate of the alloys was 50 K/s. The composition of alloys-fillers was selected so that to provide the content of quasi-crystalline phase in structure of not less than 50 % of volume. The content of elements was controlled using the methods of chemical and spectral X-ray fluores-

cent analyses. The produced alloys were crushed in the hammer mill to the fractions of 0.2–2.0 mm. The impregnation was performed by alloys-bonds on aluminium or copper base at the temperature, which by 50–100 K exceeded the melting temperature of a bond alloy. The duration of isothermal soaking during surfacing varied within the limits of 30–60 min. The structure of surfaced composite layers was investigated using the methods of quantitative metallography, scanning electron microscopy, X-ray diffraction analysis and X-ray spectral microanalysis. The rate of corrosion of composite layers in the oxide media was determined using gravimetric method. The measurements were carried out every hour at the room temperature during 4 h. The tribotechnical tests were performed according to the shaft-bushing scheme under the conditions of friction without lubrication on steel 45 at sliding speed of 20 m/s and loading of 4 MPa in the machine manufactured according to the designs [9].

Results of experiment. The alloy-filler Al-Cu-Fe has a double-phase structure consisting of quasi-crystalline icosahedral ψ -phase of $Al_{63}Cu_{25}Fe_{12}$ composition and crystalline cubic

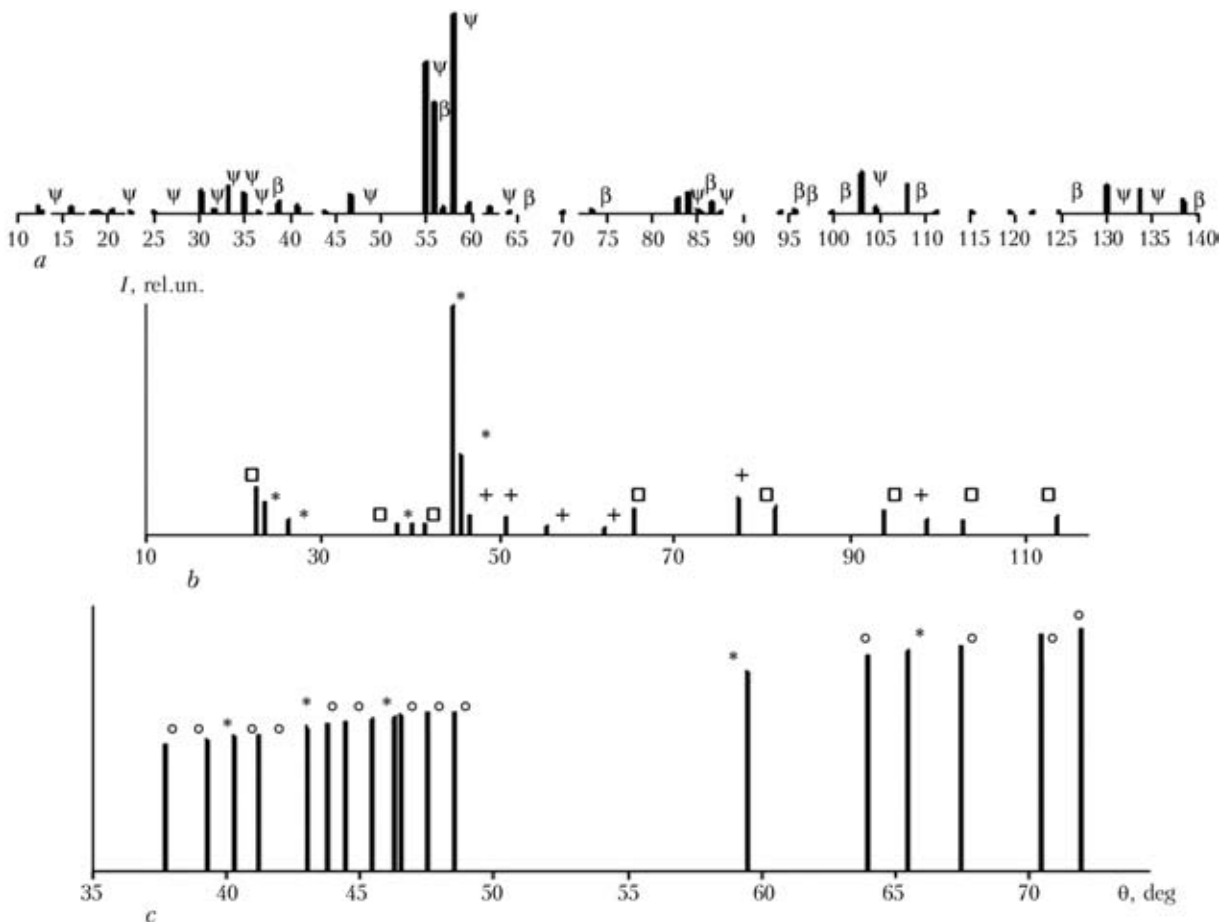


Figure 1. Marked X-ray photographs ($Fe-K_{\alpha}$ -radiation) of alloys: *a* – Al-Cu-Fe; *b* – Al-Co-Cu; *c* – Al-Co-Ni; * – D-phase; □ – $Al_4(Co, Cu)_3$; + – $Al_3(Co, Cu)_2$; ○ – $Al_9(Co, Ni)_2$

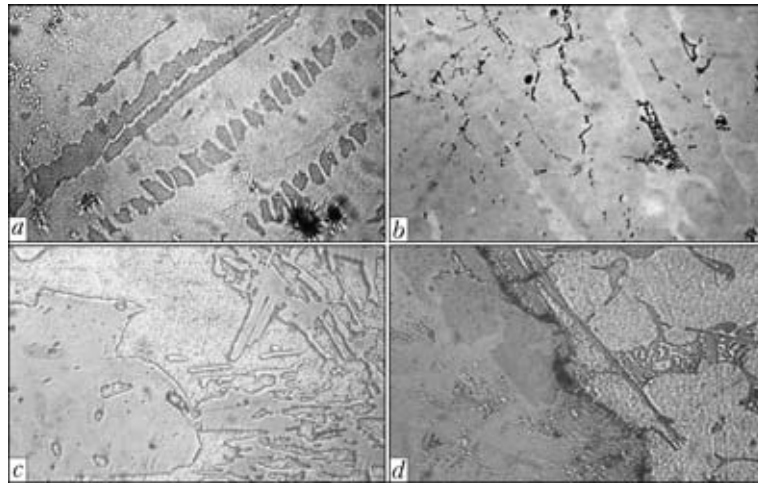


Figure 2. Microstructure of composite materials on base of aluminium alloys strengthened by Al-Cu-Fe alloy-filler: *a* – initial alloy-filler; *b* – alloy-bond (Al-6 % Mg); *c* – alloy-bond (Al-5 % Cu); *d* – alloy-bond (commercial Al) (*a*, *b*, *d* – $\times 800$; *c* – $\times 1000$)

phase FeAl (β -phase) (Figures 1, *a* and 2, *a*). The morphology of ψ -phase is defined by the presence of axis of symmetry of the fifth order and quasi-periodical long-range order in three directions [8]. The volumetric content of this phase in the structure of filler reaches 50 %.

After impregnation by the bond alloys based on aluminium the uniform distribution of particles of the filler across the section of composite material is observed (Figure 2, *b-d*). The content of alloy-filler amounts to 60–65 % and that of quasi-crystalline phase is about 35 % of material volume. At the interfaces between the filler and molten bonds the processes of contact interaction are running during surfacing, accompanied mainly by dissolution of β -phase of the filler. The quasi-crystalline ψ -phase is retained in the structure almost without changes. At next cooling the zones of contact interaction of a solution-diffusion type are formed at the interfaces due to recrystallization of dissolved regions of the filler. On the side of filler a layer is appeared, the composition of which differs from the initial composition by an increased Al content and lower Cu and Fe content. On the side of solidified Al-based alloys-bonds the copper and iron are present near the interface. The measurement of width of con-

tact interaction zones shows the intensity of processes of dissolution of crystalline phases of the alloy-filler in molten alloy-bond is decreased depending on its composition in the following row: Al \rightarrow (Al-Mg) \rightarrow (Al-Cu) \rightarrow (Al-Si). In the same sequence the porosity of surfaced composite layers is increased, reaching the maximum value of about 40 vol.%, when the alloy-bond Al-Si is applied.

With account for obtained results the specimens, surfaced by composite material Al-Cu-Fe/Al, in structure of which the content of pores does not exceed 3 vol.%, were selected for next tests. The corrosion rate of this material has the least values in solutions 5n·H₃PO₄ and 1n·HCL (Table). Coefficient of friction is within the ranges of 0.17–0.19.

Before surfacing three phases are present in the structure of alloy-filler Al-Co-Cu: one quasi-crystalline and two crystalline (Figures 1, *b* and 3, *a*). Crystals of crystalline cubic phase AlCo (β -phase) are precipitated firstly from liquid (L). Then, quasi-crystalline decagonal D-phase, having stoichiometric composition Al₆₃Co₂₄Cu₁₃, is formed by peritectic reaction L + $\beta \rightarrow$ D. Its prismatic crystals are growing mainly in the direction, parallel to axis of symmetry of the tenth

Properties of composite materials strengthened by quasi-crystalline alloys-fillers

Alloy-filler	Alloy-bond	Coefficient of friction	Wear intensity, $\mu\text{m}/\text{km}$	Corrosion rate, $\text{g}/(\text{m}^2\cdot\text{h})$			
				0.5n·H ₂ SO ₄	5n·H ₃ PO ₄	0.8n·HNO ₃	1n·HCL
Al-Cu-Fe	Al (commercial)	0.18	15.3	2.67 \pm 0.03	0.88 \pm 0.05	15.43 \pm 0.05	0.98 \pm 0.02
Al-Co-Cu	L62	0.09	7.9	1.95 \pm 0.06	0.43 \pm 0.04	9.92 \pm 0.03	0.79 \pm 0.01
	Br.Ots 10-2	0.06	4.3	2.14 \pm 0.05	0.60 \pm 0.07	13.28 \pm 0.04	0.84 \pm 0.03
Al-Co-Ni	L62	0.08	7.3	2.42 \pm 0.01	0.52 \pm 0.04	13.11 \pm 0.08	0.89 \pm 0.03
	Br.Ots 10-2	0.04	3.0	2.55 \pm 0.03	0.73 \pm 0.05	13.90 \pm 0.05	0.93 \pm 0.02

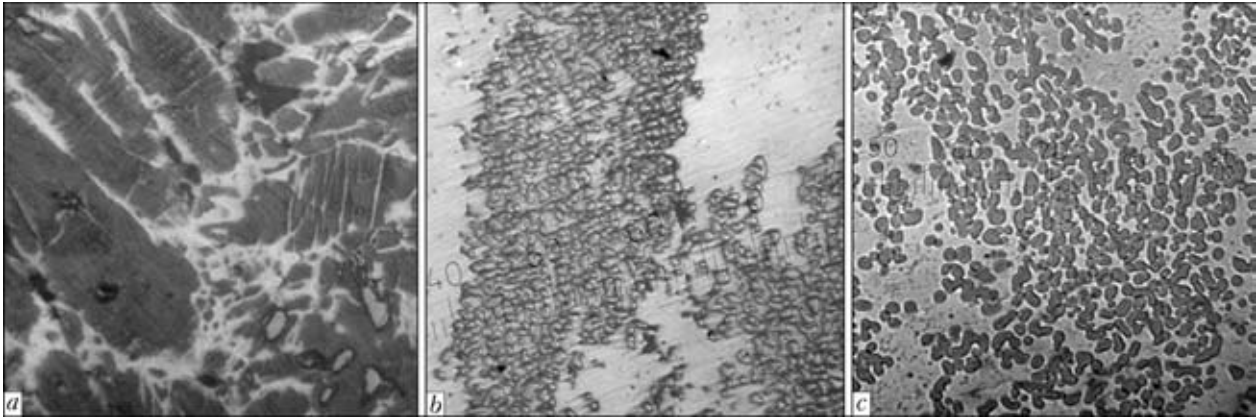


Figure 3. Microstructure ($\times 800$) of composite materials on base of copper alloys strengthened by Al-Co-Cu alloy-filler: *a* – initial alloy-filler; *b* – alloy-bond L62; *c* – alloy-bond Br.Ots 10-2

order, along which the D-phase has a periodic arrangement of atoms [10]. Quasi-periodic long-range order is observed in perpendicular plane. Volumetric content of quasi-crystalline phase in filler structure is about 80 %. Crystals of hexagonal phase $\text{Al}_3(\text{Cu}, \text{Co})_2$ (H-phase) are formed along the boundaries of quasi-crystalline phase.

Taking into account the stability of D-phase up to 1250 K, the following Cu-based alloys-bonds on were used for impregnation of particles of Al-Cu-Co alloy-filler: brass L62 and tin bronze Br.Ots 10-2. The peculiar features of structure of produced composite layers are defined by the processes of primary dissolution of crystalline H-phase of the filler. Therefore, during impregnation the molten alloys-bonds penetrate inside the filler along the boundaries of quasi-crystalline phase across the section of strengthening particles (Figure 3, *b*, *c*). This leads to a partial dissolution of D-phase, which is testified by change in its morphology from faceted to rounded one. As a result, separate inclusions of D-phase in Cu-based matrix are observed.

Due to dissolution of crystalline phases of alloy-filler in molten brass, its as-solidified composition near the interface with filler is differed

from initial composition by the presence of Al and decrease in Cu and Zn content (see Figure 3, *b*). Al, Co, Zn and Cu were observed in matrix interlayers between the crystals of D-phase. The growing intensity of processes of dissolution of filler in case of impregnation by bronze bond, as compared to brass one, leads to the violation of macro-heterogeneous constitution of surfaced composite layer. As a consequence, the non-dissolved regions of quasi-crystalline D-phase are almost uniformly distributed in the volume of the solidified bond (Figure 3, *c*). Aluminium and traces of cobalt were observed in it, except the initial components. At the periphery of inclusions of D-phase the Co and Cu content are somewhat increased, that is caused by recrystallization of non-dissolved components in bond during cooling on the surface of this phase.

Results of tests show that the corrosion rate in acid media is decreased in use of a brass bond for impregnation of alloy-filler Al-Co-Cu (see the Table), while in case of bronze bond applying the reduction of coefficient of friction and wear intensity is provided.

Alloy-filler Al-Co-Ni has a two-phase structure before surfacing (Figures 1, *b* and 4, *a*), which is mainly formed by quasi-crystalline

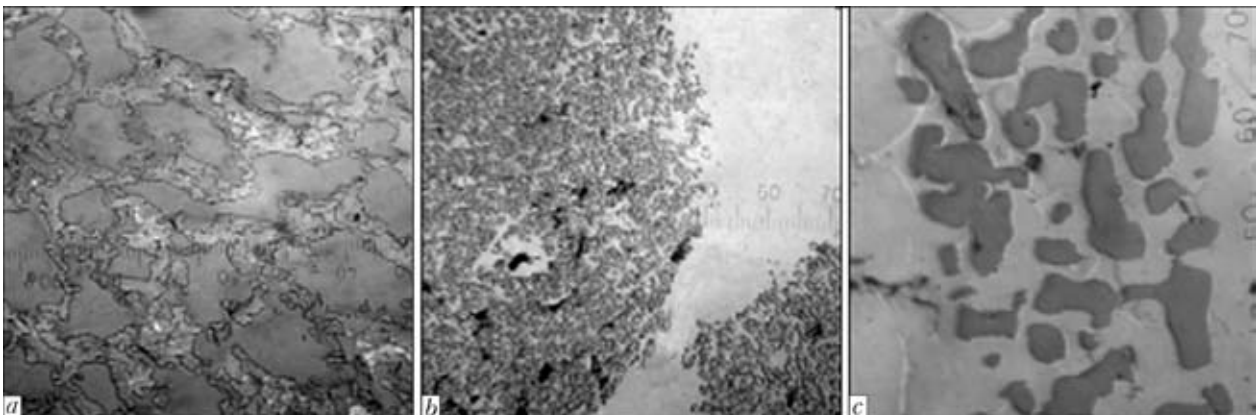


Figure 4. Microstructure of composite materials on base of copper alloys strengthened by Al-Co-Ni alloy-filler: *a* – initial alloy-filler; *b* – alloy-bond L62; *c* – alloy-bond Br.Ots 10-2 (*a*, *b* – $\times 800$; *c* – $\times 2000$)



decagonal D-phase, occupying more than 85 % of alloy volume. D-phase is crystallized directly from liquid and has stoichiometric composition $Al_{69}Co_{21}Ni_{10}$. Moreover, there is phase $Al_9(Co, Ni)_2$ in structure, formed by peritectic reaction $L + D \rightarrow Al_9(Co, Ni)_2$ [11], which has a variable composition, that can be connected with a different degree of completion of the peritectic reaction.

During furnace surfacing the impregnation of particles of Al-Co-Ni alloy-filler by copper bonds of the above-mentioned composition is accompanied by their penetration along the grain boundaries of quasi-crystalline D-phase due to more intensive dissolution of crystalline phase $Al_9(Co, Ni)_2$. As a result the structure of surfaced composite layers has separate rounded inclusions of D-phase, located after impregnation by a brass bond in the places of location of initial filler particles, and distributed uniformly in matrix after impregnation by a bronze bond (Figure 4, b, c). This proves about the high intensity of processes of contact interaction between the filler and molten bond in surfacing at the second case.

As compared with surfaced composite layers, strengthened by alloy-filler Al-Co-Cu, the content of quasi-crystalline phase in composite layers with alloys-fillers Al-Co-Ni is by 15 % higher on average and reaches 55 %. The obtained result can be explained by the higher resistance to the effect of molten bond of primary D-phase of $Al_{69}Co_{21}Ni_{10}$ composition, as compared with D-phase of $Al_{63}Co_{24}Cu_{13}$ composition formed by peritectic reaction. As a consequence, the content of components of Al-Co-Ni alloy-filler in Cu-based solidified bonds is lower than in surfaced layers strengthened by the alloy-filler Al-Co-Cu. Due to increase in content of quasi-crystalline phase, the minimum values of coefficient of friction and intensity of wear of composite layers with Al-Co-Ni alloy-filler are reached (see the Table).

Conclusion

The application of method of furnace surfacing makes it possible to produce the surfaced composite layers on aluminium and copper base, strengthened by quasi-crystalline alloys-fillers

Al-Cu-Fe, Al-Co-Cu and Al-Co-Ni. During surfacing in molten bonds the crystalline phases of alloys-fillers are mainly dissolved. In spite of a partial dissolution of quasi-crystalline phase, its content in structure of composite alloys reaches 30–55 % of their volume depending on the filler composition.

The surfaced composite layers, strengthened by quasi-crystalline alloys-fillers, are characterized by the corrosion resistance in acid solutions and high tribotechnical properties. These characteristics are correlated with content of quasi-crystalline phases, reaching the maximum values in case of composite layers of L62/Al-Co-Cu and Br.Ots 10-2/Al-Co-Ni compositions, respectively.

1. Netesa, I.V., Dudko, D.A., Maksimovich, B.I. et al. *Method of wear-resistant surfacing*. USSR author's cert. 562393. Int. Cl. B 23 K 9/04, B 22 D 19/08. Fil. 18.07.1975. Publ. 08.06.1977.
2. Danilov, L.I., Rovenskykh, F.M. (1979) Surfacing of parts of charging devices of blast furnace by composite alloy. *Metallurg*, **1**, 12–15.
3. Dudko, D.A., Maksimovich, B.I., Zelenin, V.I. et al. (1975) Wettability of wear-resistant components of composite alloys by ligaments on copper-nickel-manganese base. *Avtomatich. Svarka*, **5**, 5–6.
4. Dudko, D.A., Zelenin, V.I., Netesa, I.V. et al. (1977) Novel wear-resistant surfacing composite alloys. In: *Wear-resistant surfacing materials on the base of refractory compounds*. Kiev: Naukova Dumka, 3–5.
5. Bystrov, V.A., Bystrov, A.V., Dzodziev, G.T. et al. (1979) Investigation of properties of composite alloys on carbide titanium base. In: *Properties and tests of deposited metal*. Kiev: PWI, 131–135.
6. Borovikova, M.S. (1980) Main principles of contact interaction of refractory borides with some nontransition metals. In: *Phase interphases and their properties*. Kiev: IAM, 72–79.
7. Samsonov, G.V., Panasyuk, A.D., Borovikova, M.S. (1973) Interaction of refractory borides with liquid metals of iron family. *Poroshk. Metallurgiya*, **6**, 51–57.
8. Huttunen-Saarivirta, E. (2004) Microstructure, fabrication and properties of quasicrystalline Al-Cu-Fe alloys: A review. *J. Alloys Comp.*, **363**, 150–174.
9. Mamykin, E.T., Kovpak, M.K., Yuga, A.I. et al. (1973) Complex of machines and procedure for determination of antifriction properties of materials in sliding friction. *Poroshk. Metallurgiya*, **1**, 67–72.
10. Tsai, A.-P., Inoue, A., Masumoto, T. (1989) A stable decagonal quasicrystal in the Al-Cu-Co system. *Mater. Transact. of JIM*, **30(4)**, 300–304.
11. Godecke, T., Ellner, M. (1996) Phase equilibria in the aluminum-rich portion of the binary system Co-Al and in the cobalt/aluminum-rich portion of the ternary system Co-Ni-Al. *Z. Metallkunde*, **87**, 854–864.

Received 30.09.2013



IMPROVEMENT OF POWER EFFICIENCY OF MACHINES FOR RESISTANCE SPOT WELDING BY LONGITUDINAL COMPENSATION OF REACTIVE POWER

A.A. PISMENNY

E.O. Paton Electric Welding Institute, NASU
11 Bozhenko Str., 03680, Kiev, Ukraine. E-mail: office@paton.kiev.ua

Considered is the operation of supply system of a single-phase machine for resistance spot welding (RSW) with introducing of scheme of longitudinal compensation of reactive power into the primary circuit of welding transformer. Machines for RSW are characterized by a high consumed power, the significant part of which is a reactive component. This leads to increase in general installed power of working regions and asymmetry of loading phases of supply distribution three-phase mains. It is shown in the work that system with a longitudinal compensator is well interacted with a standard thyristor controller of power of machine and allows keeping a high value of power factor within the range of phase control up to 60° . The application of longitudinal compensation gives technological advantages of spot welding, as the power factor of machine with a compensator depends little on the resistance of welding contact. Therefore the welding of metals in the wide range of specific resistances is possible: from low-carbon steels up to some light alloys and metals with protective coatings. Low cost of additional equipping of existing machines with longitudinal compensator with a simultaneous improvement of their technological properties makes the method of longitudinal compensation challenging for industrial application. 7 Ref., 1 Table, 4 Figures.

Keywords: resistance spot welding, power system, compensation of reactive power, power factor

Welding equipment for resistance spot welding (RSW), in particular for AC welding at industrial frequency, is characterized by high consumed power. At present the problem of optimizing power consumption of power source of welding equipment is urgent for industry. The existing park of equipment for RSW consists mainly of old machines with a single-phase power supply. This is due to the fact that these machines are long-serviced and purchase of new ones with more updated systems of supply requires significant capital investments.

In works [1, 2] the ways of improving the power efficiency of supply systems are out-of-date RSW machines were analyzed. The method of longitudinal compensation of a reactive component of power in single-phase welding AC machines of industrial frequency is known [3]. The aim of the present paper is to study some peculiarities of this method as-applied to RSW machines.

It is known that any machine for resistance welding at industrial frequency current including for spot one possesses a significant reactive resistance. The reactive power, partially consumed for heating of welding transformer and current-

carrying welding circuit, is commensurable with active one consumed for heating of welding zone. Due to this the full electric power, consumed by such welding machine, is increased and total installed power of the working region is increased.

Longitudinal compensation of reactive component of power applied to RSW machine represents the connection of bank of capacitors C in series with primary winding of welding transformer T (Figure 1). General principle consists in attaining, when possible, perfect compensation of reactive resistance of circuit, that means the equality by absolute value of reactive (inductive) resistance of the secondary circuit and reactive (capacitive) resistance of bank of capacitors, reduced to the secondary side: $X_L + X'_C = 0$ (where $X_L = \omega L$ is the inductive resistance of the secondary circuit; ω is the circular frequency; L is the

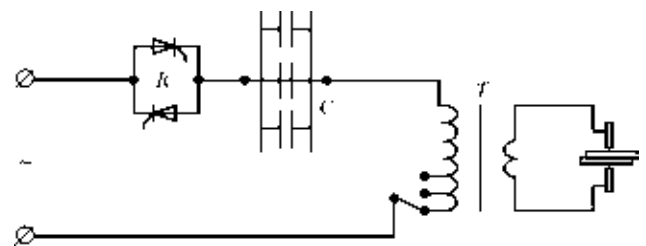


Figure 1. Scheme of supply system of RSW machine with longitudinal compensation of reactive component of power (for designations see the text)



inductance; X'_C is the capacitive resistance of bank of capacitors, reduced to secondary winding of a welding transformer). At the absence of compensation the short circuit resistance of machine is $Z_m = \sqrt{X_L^2 + (R_c + R_{w.c})^2}$.

At compensation, in a perfect case the condition is fulfilled, where Z_m reaches the minimum value, i.e. it almost becomes equal to the full active resistance of circuit R_c ($R_{w.c}$ is the active resistance of welding contact).

Thus, Z_m value is tending to the sum of values of active resistances and

$$\cos \varphi = \frac{R_c + R_{w.c}}{Z_m} \rightarrow 1.$$

At this condition the supply distribution network considers the welding machine as an active load, and full power consumed from mains is drastically decreased. Taken into account that inductive resistance X_L in RSW machines greatly exceeds the active R_c [4], the values of consumed full power can be reduced by 2 and more times.

Let us consider an example. Let the welding current of the machine without compensator be

$$I_2 = \frac{\sqrt{S'}}{\sqrt{R^2 + X_L^2}},$$

where S' is the full consumed power reduced to the secondary circuit; R is the full active resistance of the secondary circuit including resistance of the welding contact.

Let us assume that the same values should be provided by machine with the compensator:

$$I_2 = \sqrt{\frac{S'_{c.d}}{R}},$$

where $S'_{c.d}$ is the full consumed power reduced to the secondary circuit of machine with a compensating device.

Consequently, at one and the same secondary current the consumed power of machine with a compensator is

$$S'_K = \frac{S'R}{\sqrt{R^2 + X_L^2}} = \frac{S'}{\sqrt{1 + \operatorname{tg}^2 \varphi}}.$$

Reactive resistance (for larger part of RSW machines of a medium power), reduced to the secondary circuit, is not less than 150 μOhm [4], active resistance depending on design version is in the ranges of 50–100 μOhm , resistance of welding contact of steels of carbon group is 50–100 μOhm . So, in the machine without a compensator

$$\operatorname{tg} \varphi = \frac{X_L}{R} = \frac{150}{(50-100) + (50-100)} = 1.50-0.75.$$

Here, the ratio of powers is

$$\frac{S'}{S'_K} = \sqrt{1 + \operatorname{tg}^2 \varphi} = 1.80-1.25.$$

In welding of aluminium and magnesium alloys this ratio is higher as the resistance of welding contact is decreased to 10–20 μOhm :

$$\frac{S'}{S'_K} = 2.69-1.60.$$

As is seen, the use of a longitudinal compensation even in the first approximation allows obtaining the same active power at loading at the lower secondary voltage of welding transformer. Therefore, in the given case it is possible to increase the transformation factor, that respectively will decrease the secondary voltage, primary current and consumed power.

Application of longitudinal compensation of reactive power decreases load to the transformers of distribution substations, that is very important at repeated – short time mode of RSW machines operation, and also allows applying the current-carrying conductors with much smaller section for the machines connection.

At evident advantages of method of longitudinal compensation there are problems of an applied nature, requiring special investigations and calculations.

The first task is the setting up of machines with a compensator for the required welding mode. In conventional machines this is realized by switching the transformer stages. In the given case this leads to violation of compensation as the inductance is changed. It is possible to adjust the primary voltage by means of autotransformer connected between the mains and machine with a compensator, but this solution requires additional large expenses. It is more effective to apply the phase control, the peculiarities of which in using in welding machines with longitudinal compensation are given below.

The second task (the work aim) consists in possibility of attaining the full compensation under real conditions and retaining setting up during the whole operating cycle. It is known that the effect of ferromagnetic masses into welding circuit, such as dimensional and massive products being welded, improves reactive resistance of welding contour of the machine [4]. Besides, at the constant setting of mode for welding of one and the same product and from a product to product the active resistance of welding contact is



changed. If it is commensurable with active resistance of contour, then the parameters of welding mode can change dramatically.

The phase control at conventional machines for spot welding is performed using thyristor contactor K (see Figure 1). The phase of connection determines the current necessary to produce the welded joint (Figure 2).

To eliminate constant component in current and saturation of transformer, the angle of control by thyristor φ_1 should be within the ranges $\varphi < \varphi_1 < (\pi - \varphi)$. The higher φ_1 , the lower is the current, which is changed by sinusoidal low without interruption only in case if $\varphi_1 = \varphi$. At other values of this angle the pauses are occurred in steady mode between current pulses, moreover, the total pulse duration and next pause is π , and current pulse duration of semi-period is $\theta_1 = \pi + \varphi_1 - \varphi$.

If even the thyristor contactor is not used, and the welding mode is defined by selected stage of welding transformer, φ is not a constant value in practice. In traducing of dimensional ferromagnetic materials into welding circuit, as well as increase in stickout of electrodes, leads to the growth of welding circuit inductance L and angle φ . If the welding mode is defined by angle of thyristor control φ_1 , then it is necessary to find out the degree of system «recompensation» at such control.

The scheme of replacement of electrical part of RSW machine without a compensator, which is reduced to the secondary circuit and does not consider the current of transformer idle run for simplification of calculations [5], is shown in Figure 3, *a* and described by differential equation of the first order:

$$U_m \sin (\theta + \varphi + \varphi_1) = iR + X_L \frac{di}{d\theta},$$

where $\theta = \omega t$; i is the instantaneous current.

As basic values we take U_m as an amplitude value of the secondary voltage, X_L as an inductive resistance of the machine, φ_1 as an angle of thyristor control and φ as a phase angle.

Let us go on to the relative units:

$$\sin (\theta + \varphi + \varphi_1) = i \frac{X_L}{U_m} \frac{R}{X_L} + \frac{X_L}{U_m} \frac{di}{d\theta}$$

or

$$\sin (\theta + \varphi + \varphi_1) = \frac{i_e^*}{tL} + \frac{di_e^*}{d\theta}, \tag{1}$$

where

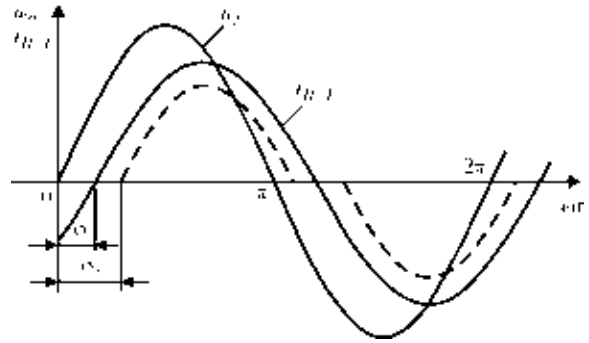


Figure 2. Dependence of instantaneous values of voltage u_2 and current $i_{R, L}$ on angle ωt for a period

$$i_e^* = i \frac{X_L}{U_m}, \quad tL = \frac{X_L}{R} = \text{tg } \varphi \quad \text{and} \quad R = R_c + R_{w.c.}$$

Using these expressions, let us define the value of welding machine χ – the power factor important for further calculations. In this case the active power for steady mode is

$$P = \left(\frac{i_e^* U_m}{X_L} \right)^2 R,$$

full power

$$S = \frac{i_e^* U_m U_m}{X_L \sqrt{2}},$$

i.e.

$$\chi = \frac{P}{S} = \frac{i_e^e U_m^2 R \sqrt{2} X_L}{X_L^2 i_e^{*2} U_m^2} = \frac{1.4 i_e^*}{tL}.$$

The simplified scheme of replacement of electric part of machine with a compensator is shown in Figure 3, *b*, where Γ -shaped scheme of transformer replacement is used (without account for circuit of open-circuit current passing). Therefore, it is taken into account that equation (1) is transformed into equation for circuit $R-L-C$ (in relative units):

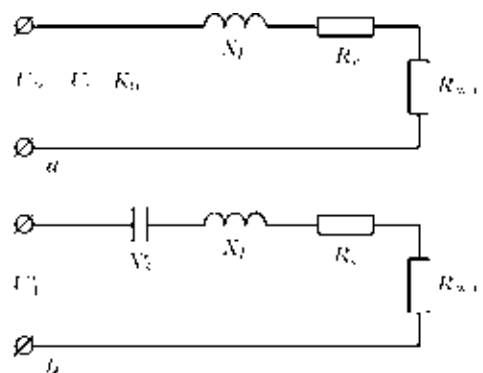


Figure 3. Scheme of replacement of welding machine without (*a*) and with (*b*) compensator reduced to the secondary side of transformer (transformation coefficient $K_{tr} = 1$; U_1 – primary voltage reduced to the secondary circuit)



Comparative characteristics of serial RSW machines

Type of machine	$R, \mu\text{Ohm}$	$X_L, \mu\text{Ohm}$	tL	χ
MT-1818	93	307	3.30	0.29
MT-1618	121	359	2.97	0.31
MT-2102	95	400	4.21	0.24
MT-2002	102	479	4.70	0.21
MT-4019	79	220	2.78	0.34

$$\sin(\theta + \varphi + \varphi_1) = \frac{i_e^*}{tL} + \frac{di_e^*}{d\theta} + \frac{X_L}{X_C} U_C t, \quad (2)$$

where $U_{C_r} = U'_C / U_m$ is the relative value of voltage at capacitor: U'_C is the voltage at capacitor reduced to the secondary side of welding transformer.

Now we shall determine how the effect from longitudinal compensation is changed at change of angle of thyristor control φ_1 using the standard power thyristor contactor. For this purpose we shall take the data of the Table [4] on serial RSW machines into consideration (values of power factors χ of machines are given at $\varphi_1 = \varphi$ in the short circuit mode).

For stationary machine with the lowest power factor (MT-2002) at different active resistances $R_{w.c}$ from 20 (in welding of light alloy parts) up to 180 μOhm (typically in welding of low-carbon steel parts) the data for three versions of connection are calculated: without compensation ($X_C = 0$), with partial compensation ($X'_C / X_L = 0.75$) and full compensation ($X'_C / X_L = 1$), tacking into account (1) and (2).

The comparison diagrams are plotted (Figure 4) illustrating dependence $\chi = f(R_c)$ at different ratios X'_C / X_L . Data for their plotting as well as program for calculation are given in [6].

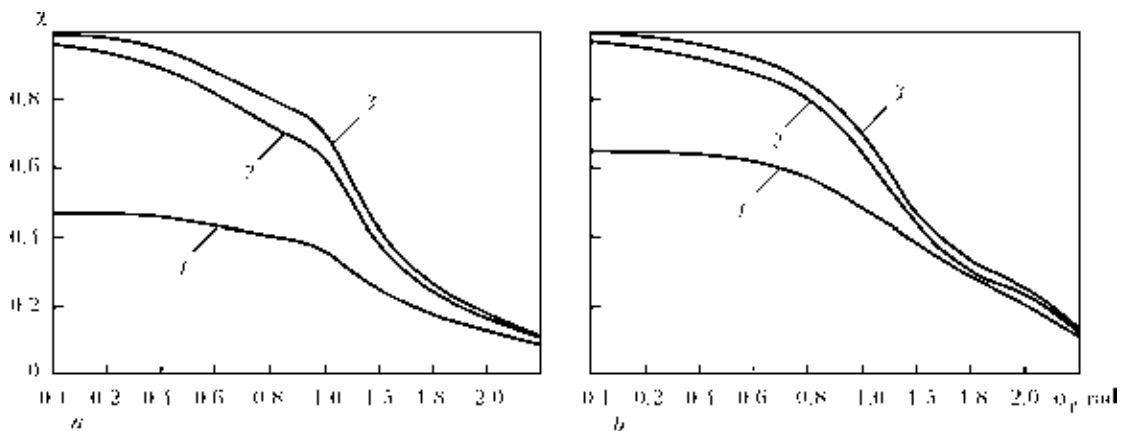


Figure 4. Dependence of power factor χ of RSW machine with longitudinal compensation on angle φ_1 of connection of thyristor contactor at $R_{w.c} = 20 \cdot 10^{-6}$ (a) and $180 \cdot 10^{-6}$ (b): 1 – without compensation; 2 – with partial compensation; 3 – with full compensation

Relative value of voltage at capacitor U'_C (reduced to the secondary side, using modulus), relative value of current i_e and power factor χ were calculated.

Diagrams illustrate the calculated values of power factors depending on active resistance of load (function of angle of thyristor contactor connection) for machines with and without compensator. The significant deviation of X_L can be caused by switching the stages of welding transformer, which can be from 4 up to 12 depending on power, and ratio of the highest voltage to the list one does not exceed usually 2.6 [5]. Therefore in many-turn transformers the transition to the next stages will not be very noticeable. It is seen from the diagram that even at a partial compensation the power factor of machines is greatly increased. In particular, in machine MT-2002 at $R_c = 20 \mu\text{Ohm}$ and $\varphi_1 = 0.8$ (about 60°) the power factor is equal to 0.71, and in machine not equipped with a compensator it is 0.39.

The diagrams illustrate negligible effect on power factor of oscillations $R_{w.c}$, changed within the wide ranges. It means that possible changes in transition resistance and specific resistance of metal during heating in the contact zone will little affect the stability of welding quality. Consequently, even in conventional single-phase machine, but equipped with a compensator, the industrial frequency of medium power (up to 100 kVA) the welding of metal is possible within the wide range of specific strengths – from carbon steels to some grade of light alloys, as well as joining of parts with a preliminary deposited protective coating with a high value of protective resistance. The mentioned possibilities are limited only by technical features of the equipment, i.e. by maximum power of welding transformer, version of the secondary welding circuit, maxi-



mum force of compression of electrodes and their configuration [7].

Compensation of reactive power allows perform welding with a great saving of electric power. Taking into account that additional equipment of serial welding machine with a compensating device depending on its capacity, adds not more than 15 % to the cost, the term of the compensator payback will be relatively small and shorter depending on the term of machine operation.

The advantages of longitudinal compensation of reactive resistance in RSW machines operating at industrial frequency are evident, and during the development of the new equipment the attention should be paid to these systems.

The continuation of works in this field can be preparation of methodology of systematized calculation of definite parameters of compensators of reactive power by real data obtained in service of updated RSW machine of up to 100 kVA capacity, taking into account the possibility of additional equipment by thyristor contactor of those models, where its application of its technology is rational.

Conclusions

1. The application of longitudinal compensation of reactive power of RSW machines allows keeping a high value of power factor in the range of phase control of up to 60° (corresponds to 5-6 stages of multi-turn welding transformer) at implicit dependence on load resistance, that corresponds to practical conditions of the welding machine service.

2. It was found that within the mentioned range of control of angle changes, there is a region

of effective application of longitudinal compensation. At further increase of making angle the values of power factors for machines, equipped with compensating devices, are commensurable with values of machines modes without application of compensation.

3. It was established that in the considered range of phase control the value of power factor of machine with a compensator scarcely depends on load resistance, that allows welding of parts in the wide range of specific resistances.

4. The practical application of systems with longitudinal compensation of reactive power is recommended in single-phase RSW machines of installed power of up to 100 kVA taking into account partial compensation within 10–25 % ranges.

1. Lebedev, V.K., Pismenny, A.A. (2001) Power systems of resistance welding machines. *The Paton Welding J.*, **11**, 28–32.
2. Lebedev, V.K., Pismenny, A.A. (2003) Power system of flash-butt welding machines with a transistor inverter. *Ibid.*, **2**, 10–12.
3. Zorin, V.V. (1960) Compensation of reactive power of resistance machines by series capacitors. *Avtomatich. Svarka*, **6**, 28–36.
4. Glebov, L.V., Filippov, Yu.I., Chuloshnikov, P.L. (1987) *Structure and operation of resistance machines*. Leningrad: Energoatomizdat.
5. Paton, B.E., Lebedev, V.K. (1969) *Electric equipment for resistance welding*. Moscow: Mashinostroenie, 59, 302, 342.
6. Pismenny, A.A. (2008) *Increase in efficiency of supply systems of resistance spot welding machines*: Syn. of Thesis for Cand. of Techn. Sci. Degree. Kiev.
7. Koubek, P. (2006) Energeticke aspekty pouzivanja zvaracich strojov s trojfazovym napajanim. *Zvaranie-Svarovani*, **10**, 288–292.

Received 27.03.2013



ANALYSIS AND PROCEDURE OF CALCULATION OF SERIES CONNECTION ELECTRONIC DEVICES FOR CONTACTLESS ARC EXCITATION

N.M. MAKHLIN¹ and A.E. KOROTYNSKY²

¹SE «PWI NRDC for Welding and Quality Control in the Field of Nuclear-Power Engineering of Ukraine»
11 Bozhenko Str., 03680, Kiev, Ukraine. E-mail: electro@paton.kiev.ua

²E.O. Paton Electric Welding Institute, NASU
11 Bozhenko Str., 03680, Kiev, Ukraine. E-mail: office@paton.kiev.ua

Considered are the issues from analysis of formation of high-voltage pulses, injected into interelectrode gap for initial arc ignition and its re-ignitions, in electronic devices with independent power supply and series connection to electric circuit of main or pilot arc, where all the elements of forming circuit are also connected in-series. The analysis of oscillating processes in the forming circuit is carried out using the solution of known linear differential equations of second degree with non-zero initial conditions. Engineering procedure based on these solutions was proposed for calculation of all components of the forming circuit in electronic devices with independent power supply for arc excitation, as well as recommendations on selection of their element base were given arising from the experimental data and experience of designing, industrial manufacture and operation of such devices. Variants of circuit solutions for oscillating constituent of electronic arc exciters with independent power supply and devices for control of switching cell of the forming circuit were described. 34 Ref., 6 Figures.

Keywords: arc and plasma welding, initial arc excitation, arc re-ignitions, electronic arc exciters, spark discharge, in-series connection, pulse-phase control

Initial ignition of arc is an important stage of arc and plasma welding cycles, having significant effect on effectiveness and efficiency of these processes and quality of welded joints. A method of arc initiation by means of electric breakdown of interelectrode gap with the help of boost devices generating high-voltage pulses [1–4] has the highest distribution among various methods of contactless excitation.

Spark-gap generators of high-frequency pulses (oscillators) were used in a course of many years as boost devices for arc ignition (arc exciters). A lot of works, results of which generalized in [2–6], were dedicated to their investigations, theory and procedure of calculation and designing. Simple structure and relatively small price should be referred to oscillator advantages. Its disadvantages are complexity of control of beginning of high-voltage pulse generation, quick attenuation of high-frequency oscillation due to losses in spark discharger, which requires periodic regulation and maintenance during operation, as well as low values of parameters of electromagnetic compatibility with electron and electric assemblies and devices of welding equipment due to high degrees of radio interferences generated by oscillator in a wide frequency range [3, 5–9].

Beginning of industrial manufacture of power semi-conductors (thyristors, symistors) with high switching and dynamic characteristics provides for the backgrounds of development of sparkless exciters and stabilizers of welding arc free from the disadvantages typical for the oscillators [3, 6, 10–13].

In recent years, series of manufacturers of welding equipment (for example, KEMPPPI) begin to use power high-voltage IGBT-transistors as switching units for oscillating circuits of arc exciters. Semi-conductor exciters and stabilizers of arc start to dominate from the beginning of 1970s and today have virtually replaced the oscillators.

Semi-conductor exciters and stabilizers of arc with in-series connection to arc circuit gained the widest application. They favorably differ from devices with parallel connection by higher efficiency, simpleness of protection of welding power sources and other assemblies and devices of welding equipment from influence of high-voltage pulses and better electromagnetic compatibility [3, 6, 9]. Figure 1 shows the circuits of in-series connection of arc exciters to the circuits of main and pilot arc of units for arc, plasma and microplasma welding, plasma and air-plasma cutting of metals, as well as welding, surfacing and spraying using plasma-tions without interelectrode insert.



Electron (semi-conductor) exciters and stabilizers of arc can be divided into two groups on structure of oscillating constituent.

The first one includes the devices, in which formation of high voltage in the energy storage (mainly capacitive one) is performed with the help of voltage multiplier or by means of resonant pumping.

Switching semi-conductor cell in the devices of the first group has in the most cases parallel connection to in-series connection of induction L and capacity C of forming circuit oscillating constituent. Devices of this group are characterized by versatility according to kind of source voltage. They can have direct supply from the arc voltage, that allows performing automatic connection of the devices during supply of open-circuit voltage to the arc gap and automatic termination of generation of high-voltage pulses or change from mode of initial ignition to mode of stabilization after arc excitation [3, 6].

However, on practice, regardless indicated advantages of the first group devices, electronic exciters and stabilizers of the second group are more widespread. These are the devices with independent power supply (as a rule from alternating current main of industrial frequency), in which switching semi-conductor cell and reaction elements L and C have in-series connection [3, 11, 12].

Formation of high-voltage output pulses injected into the arc circuit from the device, circuit of which is shown in Figure 2, *a*, is performed due to transient process, having place at periodic connections (with double frequency of source voltage) of semi-conductor cell K with double-sided conductivity, based on symictor or two thyristors of back-to-back connection.

Since the transient processes in magnetic conductor of the pulse transformer $TV1$ (see Figure 2, *a*) are not linear and $L = f(i)$, strict

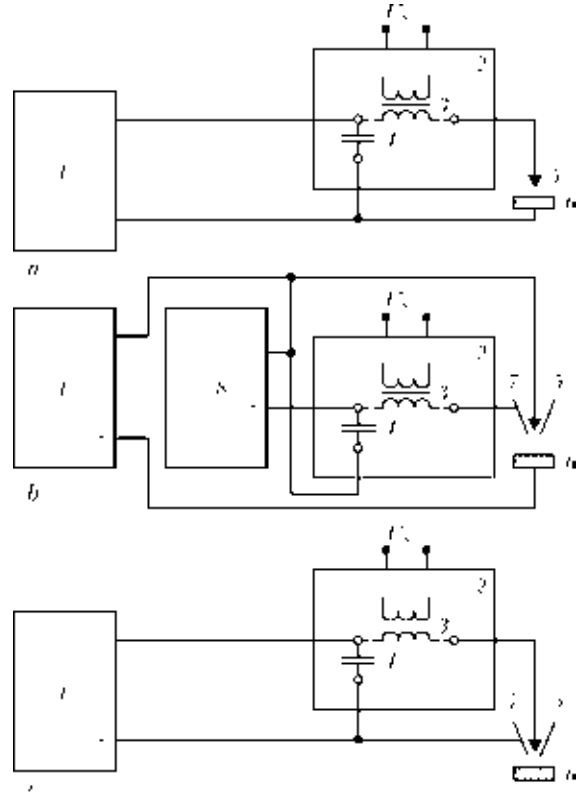


Figure 1. Circuits of in-series connection of arc exciters and stabilizers: *a* – to main arc circuit in arc welding machines; *b* – to pilot arc circuit in machines for plasma (micro-plasma) welding and surfacing, plasma and air-plasma cutting of metals; *c* – to main arc circuit in machines for plasma welding, surfacing and spraying with the help of plasmotrons without interelectrode insert; 1 – power supply unit of main arc; 2 – arc exciter; 3 – output pulse transformer of arc exciter; 4 – protective (blocking) condenser; 5 – electrode; 6 – part being welded; 7 – plasmatron nozzle; 8 – power supply unit of pilot arc

analysis of the transient process in the equivalent circuit (Figure 2, *b*) is difficult due to insufficient cleanness of the results and complexity of computations requiring solution of the system of non-linear differential equations. Therefore, in order to analyse of this equivalent circuit with small error it is relevant to assume the following assumptions:

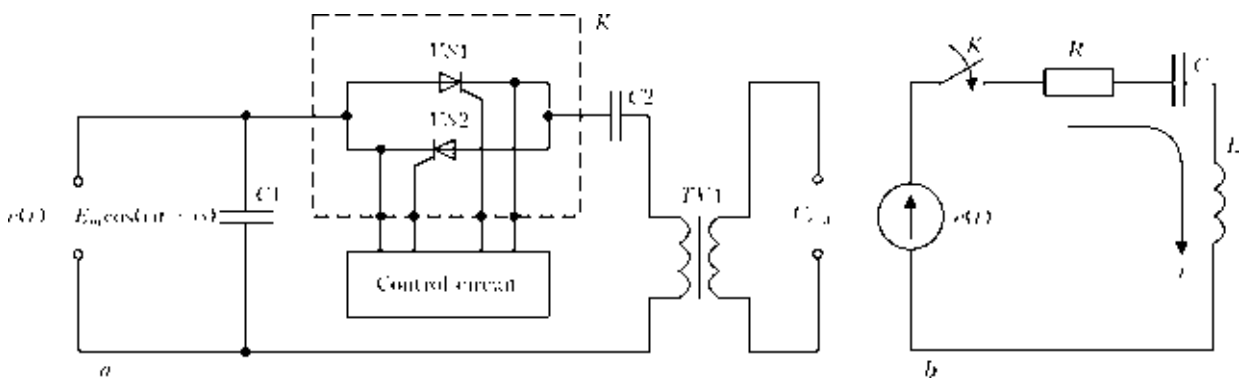


Figure 2. Basic variant of construction of arc exciters and stabilizers with independent power supply and in-series connection to switching cell and elements of forming circuit: *a* – simplified electric circuit of oscillating constituent; *b* – equivalent (calculation) circuit of oscillating constituent



1) $R = R_{K\text{ dyn}} + ESR_{C1} + ESR_{C2} + R_L + R_{c.c}$, where $R_{K\text{ dyn}}$ is the dynamic resistance of switched cell K ; ESR_{C1} , ESR_{C2} are the equivalent series active resistances of capacitors $C1$ and $C2$, respectively; R_L is the real resistance of primary winding of pulse transformer $TV1$; $R_{c.c}$ is the active resistance of connecting cables;

2) induction L of the primary winding of pulse transformer $TV1$ is linear and equals initial one, and does not depend on current passing in it;

3) $C1 > C2$, from which $C \approx C2$;

4) $\tau_{\text{trans}} \ll T/2$, where τ_{trans} is the duration of transient process; $T/2$ is the duration of semiperiod of AC input voltage (source voltage);

5) $R/2L < 1/\sqrt{LC}$;

6) $e(t) = E_m \cos(\omega t + \varphi) = E_m \sin[\omega t + (\pi/2 - \varphi)]$, where E_m is the amplitude of AC input voltage; ω is the its angular frequency and initial phase of this voltage (turn-on angle of semiconductor cell K);

7) $U_{\text{out}} = U_L W_2 / W_1$, where U_{out} is the device output voltage; U_L is the induction voltage L ; W_1 , W_2 is the number of winds of primary and secondary windings of pulse transformer $TV1$, respectively.

Considering assumptions taken for calculation circuit (see Figure 2, *b*), the transient process at non-zero initial conditions in RCL -circuit with charged capacity is described using well-known differential equation of the second order for C capacity voltage U_C [14, 15]:

$$LC \frac{d^2 U_C}{dt^2} + RC \frac{dU_C}{dt} + U_C = E_m \cos(\omega t + \varphi). \quad (1)$$

Voltage U_C is the sum of two constituents, namely $U_{C.st}$ became stationary on capacity C after attenuation of transient process, and $U_{C.f}$ voltage being the free attenuation constituent. Stationary voltage $U_{C.st}$ is determined by particular solution of equation (1) at $t \rightarrow \infty$, i.e. when $dU_C/dt = 0$ and static current $i(t) = 0$, according to which

$$U_{C.st} = U_{C_0} = E_m \frac{X_C}{Z} \cos(\omega t + \varphi - \gamma),$$

where

$$X_C = 1/\omega C; \quad Z = \sqrt{R^2 + (\omega L - 1/\omega C)^2};$$

$$\text{tg } \gamma = \frac{R}{\omega L - 1/\omega C}.$$

The free constituent of attenuating oscillations $U_{C.f}$ is described by total solution of homogeneous equation

$$\frac{d^2 U_{C.f}}{dt^2} + \frac{R}{L} \frac{dU_{C.f}}{dt} + \frac{1}{LC} U_{C.f} = 0. \quad (2)$$

For $R/2L = \delta$, $1/LC = \beta_0^2$ and $\beta = \sqrt{\beta_0^2 - \delta^2}$ designations and assumption $\beta_0^2 > \delta^2$, the solutions of equations (1) and (2) can be represented in the form

$$U_C = U_{C.st} + U_{C.f} = E_m \frac{X_C}{Z} \cos(\omega t + \varphi + \gamma) + e^{-\delta t} \left\{ E_m \frac{X_C}{Z} [\cos(\omega t + \varphi + \gamma) - \cos(\varphi + \gamma)] \times \right. \\ \left. \times \frac{\beta_0}{\beta} \sin(\beta t + \gamma) + E_m \frac{X_C}{Z} \sin \frac{\omega}{\beta} \sin \beta t \right\}; \quad (3)$$

$$i = \frac{E_m}{Z} \sin(\omega t + \varphi - \gamma) + \frac{E_m}{Z} e^{-\delta t} \times \left[\frac{\beta_0^2}{\omega \beta} \cos(\varphi - \gamma) + \frac{\delta}{\beta} \sin(\varphi - \gamma) - \sin(\varphi - \gamma) \cos \beta t \right]. \quad (4)$$

It follows from (3) that C capacity, overvoltage which 3.2 time exceeds E_m value, takes place during connection of switching cell K at the moment, when $e(t)$ achieves the maximum being in antiphase with C charged capacity voltage, i.e. at $e(t) = E_m$, $\varphi = -\gamma$, $U_{C_0} = -E_m$.

Considering relationship $U_L = L \frac{di}{dt}$, L induction voltage is determined using expression

$$U_L = E_m \frac{X_L}{Z} \left\{ \cos(\omega t + \varphi - \gamma) - \frac{\delta}{\omega} e^{-\delta t} \times \right. \\ \left. \times \left[\frac{\beta_0^2}{\beta} \cos(\varphi - \gamma) + \frac{\delta}{\beta} \sin(\varphi - \gamma) - \right. \right. \\ \left. \left. - \sin(\varphi - \gamma) \cos(\beta t + \beta) \sin(\varphi - \gamma) \sin \beta t \right] \right\}, \quad (5)$$

where $X_L = \omega L$.

In (3)–(5) β is the oscillation angular frequency during transient process in RCL -circuit; δ is the coefficient of their attenuation.

Since resistance of the interelectrode gap is sufficiently high (from several tens to hundred of kilohms) during breakdown and spark discharge, which are referred to the independent unsteady discharges in the gases, then it could be assumed that expressions (3)–(5) are true for open-circuit mode of arc exciter, as well as spark discharge (up to the moment of transfer of spark discharge in the interelectrode gap into stationary arc discharge). At that, the effect of welding circuit, including secondary circuits of boost device, on parameters of elements of arc exciter oscillatory constituent is negligibly small.



Expressions (3)–(5) and results of the experimental investigations and many years of experience of development, serial production and operation of exciters and stabilizers of arc of in-series connection can be used for calculation of parameters and selection of components for basic variant of similar devices.

Condenser C1 (see Figure 2, a) is chosen from the condition $C1 > (2-4)C2$, frequency properties which should correspond to index β in (3)–(5), *ERS* value (not more than 10 mOhm), allowable value of $I_{R.M.S}$ variable component of current through the condenser and $U_{VAC\ al}$ allowable effective value of AC voltage on this condenser depending on the biggest value of input voltage (source voltage) U_s .

Usually, $C1 = 4-6 \mu F$ at $U_{s,nom} = 380 V$, and $6-15 \mu F$ at $U_{s,nom} = 220 V$, respectively, $I_{R.M.S}$ values, determined from relationship $I_{R.M.S} = E_m / X_{C1}$ (where $X_{C1} = \omega C1$) make 0.74–1.11 and 0.68–1.08 A and $U_{VAC\ al}$ value being 600 and 250 V, correspondingly (at $U_s = 1.1U_{s,nom}$).

Metal-film condensers with polypropylene or polycarbonate dielectric, in particular, condensers of K75-15, K75-24 series, or PHC, PWM or PMB series of ICEL company or similar one of other company-manufacturers, are the most suitable for application as condenser C1 based on combination of characteristics (including frequency ones) and parameters. Values of *ERS* do not exceed 3.5 mOhm and allowable values of $I_{R.M.S}$ make not less than 9 A [16] in such condensers at the indicated range of their capacities and voltages $U_{VAC\ al}$. From point of view of optimum thermal mode and indices of safety, good results could be achieved at dissipative (parallel) connection of two or three such condensers of corresponding capacity.

Capacity of condenser C2 (see Figure 2, a) can be determined based on necessary value of energy of pulses injected in the arc circuit using relationship $W_i = CU_{C2}^2 / 2$ (where W_i is the pulse energy, U_{C2} is the condenser C2 voltage in the moment of switching cell connection), i.e. at $t(0)$. Since such cell connection is symmetric in each semi-period of input voltage (source voltage), then C2 condenser voltage is determined as $U_{C2} = k_{min} 2E_m \sin \phi$ (where k_{min} is the coefficient considering the smallest value of E_m in oscillation of input voltage). As a rule, $k_{min} \geq 0.85$. Based on this, the expression for C2 condenser capacity can be represented as

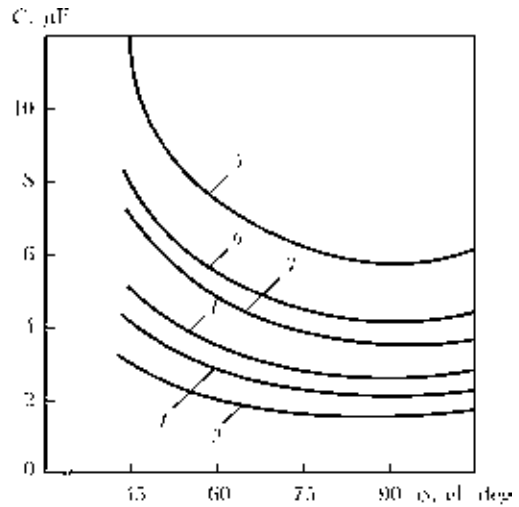


Figure 3. Dependence of capacity C on turn-on angle of cell K of forming RCL-circuit at pulse energy of 0.3, 0.5 and 0.8 J, respectively, and effective value of source voltage of 187 (1, 3, 5) and 220 (2, 4, 6) V

$$C = \frac{2W_i}{U_{C2}^2} = \frac{W_i}{2(k_{min} E_m \sin \phi)^2} \quad (6)$$

According to the earlier investigations and experimental data, providing of effective arc excitation in DC units with single-phase rectification requires (90 ± 5) el. deg turn-on angle of switching cell (angle ϕ), that in units with three-phase rectification should be (90 ± 10) el. deg, and angle ϕ in the AC units makes (75 ± 5) el. deg [3, 6, 11, 12] based on that $\sin \phi = (0.94-1)$. As it is seen from Figure 3, C2 condenser capacity should be from 2 to 6 μF at reduced ($U_s = 0.85U_{s,nom}$) and nominal ($U_{s,nom} = 220 V$) values of source voltage and pulse energy from 0.3–0.8 J, and it should be from 0.5 to 2.0 μF at $U_s = 0.85 \cdot 380 V$, according to (6). Considering that the transient process in RCL-circuit (see Figure 2, b) is accompanied by determined (3) condenser C2 overvoltage (see Figure 2, a), the allowable amplitude value of DC voltage of this condenser is taken from the condition

$$U_{VDC\ max} \geq 3.2E_m \quad (7)$$

The requirements to frequency properties and *ESR* of condenser C2 are similar to the requirements to condenser C1. Dissipative (parallel) circuit of connection of two-four frequency metal-film condensers, for example, K75-24 series or ICEL PPA, PWM or PMB series [16, 17], are also relevant for C2.

Values of the active resistance R (see Figure 2, b) of forming RCL-circuit are determined using the reference data given, for example, in [16–18]. In the most cases, *ESR* of one metal-film condenser with polypropylene dielectric and $U_{VDC\ max} = 1000-2000 V$ do not exceed 4 mOhm,



and $R_{K\ dyn}$ values for number of thyristors of domestic and foreign manufacture, including low-voltage thyristors of unified series T122-25–T141-40, lie in 3.3–11.0 mOhm range. Sum of active resistances $R_{c,c}$ of the wires, connecting components of oscillatory constituent of arc exciter, and resistance R_L of the primary winding of pulse transformer do not exceed 12 mOhm. Respectively, the value of active resistance of the forming RCL -circuit makes not more than 40 mOhm.

Induction L of the forming RCL -circuit (see Figure 2, *b*) should meet a series of requirements. The most significant from them lie in the fact that providing of oscillatory character of the transition process at K cell turn-on requires fulfillment of necessary condition $2\sqrt{L/C} > R$ (in semi-conductor exciters and stabilizers of arc this condition is fulfilled virtually in any case), and no-fault operation of semi-conductor cell K demands having L value so that $I_m \ll I_{TRM}$ and $(di/dt)_K < (di_{o-s}/dt)_{cr}$ (where I_m is the maximum amplitude value in the forming RCL -circuit; I_{TRM} is the maximum allowable repetitive on-state current of cell K ; $(di/dt)_K$ is the maximum value of rate of current rise in the forming RCL -circuit; $(di_{o-s}/dt)_{cr}$ is the value of critical rate of current rise of on-state cell K).

Considering that period of sine source voltage (supply main voltage) significantly (not less that by order) exceeds the duration of transient process in the forming RCL -circuit, and after performance of some simplification of expression (4), omitting constituents having insignificant influence on final result, the expression for transient current passing in RCL -circuit can be represented in the form

$$i = \frac{E_m}{\beta L} e^{-\delta t} \sin \beta t. \tag{8}$$

According to (8) the biggest amplitude value of current in the forming RCL -circuit can be determined on relationship

$$I_m = \frac{E_m}{\beta_0 L} = E_m \sqrt{\frac{C}{L}}, \tag{9}$$

and the maximum value of rate of current rise in this circuit is made on expression

$$(di/dt)_K = 4I_m\beta_0 = \frac{4I_m}{\sqrt{LC}}. \tag{10}$$

Calculations and experience of development and designing of arc exciters, in which switching cell and elements of the forming circuit have in-series connection, show that induction L makes

as a rule around 20 mH at the limitations caused by electromagnetic and structural parameters of ferritic cores of real pulse transformers. Such (or close to this) value of induction L provides for fulfillment of the condition of oscillatory behavior of transient process in the forming RCL -circuit, as well as the values $I_m \leq 180$ A and $(di/dt)_K \leq 80$ A/ μ s at supply main voltage 220^{+22}_{-33} V, that is verified by corresponding oscilografic measurements. At typical values of R , C and L calculated in accordance with (6)–(10), the frequency $\beta_0/2\pi$ of own (free) attenuating oscillations in the forming RCL -circuit makes 15–20 kHz and relation of frequencies β_0/β are close to one.

High-voltage pulse transformer $TV1$ (see Figure 2, *a*) is the critical and most complex on design unit of arc exciters. The requirements, made to this transformer, are highly controversial [3, 6, 10–12]. First of all, such a transformer with increased dissipation should correspond to the norms and rules of high-voltage transformers construction. Secondly, its mass-and-dimension indices and cost should be noticeably smaller in comparison with the similar indices of all engineering unit. Besides, surface effect caused by high frequency of pulse currents flowing around the transformer windings, the biggest value of arc current passing through secondary winding of the transformer, as well as electromagnetic and structural parameters of serially manufactured in industry ferritic cores, providing calculation (set) L value should be considered during calculation and designing of the transformer.

Number of works, for example [19–25], are dedicated to the theoretical fundamentals, analysis of the processes and procedures of calculation of inductive elements with ferromagnetic cores, including pulse transformers of ultrasonic and high frequencies. Therefore, present work considers only some aspects of simplified calculation and designing of high-voltage pulse transformer (PT) of arc exciters of in-series connection.

Requirements made to PT of arc exciters are caused by idea of performance of their windings with minimum possible number of winds, following from what the number of winds of the primary circuit $W1$ of such PT makes as a rule 1 or 2. According to (5) at $e(t) = -E_m$ and $\varphi = -\gamma$, the maximum value of primary winding voltage of PT is 2.1 times higher than the E_m value, and at reduced U_s makes

$$U_{L\ max} = 2.1 k_{min} \sqrt{2} U_s. \tag{11}$$



For example, $U_{L\max} = 555\text{ V}$ at $U_s = 220\text{ V}$ and $k_{\min} = 0.85$.

Amplitude value of open-circuit voltage of PT secondary winding (U_{out}) should correspond to the levels providing breakdown of the interelectrode gap of technologically grounded length, and appearing after that spark discharge, i.e. $U_{\text{out}} \geq U_{\text{br}}$ should be fulfilled (where U_{br} is the voltage of interelectrode gap static breakdown). Since, up to now there is no theory of arc discharge, explaining all combination of effects, which accompany the processes of interelectrode gap breakdown and arc discharge in it, so entering of analytical expression for U_{br} in form acceptable for engineering calculations is very complicated. Therefore, experimental data verified by accumulated experience of application of arc exciters [3–7, 10–12] is reasonable for application at determination of necessary U_{out} value. According to these data $U_{\text{out}} = 3\text{--}6\text{ kV}$ in the arc exciters of units for arc welding and most units for plasma welding, surfacing and spraying, $U_{\text{out}} = 10\text{--}12\text{ kV}$ in the arc exciters of units for arc-plasma cutting, and in some cases it equals 16–20 kV. Based on this and considering well-known relationship $W_2 = W_1 U_{\text{out}} / U_{L\max}$ at $W_1 = 1\text{--}2$ winds, the number of winds W_2 of the secondary PT winding usually makes 9–18 in the arc exciters of units for arc and plasma welding, surfacing and spraying in inert gas atmosphere, 18–36 in the exciters of pilot arc of units for air-plasma cutting, and 32–48 in the arc exciters of units for CO₂ plasma welding.

Influence of the surface effect on sizes of conductors of PT windings is characterized by penetration depth of high-frequency current D_{pen} , which could be determined in millimeters for conductors from copper with sufficient for practice level of accuracy [25]:

$$D_{\text{pen}} = \frac{75}{\sqrt{\beta_0/2\pi}}. \quad (12)$$

According to (12), section area of conductor of the primary winding should be not more than 1.15 mm², and thickness of rectangular conductor of the secondary winding makes not more than 1.2 mm for rational application of section of conductors of PT winding at typical values of β_0 .

Rectangular strips from soft copper (for example, copper strips with heat-resistant film coating of PMLBN grades on TU 16.K50-088–2006, PMGLBN on TU 16.K50-009–2007 or bare strips of LMM type on GOST 434–78) are reasonable for application as a conductor of PT secondary winding. At that, dimensions of such strips should be chosen considering number of winds

of the secondary winding, D_{pen} value and necessary cross-section area $S_{\text{cr.s}}$.

Soft manganese-zinc ferrites of 2500NMS1 and 3000NMS1 grades or ferrites from 3S8 material, designed for operation in power magnetic fields, are the most suitable for application as PT core material. The assumptions are made in order to simplify the process of selection and determination of the main parameters and dimensions of PT core. According to them, the value of magnetic induction B is changed symmetrically relatively to zero of characteristics of magnetization, distribution B and magnetic field intensity H are homogeneous, value of magnetic permeability μ_R is constant, i.e. B/H core characteristic is linear. Shell-type transformers received the highest application in the exciters and stabilizers of arc and bar-type PT are rarely used. As a rule, the cores of such PT have II- or E-shaped configuration with rectangular or round shape of section of cores and yokes.

Application of cores of E-shape configuration, for example, E55/28/21 for PT of exciters of pilot arc or E80/38/20 for PT of exciters of main arc, are the most reasonable for minimizing of mass-and-dimension parameters of PT in the exciters of pilot arc and in the exciters of main arc, current of which does not exceed 160 A. Usage of II-shaped cores, for example, PK 40×18 from ferrite 2500NMS1 or 3000NMS1 or cores UU 93/152/16 from ferrite 3S8, is acceptable in the exciters of main arc, the nominal current of which makes from 160 to 315 A. II-shaped cores having developed window area A_W , for example, UU 101/152/30 or UR 114/78/38, are good for PT exciters of arc, the nominal current of which varies from 315 to 500 A, and for PT exciters of arc of machines for CO₂ plasma welding.

When selecting the PT core, determination of total effective cross-section of core A_E based on specified induction value L of PT primary winding, can be done using relation

$$L = A_L W_1^2, \quad (13)$$

where A_L is the integral parameter, specified in technical data of the core and determining a value of winding induction located in this core, depending on square of its winds (for PT – depending on square of primary winding winds). At that, two approaches are possible. The first one assumes application of single core that requires fulfillment of condition $W_1 \geq \sqrt{L/A_L}$, so that in real PT the number of winds should be not less than 2 and, respectively, $W_2 \geq 20$. Such an approach is sufficiently suitable in designing



of PT exciters of pilot arc and limited for PT exciters of main arc, the nominal current of which does not exceed 250 A. According to the second approach, necessary value of A_L at set L and W_1 values is achieved through application in PT of the core consisting from several single cores, number of which is determined on expression

$$n_c = \frac{L}{W_1^2 A_{LS}}, \quad (14)$$

where n_c is the rounded upward number of single cores; A_{LS} is the A_L parameter of single core. Namely, the second approach is typical for PT exciters of main arc, the nominal current of which makes more than 250 A.

The necessary area of core window A_W is determined using standard procedure, given, for example, in [20, 23, 25], through calculation of total area of the window covered by conductors of PT windings considering the thickness of inter-wind and inter-winding insulation and increased temperature of PT at it cooling due to natural convection.

A_E and A_W values received with the help of reference data allow performing preliminary selection of standard size of PT core, after what correspondence of electromagnetic mode of chosen core to $B_{max} < B_S$ condition (where B_{max} is the value of magnetic induction at peak value H_{max} of magnetic field intensity in the core, and B_S is the value of saturation magnetic induction of the core) should be checked.

If, according to the data given [25–27], it is assumed that the maximum allowable value $B_{max} = 0.2$ T and values of relative μ_0 and effective μ_{ef} magnetic permeability of the core are equal, then for section of $B = f(H)$ curve of places of hysteresis loop of 2500NMS1, 3000NMS1 or 2S8 ferrites, in which $B/H = \text{const}$, the maximum allowable value H_{max} at core temperature not more than 120 °C is calculated on expression

$$H_{max} = \frac{1.592 \cdot 10^5}{\mu_{ef}}. \quad (15)$$

Since usually $\mu_{ef} = (1.70–1.99) \cdot 10^3$, then H_{max} values lie in the ranges 94–80 A/m.

Besides, H_{max} values should be determined depending on amplitude value I_m wrapping the PT primary winding, number of winds of these winding and size of selected core, using expression

$$H_{max} = \frac{I_m W_1}{l_{ef} n_c}, \quad (16)$$

where l_{ef} is the reference value of effective length of magnetic line path. If H_{max} value, calculated

on (16), exceeds the value, received on expression (15), then it is necessary to choose size of the core with larger l_{ef} or increase n_c of single cores, forming PT core, after what carry out checking calculation again.

Low frequency of passing of pulses of output voltage U_{out} , significant level of transient current and voltage on the elements of circuit forming these pulses and their high relative duration (not less than 10) provide for the relevance of application of low-frequency thyristors as a cell K (see Figure 2, a) in the arc exciters with independent power supply. They together with high switching capabilities have relatively low values of $R_{K \text{ dyn}}$ in on-state, control power insignificant in comparison with switching power, high service safety, mass production and application and relatively small cost. The most preferable among such thyristors are the domestic ones of unified series T122-25 or T131-40 at nominal source voltage (supply main voltage) 220 V, and T132-25 or T141-40 series at nominal source voltage 380 V, or their foreign analogues.

Class of thyristors based on repetitive pulse back voltage U_{RRM} is chosen from the relationship

$$U_{RRM} = 100 + 3.2E_m. \quad (17)$$

Thyristors of the 12th class can be recommended considering (17) at supply main voltage 220 V, and that of the 20th class at 380 V.

The maximum average and active current values, passing through thyristor in its on-state can be determined by means of approximation of exponential bidirectional radiopulse of current i , passing in forming RCL -circuit, by unidirectional video pulse of rectangular shape. According to this, the maximum average value of current I_{TAV} , passing through thyristor in its on-state, is calculated on expression

$$I_{TAV} = 0.5I_m \frac{\tau_p}{T_p}, \quad (18)$$

where τ_p is the duration of exponential bidirectional radiopulse of current i (or corresponding to it unidirectional videopulse), determined as $\tau_p = 1/\delta = 2L/R$; T_p is the period of frequency of pulse passing, being equal to the period of doubled frequency of power supply voltage of arc exciter. The maximum active I_{TRMS} value of current passing through the thyristor can be determined from the relationship

$$I_{TRMS} = 0.5 \frac{I_m}{\sqrt{T_p/\tau_p}}. \quad (19)$$



It follows from (18) and (19) that, for example, the maximum average and active values of current passing through thyristor in its on-state make $I_{TAV} = 9.0$ and 28.5 A, respectively, at given typical values of R , C , L and I_m . Therefore, in this case, the thyristors of T122-25 series, in which maximum allowable average current is 25 A and limiting allowable active value of current is 31.4 A [18], can be used.

Critical rate of current rise di_{on}/dt in on-state for low-frequency thyristors of unified series makes not less than 100 A/ μ s, and, therefore, $(di/dt)_K < di_{on}/dt$ requirement for the arc exciters with independent power supply (see Figure 2, a) is fulfilled virtually in any case.

Output impedance of the exciters with in-series connection to arc circuit, mainly depending on induction and effective resistance of PT secondary winding, makes from 1.2 to 9.0 kOhm, that predetermines presence of dropping external volt-ampere characteristics in the arc exciters.

Control of turn-on of thyristor switching cell K (see Figure 2, a) and, respectively, the moments of beginning of output pulse U_{out} generation, is performed by means of widely distributed synchronous pulse-phase control. It differs by control pulse feed angle, often from phase, corresponding to moments of zero values of supply main voltage. Realization of pulse-phase control can be performed using number of circuit solutions for phase-shifting devices (PSD), designed on such semi-conductor devices as diode, transistors, thyristors or analogues or digital microcircuits, or combination of the first and the second [10, 22, 24, 28]. PSD designed on the basis of unijunctional transistors (double-base diodes) have the widest distribution in the arc exciters with independent power supply. Analysis, calculation procedure and recommendations on selection of double-base diode PSD are given in [28], and Figure 4 shows a typical circuit solution of PSD, applied in the arc exciters with independent power supply. Synchronizing voltage in such PSD is formed with the help of stabilatron tube $VD2$ and regulation of moment for generation of turn-on pulse of thyristors of arc exciter switching cell is carried out with the help of variable resistor $R4$. Detailed description of this PSD and voltage diagrams in different points of its circuit are given in [12].

Thyristors of the switching cell K can break down due to exceeding of allowable value of current overloading. It will inevitably happen in the case of saturation of PT core, the secondary winding of which has in-series connection to circuit of DC arc. Therefore, the oscillating constituent

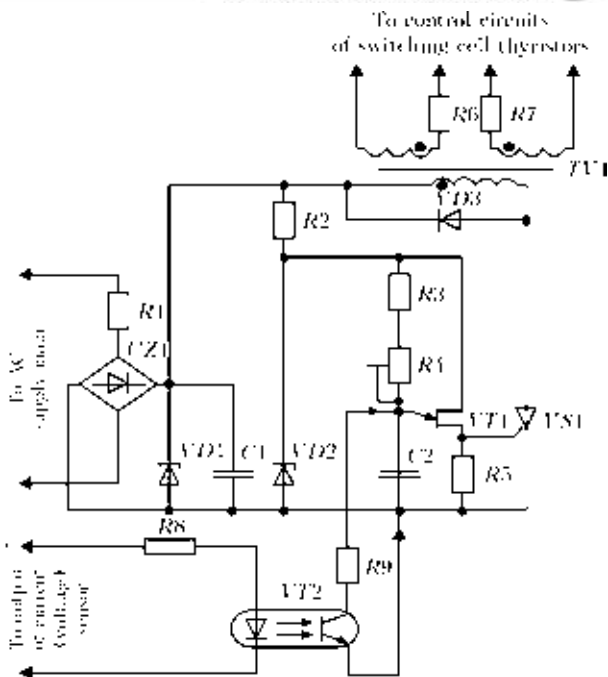


Figure 4. Typical electric schematic of PSD of arc exciters with independent power supply

of arc exciter should automatically switch off during setting into the interelectrode gap of stationary arc discharge. In PSD (see Figure 4) such switch off is carried out with the help of assembly, consisting of fast-operating transistor optical coupler $VT2$ and current-limiting resistors $R8$ and $R9$. Shunting of condenser $C2$ is provided when signal from the output of arc (voltage) current sensor comes to the input of this assembly. The sensors operating on Hall effect are often used as the sensors of arc current in modern machines and welding power supplies. If such a current sensor is absent in the machine control system, then current shunt set in the arc circuit can be used as an arc current sensor. Figure 5 shows a variant for current sensor construction, including shunt $RS1$, linear noninverting shunt amplifier based on microcircuit $DA1$ and comparator unit based on microcircuit $DA2$.

A signal, level of which is proportional to the arc current, is formed during appearance of cur-

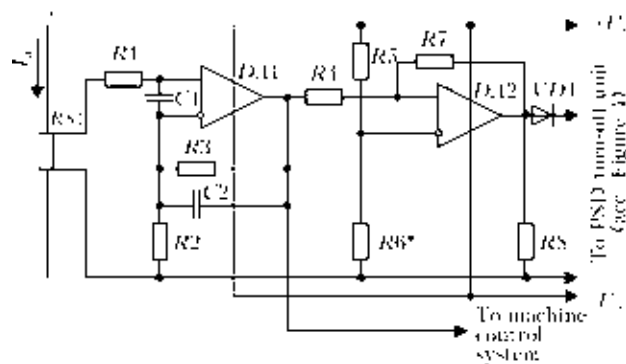


Figure 5. Electric schematic of variant of construction of arc current sensor

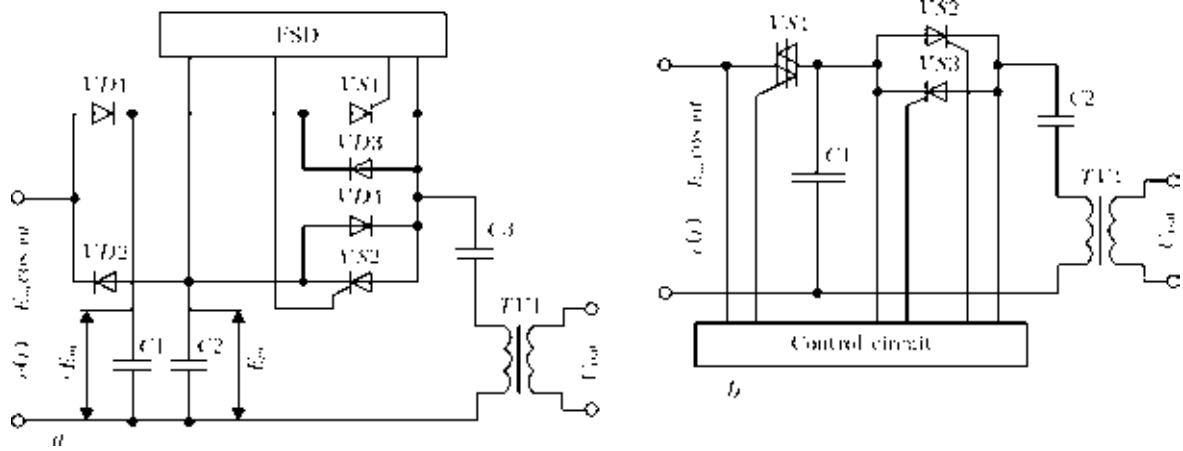


Figure 6. Electric schematic variants of construction of oscillatory constituent in arc exciters with power supply of forming *RCL*-circuit from energy storage devices: *a* – circuit of arc exciter with double-channel energy storage; *b* – circuit of device for arc excitation with single-channel energy storage

rent in the arc circuit at the output of microcircuit *DA1*. This signal is fed into the machine control system and to the input of comparator unit based on microcircuit *DA2*, operation threshold of which is set with the help of resistor *R6*. The voltage from the output of comparator unit is fed to the input of *PSD* turn-off unit (see Figure 4). In the case, when determination of moment of setting of stationary arc discharge in the interelectrode gap is carried out by arc voltage sensor, the signal proportional to this voltage can be fed to the input circuit of comparator unit based on microcircuit *DA2* (see Figure 5), i.e. through resistor *R4*.

The disadvantages of arc exciters with independent power supply designed on basic variant (see Figure 2, *a*) are the dependence of amplitude and energy of output pulses on turn-on angle of thyristors of switching cell *K* and oscillations of source voltages (supply main voltage) as well as the necessity of preliminary regulation (using *PSD*) of the moments of beginning of output pulse generation, in particular, at excitation and stabilization of AC arc.

Effect of supply voltage fluctuations on parameters of output pulses can be minimized to acceptable level by means of application of reactive elements and *PT* in the forming *RCL*-circuit. They are calculated in accordance with given in present work procedure for minimum allowable supply voltage making, as a rule, 85–90 % of nominal values.

Dependence of parameters of output pulses of the arc exciters with independent power supply on the turn-on angle of thyristors of switching cell *K* can be eliminated due to power supply of forming *RCL*-circuit from energy storage devices (mainly of capacitor type). Figure 6 shows the examples of circuit solutions for such devices.

Condensers *C1* and *C2* are the energy storage devices in the arc exciter, constructed based on schematic from Figure 6, *a* [29]. Their charging to the source voltage amplitude value $\pm E_m$ (supply main voltage) is carried out through separation diodes *VD1* and *VD2*.

Arc exciters made based on schematic, presented in Figure 6, *a*, provide the possibility of generation of output pulse, stabilized on amplitude and energy, virtually at any moment of each semi-period of source voltage. At that, discharge of each storage condensers takes place in those semi-periods of source voltage, when the separation diodes connected to these condensers are in nonconducting state. This provided the possibility of application of the arc exciters, built on circuit given in Figure 6, *a*, as universal devices for preliminary excitation of DC and AC arc as well as for stabilizing (re-ignitions) of AC arc [6, 12].

Charging of the storage condenser *C1* in single-channel device, schematic of which is given in Figure 6, *b* [30], starts in the beginning of each semi-period of source voltage at turning on of thyristor cell with double-side conductivity (symistor) *VS1*. Symistor *VS1* is switched on and condenser *C1* is charged till the voltage of *C1* condenser achieves the amplitude value of source voltage. Generation of stabilized amplitude and energy output pulse starts from switching of thyristors *VS2* and *VS3* using the control circuit at any moment of the second part of semi-period of source voltage, but not earlier then 500–700 μ s after turn-off symistor *VS1*. Based on this, area of application of single-channel device (Figure 6, *b*) is an initial excitation of direct current. On practice such devices are used for striking of pilot arc in the plasmatrons for metal welding and cutting.



It should be noted that the devices, circuits of which are shown in Figure 6, do not have wide distribution, regardless some advantages, since in comparison with basic variant of construction of arc exciters (see Figure 2, *a*), the devices with energy storage units (Figure 6) require larger number of semi-conductor devices and passive elements for their realization, therefore have higher static and dynamic losses, more complex structure and lager price.

Necessity of preliminary regulation or adjustment of turn-on angle of thyristors of switching cell for providing effective initial ignition of the DC arc with the help of arc exciters, made on the circuit shown in Figure 2, *a*, can be eliminated using PSD. It is designed on principle of detection of power supply voltage amplitude. One of the examples of circuit solution for such PSD is given in [31].

PSD, which uses differential method of formation of control pulses for switching cell thyristors and based on generation of these pulses at rapid changes of arc voltage, can be used for elimination of necessity of preliminary regulation or adjustment of moments of beginning of generation of output pulses in exciters and stabilizers of arc universal by current type. Example of construction of such PSD can be a control circuit of exciter-stabilizer of arc VSD-03 UZ, given in [3].

Industrial large-scale production of arc exciters with independent power supply and in-series connection to arc circuit, made in form of separate monolithic devices, was mastered at Ukrainian enterprises for the first time in 1975. More than 25,000 of units of arc exciters of UPD-1, UPD-2 and UPD-3 series and their different modifications were manufactured during 1976–1993. They found wide application as devices for contactless initial arc ignition, as well as stabilizers of AC arcing, including during argon-arc welding of aluminum and its alloys [3, 9, 11, 12, 32–34]. Such arc exciters are used in the machines and units for arc and argon-arc (TIG) welding (in particular, in the machines and units of I-118, I-190, UDG-310M, UKhL4 types), in machines for plasma and microplasma welding, surfacing and spraying (for example, UPS-301, UPS-501, UKhL4, UN-150, «Kiev-7», N-155, UMPDS-0605 UKhL4), in the machines for plasma and air-plasma cutting such as «Kiev-4», in gas-cutting machines with program control of «Cristall» type, in the assembly stations for arc and TIG DC and AC welding and in other welding equipment of domestic and foreign manufacture.

Due to change of economic conditions in 1991 the volume of domestic manufacture of electronic

arc exciters has dramatically reduced, however, today their production is carried out in series of foreign countries (mainly as a constituents of technological units) as well as by small batches in Ukraine and Russia. Works on improvement of such devices continue at that.

Conclusions

1. Using the solutions of well-known linear differential equations of the second order, the analysis of electromagnetic processes in the circuit of basic variant of construction of electronic arc exciters with independent power supply and in-series connection to arc circuit, which have found the widest distribution among the boost devices for contactless initial arc ignition and arcing stabilization, was performed.

2. Engineering procedure for calculation of such devices was developed based on carried out analysis and considering experience of development, designing, manufacture and operation of the arc exciters with independent power supply and in-series connection to arc circuit.

3. In recent years the electronic arc exciters, which use voltage multiplication and resonant pumping for formation of increased voltage in oscillation component, gain more and more application. At that, semi-conductor switching cell has parallel connection to in-series connection of capacitor storage device and primary winding of output pulse transformer. Analysis and procedure for calculation of such devices require separate study that is not covered in present work.

Authors would like to express their thanks to engineers V. Yu. Buryak, A. G. Skirta and D. S. Oliyanenko for valuable help in preparation of this work.

1. Paton, B.E., Zavadsky, V.A. (1956) Pulse ignition of arc in gas and manual arc welding. *Avtomatich. Svarka*, **3**, 26–35.
2. Golosubov, V.I. (2005) *Welding power supplies*. Kiev: Aristej.
3. (1986) *Arc welding equipment*: Refer. Book. Ed. by V.V. Smirnov. Leningrad: Energoatomizdat.
4. Pentegov, I.V., Dymenko, V.V., Sklifos, V.V. (1994) Welding power supplies with a pulse arc ignition. *Avtomatich. Svarka*, **7**, 36–39.
5. Gufan, R.M. (1967) *Study of welding oscillators*: Syn. of Thesis for Cand. of Techn. Sci. Degree. Rostov-na-Donu.
6. Temkin, B.Ya. (1981) *Theory and calculation of welding arc exciters*: Syn. of Thesis for Cand. of Techn. Sci. Degree. Leningrad.
7. Gufan, R.M., Zolotykh, V.G., Budnik, N.M. et al. (1966) Universal welding oscillator ISO. *Avtomatich. Svarka*, **8**, 50–53.
8. Leskov, G.I., Lugin, V.P., Svetlov, A.T. (1976) Suppression of radio interference created by exciters and stabilizers of arc discharge. *Ibid.*, **10**, 56–59.



9. Makhlin, N.M., Fedotenkov, V.G., Livshits, D.M. et al. (1979) Suppression of radio interference created by arc exciters of UPD-1 type. *Ibid.*, **12**, 55–57.
10. Lankin, Yu.N., Lapchinsky, V.F., Masalov, Yu.A. (1969) Pulse generator for ignition of welding arc. *Ibid.*, **10**, 61–63.
11. Dudko, D.A., Fedotenkov, V.G., Makhlin, N.M. (1980) Thyristor pulse generators of UPD-1 type. *Ibid.*, **6**, 61–63.
12. Fedotenkov, V.G., Makhlin, N.M., Temkin, B.Ya. (1981) Pulse generator for ignition and stabilization of alternating current arc. *Svarochm. Proizvodstvo*, **8**, 33–34.
13. Paton, B.E., Zaruba, I.I., Dymenko, V.V. et al. (2007) *Welding power supplies with a pulse stabilization of arcing*. Kiev: Ekotekhnologiya.
14. (2008) *Theoretical principles of electrical engineering*: Refer. Book on theory of electric circuits. St.-Petersburg: Piter.
15. Levinshtejn, M.L. (1972) *Operational calculus in problems of electrical engineering*. Leningrad: Energiya.
16. <http://www.dacpol.com.pl>
17. <http://www.elcod.spb.ru>
18. Zamyatin, V.Ya., Kondratiev, B.V., Petukhov, V.M. (1988) *Power semiconductor devices. Thyristors*: Refer. Book. Moscow: Radio i Svyaz.
19. Ermolin, N.P. (1969) *Calculation of low power transformers*. Leningrad: Energiya.
20. Baev, E.F., Fomenko, L.A., Tsybalyuk, V.S. (1976) *Inductive elements with ferromagnetic cores*. Moscow: Sov. Radio.
21. Volgov, V.A. (1977) *Parts and components of electronics*. Moscow: Energiya.
22. Pisarev, A.L., Detkin, L.P. (1975) *Control of thyristor transducers*. Moscow: Energiya.
23. Zeman, S., Osipov, A., Sandyrev, O. (2007) Specifics of operation of high-frequency transformer in circuit of series-resonant inverter. *Silovaya Elektronika*, **1**, 67–72.
24. (2001) *Microcircuits for pulse power supplies and their application*. 2nd ed. Moscow: Dom Dodekaxxi.
25. (1988) *Reference book on electrotechnical materials*. 3rd ed. Leningrad: Energoatomizdat.
26. <http://www.epcos.com>
27. (1971) *Thyristors* (Technical Refer. Book). 2nd ed. Moscow: Energiya.
28. Gottlib, I.M. (2002) *Power supplies. Inverters, converters, linear and pulse stabilizers*. Ed. by S.A. Luzhansky. Moscow: Postmarket.
29. Shmakov, E.I., Fedotenkov, V.G., Kolesnik, G.F. *Device for excitation and stabilization of arcing process*. USSR author's cert. 567563. Publ. 1977.
30. Fedotenkov, V.G., Makhlin, N.M., Turchin, P.S. *Device for arc excitation*. USSR author's cert. 1202768. Publ. 1986.
31. Ivanov, Yu.E., Kozak, V.V., Likhoded, V.P. et al. *Device for switching of thyristors*. USSR author's cert. 1115174. Int. Cl. N 02 M 1/08. Publ. 1984.
32. Shmakov, E.I., Makhlin, N.M., Fedotenkov, V.G. et al. (1978) Application of alternating current for welding of low-alloyed and alloyed steels, aluminium and its alloys. *Montazh. i Spets. Raboty v Stroitelstve*, **4**, 20–22.
33. Bugaev, P.N., Sidoruk, V.S., Makhlin, N.M. et al. (1986) Application of manual arc welding at modulated current in fabrication and assembly of small diameter pipelines. *Montazh. i Spets. Stroit. Raboty*. Series 19: Assembly and adjustment of automation and communication means, **11**, 26–28.
34. Chigarev, V.V., Granovsky, N.A., Kondrashov, K.A. et al. (2007) Power exciter as a stabilizer of welding arc. *Svarochm. Proizvodstvo*, **7**, 14–16.

Received 15.07.2013

WELDED STRUCTURE OF KIEV TV-TOWER IS 40 YEARS OLD

L.M. LOBANOV, E.F. GARF, L.N. KOPYLOV and A.G. SINEOK

E.O. Paton Electric Welding Institute, NASU

11 Bozhenko Str., 03680, Kiev, Ukraine. E-mail: office@paton.kiev.ua

The basic moments connected with the fulfillment of assembly-welding works during building of Kiev TV-tower are described. The peculiar attention is paid to the application of automatic welding in increment of tower supports, as such solution was at the first time applied in practice of building of high-level constructions. 5 Figures.

Keywords: *tower, welding, automatic welding, manual arc welding, pipes, assemblies*

It has been 40 years since the day when the Kiev TV-tower was put into operation. During building of the tower the new design and technological solutions were used to demonstrate the successes and achievements of Kiev school of designing in the field of metal construction and capabilities of modern welding technologies. In spite of fierce resistance to the proposed project of the TV-tower from the side of the All-Union Association on Designing of Building Metal Structures, and also due to active support of Boris E. Paton, the President of the AS of Ukraine, and the UkrSSR Government, it was defended and realized.

Among the main advantages of the TV-tower project, which can serve as an example to follow even today, it cannot be but mentioned, first of all, the following:

- use of tubular sections for the tower elements manufactured of high-strength steel;
- application of connection of assemblies with direct attachment of elements to each other;
- manufacture of all-welded construction with a high rate of using automatic welding;
- application of erection of tower using the method of «increment» for the first time in the domestic practice of such constructions.

The essential component for successful realization of these progressive innovations was welding. We should note that volume of welding during erection of tower was very high, as the pipes were manufactured of a sheet and enlarged using circumferential butts. During erection all the joints were also produced using welding.

During construction of tower the automatic CO₂ welding and manual electric arc welding using consumable electrode were used.

Manufacture of pipes. The pipes were manufactured of a sheet at the Zhdanov Heavy Machine-Building Plant. The technological process of manufacture of pipes envisaged the following succession of operations:

- edges preparation and chamfering for two longitudinal butt welds;
- cold stamping of billets (semi-pipes) of 4000 mm length;
- assembly and welding of pipes in a specially manufactured stand. The welding of outer and inner longitudinal butt welds was performed in accordance with the technology developed by the E.O. Paton Electric Welding Institute and the Laboratory of Central RSI of Shipbuilding Technology. Moreover, a specially developed small-sized tractor TS-42 for submerged arc welding of inner longitudinal welds was used. For the automatic submerged arc welding, wire Sv-08N2M in combination with flux 138KF-1 was applied;
- quality control of welded joints;
- heat treatment of pipes for removal of inner stresses in the pipe formed in the process of formation of chutes and welding of longitudinal welds;
- calibration of pipe ends in the cold state allowing the performance of their alignment without special difficulties;
- final operation was chamfering for welding on the ends of pipes.

Automatic welding of circumferential butts of girths during erection of tower. The method of erection by «increment», accepted during development of the project of the tower, allowed performing all the basic welding-assembly works on welding the columns of the tower trunk from the stationary assembly sites, located at the height of 18 m from the ground surface and fastened on the guiding jig located inside the trunk of the tower (Figure 1).



Figure 1. Removable erection platform for performance of automatic welding

This allowed applying the automatic welding during increment of the most critical elements of the tower (8 vertical columns of girth pipes of 550 mm diameter with the wall thickness of 18 and 22 mm), and thus realizing all the advantages of automatic welding both from the point of view of quality guaranteeing, as well as from the position of labor capacity.

At the initial stage the works on development of the technique and technology of welding were fulfilled. The basic tasks solved at this stage: to provide the high quality of a weld and strength of welded joint not lower than the strength of



Figure 2. Macrosection of welded joint of a pipe produced using automatic CO₂ welding

base metal, and to obtain maximum efficiency of the welding process.

The experimental works on the development of technological process of automatic welding were performed by a group of associates (V.S. Krivosheya, the supervisor, L.N. Kopylov and V.M. Zil, leading engineers) under the leadership of B.Ya. Dubovetsky, the Laureate of the Lenin Prize, and Prof. B.F. Lebedev. PWI Research laboratories were also involved in the work. For the experimental research on development of technique and technology of welding of horizontal welds in a vertical plane the laboratory installation was mounted, on which the full-scale specimens of pipes were welded.

After welding of shells the quality of a weld was tested (ultrasonic flaw detection, gamma-ray examination), then the plates were cut out from the welded joint, the specimens for mechanical and metallographic investigations were manufactured. From the test results the correction of parameters of welded process was carried out, which was considered during fulfillment of the following experiments.

The girth pipes of the tower trunk were manufactured of steel IZ-138 with the increased strength characteristics. This steel melted at the Izhorsky Metallurgical Plant was at the first time applied in the practice of building of the objects of the tower type, therefore it was necessary to perform a large volume of investigations on its weldability. During conduction of experiments a number of difficulties were encountered. In particular, at the initial stage of investigations, during conduction of mechanical tests of welded joints, the positive results during bending tests of specimens (the requirement – 180°) were not achieved. The required results were achieved after application of the simple technological method of surfacing of four-five annealing beads on the lower and upper edges of a butt (Figure 2).

As a result of fulfilled experimental works the optimal V-shape edge preparation of butt joint of a pipe with minimum cross section area of a weld was found. Bevel of a low edge was equal to 11°, the upper one to 27°. The basic parameters of technological process were determined, the technique of automatic welding of horizontal circumferential welds in the vertical plane was developed providing the defect-free welded joints.

The developed technological process provided the equal strength of welded joint and base metal of pipes.

Basing on the data obtained during development of technique and technology of welding, the Technological Manual on welding of erection

butts of girth pipes of tower trunk and the Technical Assignment on designing of the equipment for automatic welding of horizontal circumferential butts were worked out.

The development of the design of the equipment for welding of assembly butts of girth pipes of the tower trunk was performed under the supervision of Vladimir E. Paton. The main performers of design documentation were Yu.I. Saprykin and V.N. Kotov. During development of the design it was assumed that at erection of the tower trunks the loads would relieve simultaneously from two diametrically opposite vertical columns. Thus, the simultaneous welding of two butts could be performed. Therefore, to reduce the costs on reinstallation of welding equipment and to provide maximum labor efficiency of welding works, the decision was adopted to use simultaneously two sets of welding automatic machines during erection of the tower and to arrange the automatic machines on the transport carriage for convenient transportation of the equipment during welding of the following butts.

The team of designers of the PWI Experimental Design Bureau developed the design of specialized welding automatic machine A-1311 composed of the welding head with the guiding rail (Figure 3).

At the PWI Pilot Plant of Welding Equipment two sets of welding automatic machines A-1311 were manufactured. The equipment passed technological tests and was transferred to Construction and Election Organization of the UkrSSR Minmontazhspejsstroj.

The specialists of the E.O. Paton Electric Welding Institute conducted training of the welders team of the erection organization, which mastered successfully the technique of automatic welding and methods of work on welding automatic machines within a short period and were attested and obtained the permission to perform the works on automatic welding of site butts of girth pipes of the tower. For quality performance of automatic welding a number of organization-technical measures was carried out:

- at the building site the stand for preliminary control assembly of pipes being welded was equipped;
- in the zone of erection sites the tracks were mounted providing possibility of transportation of welding automatic machines from butt to butt;
- removable platforms were equipped mounted during welding of site butt and lowered during rise of the tower;
- quick-detachable tents protecting the erection site from wind during welding were manufactured;

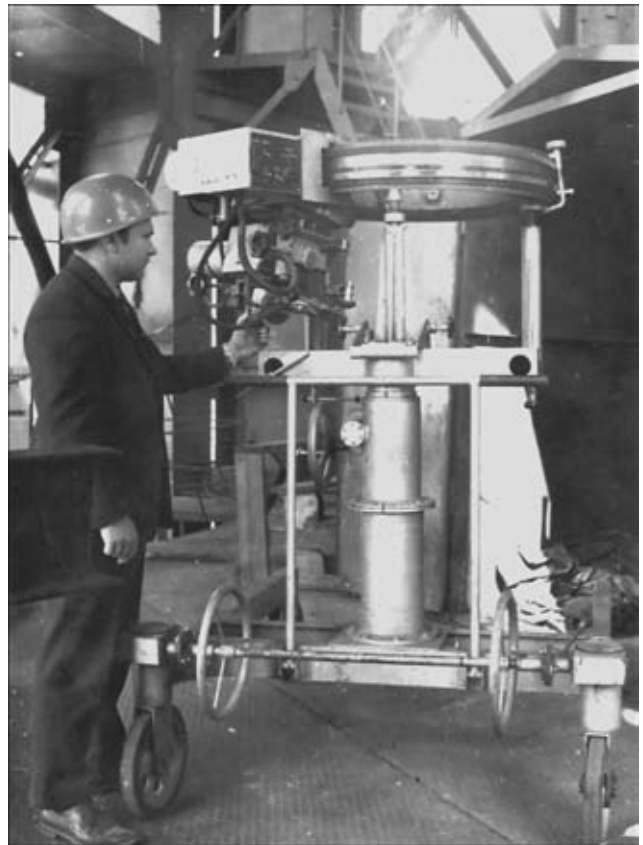


Figure 3. Welding machine A-1311 on the technological transport carriage

- erection sites for welding were provided with illumination.

The works on erection of the tower and also automatic welding of site butts of girth pipes were conducted in two shifts. The technological process of their assembly and welding was optimized.

On the stand for reference assembly of pipes two pipes were laid, which had to be aligned with each other, the most favorable arrangement of abutted ends was selected. To the end of the pipe, which will be the lower during assembly of the erection butt, a barrel-like metallic backing ring of 4 mm thickness was mounted. Then, on the side of the outer surface the ring was welded on to the root area of the pipe by a solid weld around the whole perimeter of the ring. At the outer surface of pipes a mark was made by a paint allowing the repeating of given position of pipes during the assembly. After the unloading of two diametrically arranged jacks providing the lifting of tower, a lower pipe was installed on the jacks pushers, a pipe was brought to the lower end of the upper pipe using jacks and the technological gap in the root was set.

Before welding the automatic machine was moved to the place of welding, fastened on the butt being welded, the carriage was removed from



Figure 4. Quality control of assembly of circumferential butt

the erection site, and protective tent was installed.

The site butt was assembled at the technological gap of 3–4 mm in the root. The multipass welding of the site butt was performed with the preliminary heating of edges up to 180–200 °C. For preheating the multi-flame gas oxygen-free torch was used, which was fastened on the welding machine ahead the welding nozzle. After heating of the initial area of a butt to the necessary temperature the welding process started.

For welding the electrode wire Sv-10GSMT of 1.2 mm diameter was applied. The welding of inner passes of a weld was performed at the current of 230–250 A and arc voltage of 23–24 V. The conditions of the finishing passes were the following: 50–180 A current, 19–21 V voltage. Depending on the thickness of the pipe wall (18 or 22 mm) to fill the groove it was necessary to deposit 16–20 passes. The linear speed of welding of separate passes was 13–15 m/h.

During welding the periodic cleaning of the weld surface from a slag was performed using an abrasive tool. After completion of welding of a butt the cleaning of the surface of welded joint was performed using an abrasive tool, and the weld was given a barrel-like shape. Such a treatment improves the service characteristics of welded joint and enables the quality performance of ultrasonic testing of a weld.

Then 100 % ultrasonic testing of welded joint was carried out. When it was necessary to specify

the results, the gamma-ray examination was applied. Within the whole period of construction there was no a single case of repair of weld defects.

The total time of welding of one butt with the setting up of equipment, installation and disassembly of protective tent did not exceed 2.5 h, where the duration of welding was not more than 1.5 h.

Within the whole period of construction of Kiev TV-tower the specialists from the E.O. Paton Electric Welding Institute provided the author's supervision at all the stages of assembly-welding works of metal structures of the tower trunk (Figure 4) which contributed to the increase of quality of welded joints.

Manual electric arc welding. The considerable volume of works during construction of the tower was performed using manual consumable electrode arc welding. The control of all the operations connected with manual welding was performed by the PWI group of associates, headed by V.A. Kovtunenکو.

The method of erection using «increment» allowed welding the elements of the grate (steel 20) with the tower supports not at a great height, within the range of two tiers. As the joining of elements of grate with the supports was performed by direct attachment along the spatial curve, a great attention was paid to cutting-on of pipe ends of grate elements (Dnepropetrovsk I.V. Babushkin Steelwork Plant). For this purpose the Plant together with the All-Union RSI «Avtomat» and Odessa Plant «Avtogenmash» manufactured the machine providing cutting-on of ends of the required quality. Only in single cases during erection the fitting-up was required to provide the required gaps.

The assembled joints of elements were admitted to welding after their acceptance by a representative from the E.O. Paton Electric Welding Institute and a welding inspector of C&EO with registration in the log book of assembly works. The marking was made on the joint allowing welding to be performed.

The welding was performed using low-hydrogen electrodes of 48N-1 grade providing the mechanical properties of welded joint on the level of steel of S-60 class. The welding was performed at the temperature of not lower than –15 °C. Independently of the temperature of the environment, in welding of assembly joints the preheating to 50–60 °C was applied to remove condensate. The welding was performed using in-line multilayer welds (Figure 5).

Sticking between the beads was regulated within the range of 1.0–1.2 mm with a smooth transition from weld metal to base metal.

The joints on the areas of complete penetration were tested using ultrasonic method. In some spots, which required profound decoding of testing results, the gammagraphy was applied. The development of procedures and control were performed by the PWI associates.

Using manual electric arc welding a considerable amount of butt joints of pipes in the support part, in the support of grate part of the antenna «Altaj» and stem of the antenna were performed.

The butt joints were performed on the backing ring using the same welding consumables. At the E.O. Paton Electric Welding Institute the technology and technique of welding, optimal conditions providing the stable quality of welded joints were tested. All the welders passed qualification selection with the obligatory welding of reference specimens. In welding of steel of grade 14KhGN2MD (IZ-138) the preheating up to 160–200 °C was necessary. In the rest the requirements to welded joints were similar to those accepted for assembly joints.

The other joints (frame of the building, links, platforms) were also made using manual electric arc welding.

In conclusion one cannot but note that even after 40 years the Kiev TV-tower is the example of perfection of engineer idea and also a high level of design and technologies used during construction.

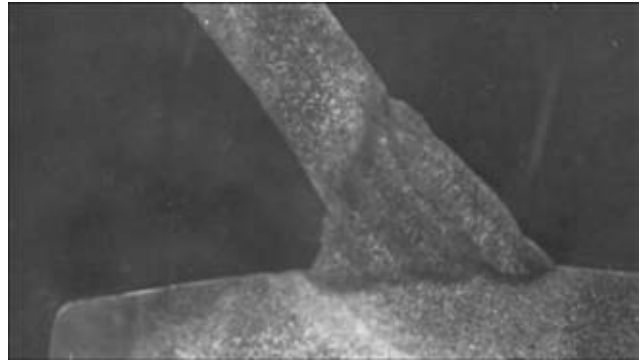


Figure 5. Macrosection of joint produced using manual electric arc welding

In building of the tower a great number of engineers-designers, scientists, erectors, engineers and workers of building specialties took part. Each of them made his great contribution into the creation of a unique construction, decorating Kiev even today. On the occasion of anniversary date from the day of creation of the tower the contribution of O.I. Shumitsky and V.I. Novikov should be especially marked, who made great efforts to realize the project in a form in which it was realized, decided to implement new and extraordinary for that time engineering solutions. And one should note also the support of new ideas on the side of B.E. Paton, without which the realization of the project under those conditions would be unreal.

Received 16.07.2013

CALCULATION OF UPSETTING FORCE IN FLASH BUTT WELDING OF CLOSED-SHAPE PRODUCTS

P.N. CHVERTKO, A.V. MOLTASOV and S.M. SAMOTRYASOV

E.O. Paton Electric Welding Institute, NASU

11 Bozhenko Str., 03680, Kiev, Ukraine. E-mail: office@paton.kiev.ua

In structure elements of flying vehicles the ring-type parts of high-alloy steel and alloys are widely applied. To manufacture such structure elements different methods of fusion welding are applied including flash butt welding (FBW). Technology of FBW of such parts requires high upsetting speeds $\geq 50\text{mm/s}$ with a specific force of not less than 120–200 MPa. In FBW of parts of a closed shape it is important to determine the value of necessary upsetting force. At unlimited or insufficient upsetting force the necessary conditions for joint formation in a solid phase will not be provided, and during overheating the part shortening will be rather large. Both conditions will lead to violation of shape of ring-type parts, in particular, in perimeter. In the process of welding the elastic forces appear in product being welded, hindering the joint formation, which should be determined in the development of technology and equipment for welding. Besides, in welding of ring-type billets of a large section, which are characterized by a significant elasticity, it is necessary to take into account the possibility of a welded butt rupture due to elasticity of billet at insufficient time of upsetting without passing of electric current. Calculation of the above-mentioned forces was carried out according to the theory of thin rods under the conditions, when stress-strain state was considered to be linear. Also the calculation of given forces using the methods of elasticity theory was carried out, and as a result the plain problem of elasticity theory was solved. The comparison of results of calculation of eight rings with different characteristic sizes showed that maximum difference of values of upsetting force, calculated by the theory of thin rods and formulae of plane problem, was about 2 %, and the values of forces, rupturing a butt after welding, was less than 1 %. Moreover, in decrease of ratio of external radius of the ring to its internal radius the accuracy of calculation according to the theory of thin rods is increased. 7 Ref., 1 Table, 4 Figures.

Keywords: *flash butt welding, rings, high-alloyed steels, stress-strain state, upsetting force, theory of thin rods, plain problem*

In industry, to manufacture the parts and structures of a closed shape of different purpose (elements of engines, different bandages, turntables, bearings, flanges, etc.), different methods of welding are applied (arc, electron beam, flash

butt, etc.) on which the service characteristics of welded joint greatly depend.

One of the most saving and technically simple processes of manufacture of ring-type billets is FBW [1]. This method provides high stable quality of welded joints, unites welding and assembly operations in one cycle and does not require application of auxiliary consumables (electrodes, fluxes, welding wires, shielding gases, etc.).

At the E.O. Paton Electric Welding Institute the technology and equipment [2] for FBW of ring-type parts under the industrial conditions were developed (Figure 1). The technology was based on the method of FBW with pulsating flashing [3], which provides the highly-concentrated heating, due to which the HAZ is decreased.

The calculation diagram of loading the ring, on which the upsetting force P and reactive moment M from the movable clamping device of the machine, corresponding to Figure 1, are affected, is given in Figure 2.

It can be assumed as the first approximation that the sizes of the cross section of the ring are

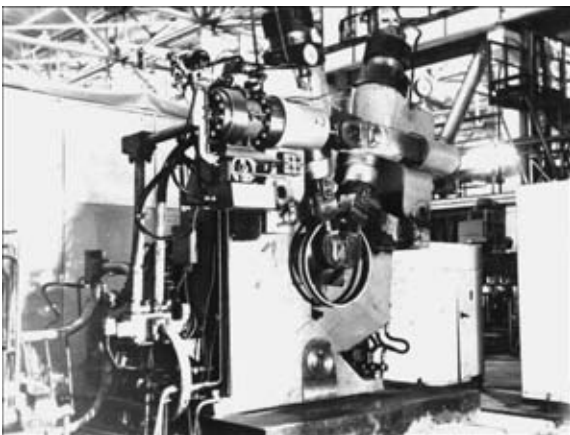


Figure 1. Ring-type billet in the clamping devices of butt welding machine K607

small as compared to its average radius, then the problem can be solved using the thin rods theory.

To determine forces P it is rationally to relate it with the value of elastic movement δ_{el} from the initial gap up to the final position considering the shortening of part due to flashing and upsetting. The value of elastic movement in a curvilinear contour should be determined using More integral:

$$\delta_{el} = \int_S \frac{\overline{M}M_p ds}{EI_z}, \quad (1)$$

where \overline{M} is the expression for moment from single force applied in the direction of force P ; M_p is the expression for the moment from active and reactive forces; I_z is the moment of section inertia; E is the elasticity modulus of the first kind.

Using canonic equations of method of forces [4], the value of reactive moment $M = P(a + b)/2$ was found. Considering that the expression for bending moment in ring sections has a form

$$M_p = \frac{1}{2} P(a + b) \cos \theta. \quad (2)$$

Expression for determination of moment from action of single force $P = 1$ will be written in a form

$$\overline{M} = \frac{1}{2} (a + b)(1 - \cos \theta). \quad (3)$$

Substituting expressions (2) and (3) into (1), the value of elastic movement was determined:

$$\delta_{el} = \frac{1}{EI_z} \times \left[2 \int_0^\pi \frac{1}{2} P (a + b) \cos \theta \frac{1}{2} (a + b) (1 - \cos \theta) \frac{1}{2} (a + b) d\theta \right] = \frac{\pi P(a + b)^3}{8EI_z},$$

from which it is possible to obtain the upsetting force

$$P = \frac{8EI_z}{\pi(a + b)^3} \delta_{el}. \quad (4)$$

We obtain the more precise solution of this problem by solution of plane problem of theory of elasticity. This solution belongs to Kh.S. Golovin and is described in work [5]. Therefore, we give only expressions for stresses:

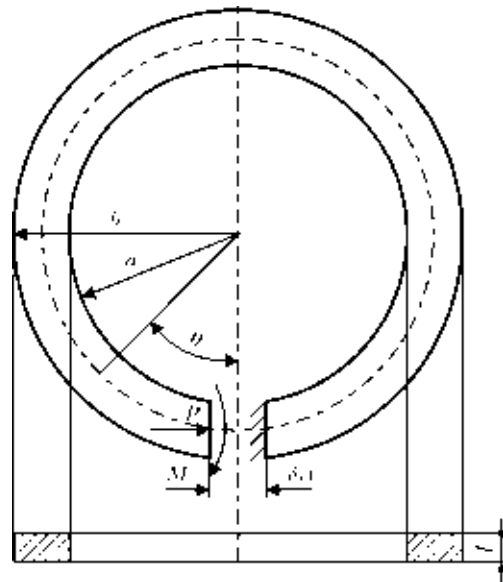


Figure 2. Schematic of ring loading in FBW

$$\begin{cases} \sigma_r = \frac{\partial \varphi}{r \partial r} + \frac{\delta^2 \varphi}{r^2 \partial \theta^2} = \left(2Ar - \frac{2B}{r^3} + \frac{D}{r} \right) \cos \theta, \\ \sigma_\theta + \frac{\partial^2 \varphi}{\delta r^2} = \left(6Ar + \frac{2B}{r^3} + \frac{D}{r} \right) \cos \theta, \\ \tau_{r\theta} = - \frac{\partial}{\partial r} \left(\frac{\partial \varphi}{r \partial \theta} \right) = \left(2Ar - \frac{2B}{r^3} + \frac{D}{r} \right) \sin \theta, \end{cases} \quad (5)$$

where A , B and D are the constants determined by the boundary conditions. In our case they are equal:

$$A = \frac{-P}{2R}; \quad B = \frac{Pa^2b^2}{2R}; \quad D = \frac{P}{R} (a^2 + b^2). \quad (6)$$

Moreover

$$R = a^2 - b^2 + (a^2 + b^2) \ln \frac{b}{a}.$$

Unlike work [5] where during study of movements the functions of complex variable were used, we used the method, which was applied in [6] for solution of problem about the action of tangent force applied at the end of a curvilinear rod.

The components of deformation in the polar coordinates has the following form:

$$\varepsilon_r = \frac{\partial u}{\partial r}; \quad \varepsilon_\theta = \frac{u}{r} + \frac{\partial v}{r \partial \theta}; \quad \gamma_{r\theta} = \frac{\partial u}{r \partial \theta} + \frac{\partial v}{\partial r} - \frac{v}{r}. \quad (7)$$

Through the components of stress (5) the components of deformation in plain-stressed state are expressed in the following way:

$$\varepsilon_r = \frac{1}{E} (\sigma_r - \mu \sigma_\theta); \quad \varepsilon_\theta = \frac{1}{E} (\sigma_\theta - \mu \sigma_r); \quad \gamma_{r\theta} = \frac{\tau_{r\theta}}{G}, \quad (8)$$

where

$$G = \frac{E}{2(1 + \mu)}$$

Having compared the expressions for ϵ_r from (7) and (8) considering (5), we obtained after integration

$$u = \frac{\cos \theta}{E} \times \left[Ar^2(1 - 3\mu) + \frac{B}{r^2}(1 + \mu) + D(1 - \mu) \ln r \right] + f(\theta), \quad (9)$$

where $f(\theta)$ is the function depending only on the argument θ , which will be determined below. By substitution of obtained expression (9) into expression for ϵ_θ from (7) considering (8) we shall obtain after integration

$$v = \frac{\sin \theta}{E} \times \left[Ar^2(5 + \mu) + \frac{B}{r^2}(1 + \mu) + D(1 - \mu)(1 - \ln r) \right] - \int f(\theta) d\theta + F(r), \quad (10)$$

where $F(r)$ is the function depending only on the argument r , which also will be determined below. Substituting obtained expression (10) together with expression (9) into expression for $\gamma_{r\theta}$ from (7) considering (8) we shall obtain

$$\frac{4D \sin \theta}{E} = r \frac{dF}{dr} + \int f(\theta) d\theta - F(r) + \frac{df(\theta)}{d\theta},$$

which should comply with functions $f(\theta)$ and $F(r)$. These functions were determined by the authors in the following form:

$$f(\theta) = \frac{2D}{E} \theta \sin \theta + K \sin \theta + L \cos \theta; F(r) = Hr, \quad (11)$$

where K, L, H are the arbitrary constants determined from the conditions of clamping.

Considering (11) the expressions for components of movement have a form

$$\left\{ \begin{aligned} u &= \frac{2D}{E} \theta \sin \theta + \frac{\cos \theta}{E} \times \\ &\times \left[Ar^2(1 - 3\mu) + \frac{B}{r^2}(1 + \mu) + \right. \\ &\left. + D(1 - \mu) \ln r \right] + K \sin \theta + L \cos \theta; \\ v &= \frac{2D}{E} \theta \cos \theta + \frac{\sin \theta}{E} \times \\ &\times \left[Ar^2(5 + \mu) + \frac{B}{r^2}(1 + \mu) + \right. \\ &\left. + D[(1 - \mu)(1 - \ln r) - 2] \right] + K \cos \theta - L \sin \theta + Hr. \end{aligned} \right. \quad (12)$$

Tangential movement of a free end can be obtained by substituting value $\theta = 0$ into expression for v , then

$$v(\theta = 0) = K + Hr. \quad (13)$$

Constants K, H are determined from the conditions on stationary fixed end $\theta = 2\pi$, where $v = 0, \partial v / \partial r = 0$. Substituting that into expression for v from (12) the unknown constants were determined:

$$K = -\frac{4\pi D}{E}; H = 0. \quad (14)$$

Thus, using formulae (6) we will find at $\theta = 0$

$$v = \delta_{el} = -\frac{4\pi P(a^2 + b^2)}{E \left[a^2 - b^2 + (a^2 + b^2) \ln \frac{b}{a} \right]}. \quad (15)$$

From formula (15) we shall determine the upsetting force:

$$P = \frac{E \delta_{el} t}{4\pi(a^2 + b^2)} \left[a^2 - b^2 + (a^2 + b^2) \ln \frac{b}{a} \right]. \quad (16)$$

The character « \rightarrow » evidences that direction of movement v does not coincide with the direction of growth θ . It should be noted that thickness t was introduced to formula (16) as for the solution of plane problem we would obtain the force per a unit of thickness. Rejects and defects in welding are mainly detected after operation of calibration or in the process of subsequent mechanical treatment. Those rings can be considered defective, in which during removal of upsetting force the cracks are formed in a butt or fracture along the welded butt is occurred.

During determination of force tending to rupture the butt joint after welding, it is necessary to consider that during removal of the upsetting force the reactive moment stops acting as far as clamping device creating this reaction is open. Thus, when a weldment is trying to obtain the previous geometric shape, the stressed state is predetermined only by the effect of the force P , directed to the opposite direction to the upsetting force (Figure 3).

To solve this problem by the theory of thin rods it is sufficient to substitute into expression (1) instead of (2)

$$M_p + \frac{1}{2} P(a + b)(1 - \cos \theta). \quad (17)$$

Then we shall obtain

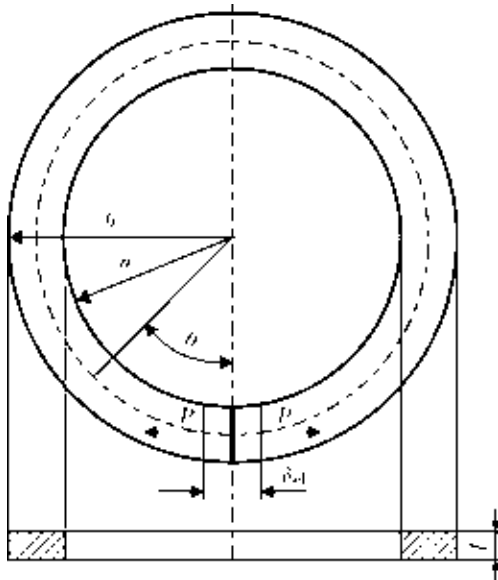


Figure 3. Schematic of ring loading after welding

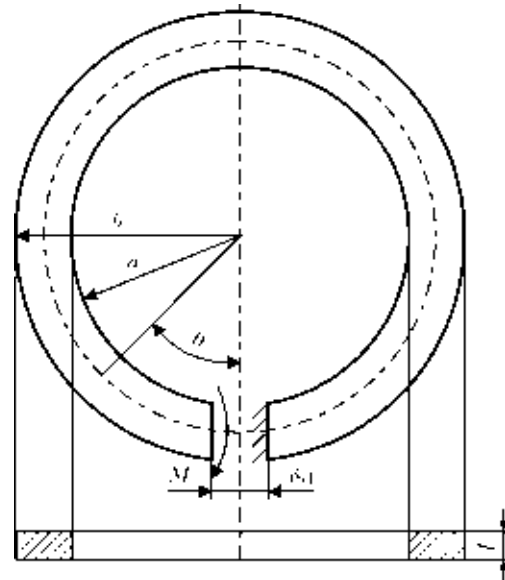


Figure 4. Calculation scheme of ring under bending by moment in curvature plane

$$\delta_{el} = \frac{1}{EI_z} \times \left[1 \int_0^\pi \frac{1}{2} P(a+b)(1-\cos\theta) \frac{1}{2} (a+b)(1-\cos\theta) \frac{1}{2} (a+b)d\theta \right] = \frac{3\pi P(a+b)^3}{8EI_z}$$

from where it is possible to obtain the force, tending to rupture the butt joint after welding:

$$P = \frac{8EI_z}{3\pi(a+b)^3} \delta_{el} \tag{18}$$

As is seen from expression (18), in the frames of theory of thin rods the force P , tending to rupture the butt joint after welding, is always 3 times less than the upsetting force determined by formula (4).

It should be noted that formula (18) coincides with formula, obtained in work [7], in another way. To solve this problem using methods of theory of elasticity it is necessary to subtract stresses,

arising under the action of moment, from expressions (5) (Figure 4):

$$v = \frac{8\pi M(a+b)(b^2-a^2)}{E \left[(b^2-a^2)^2 - 4a^2b^2 \left(\ln \frac{b}{a} \right)^2 \right]} \text{ at } \theta = 2\pi. \tag{19}$$

The solution of this problem also belongs to Kh.S. Golovin and is available in literature [5, 6].

The value of elastic deformation δ_{el} consists of movement, given by formula (15), taken with an opposite sign, and movements given by formula (19). Taking into account that $M = P(a+b)/2$ and multiplying by thickness t , we shall obtain expression for the force acting on the butt joint after welding

$$P = \frac{E\delta_{el}t}{4\pi N}, \tag{20}$$

where

Results of calculation of upsetting forces and forces rupturing butt joint after welding

a , mm	b , mm	t , mm	δ_{el} , mm	P_w , kN (4)	P_w , kN (16)	ΔP_w , %	P_r , kN (18)	P_r , kN (20)	ΔP_r , %
160	210	10	13	13.62	13.48	1.08	4.54	4.52	0.52
180	230	12	14	12.94	12.83	0.88	4.31	4.29	0.43
255	347	14	20	42.44	41.86	1.37	14.15	14.05	0.67
243	323	16	19	36.45	36.03	1.18	12.15	12.08	0.57
241	351	16	22	95.89	94	2.01	31.96	31.65	0.98
175	215	22	16	16.13	16.03	0.63	5.38	5.36	0.31
181	216	25	16	11.64	11.58	0.46	3.88	3.87	0.26
356	421	25	21	13.05	13	0.42	4.35	4.34	0.23



$$N = \frac{(a^2 + b^2)}{a^2 - b^2 + (a^2 + b^2) \ln \frac{b}{a}} + \frac{(a^2 + b^2)(b^2 - a^2)}{(b^2 - a^2)^2 - 4a^2b^2 \left(\ln \frac{b}{a} \right)^2}$$

Results of calculations for eight typical rings of steel 12Kh18N10T ($E = 200,000$ MPa), which are used in the structure elements of flying vehicles manufactured at the SE «A.M. Makarov Yuzhny Machine Building Plant», are given in the Table.

In the Table according to results of calculation of upsetting force, made using the theory of thin rods (4) and the method of theory of elasticity (16), maximum deviation ΔP_w is about 2 %. Similarly using formulae (18) and (20) the forces, tending to rupture the butt joint after welding, were calculated, maximum deviation ΔP_r here was less than 1 %. It evidences that in this case the theory of thin rods gives very accurate results. Besides, it can be noted that the error is decreased at decrease of b/a ratio (in fact, if b is tending to a , we shall obtain a thin rod and the error will tend to zero).

Conclusions

1. Using two analytical methods of calculation the expressions for determination of upsetting

force necessary in FBW of ring-type billets and the force tending to rupture the butt joint after welding were obtained.

2. The results of calculations by formulae are given, obtained on the basis of different calculation methods, for eight typical rings. The maximum deviation of value of upsetting force was about 2 % and that for rupture was less than 1 %.

3. The technology and equipment were developed for industrial manufacture of rings of heat-resistant alloys and steels of types 12Kh18N10T, EI711 and EI712 with the diameter of middle surface from 370 to 777 mm and 500–1760 mm² cross section area.

1. Kuchuk-Yatsenko, S.I. (1992) *FBW*. Kiev: Naukova Dumka.
2. Kuchuk-Yatsenko, S.I., Chvertko, P.N., Semyonov, L.A. et al. (2013) FBW of products of high-strength alloys based on aluminium. *The Paton Welding J.*, **7**, 2–6.
3. Kuchuk-Yatsenko, S.I., Didkovsky, V.A., Bogorsky, M.V. et al. *Method of resistance butt welding*. Pat. 46820 Ukraine. Publ. 17.06.2002.
4. Pisarenko, G.S., Yakovlev, A.P., Matveev, V.V. (1975) *Handbook on strength of materials*. Kiev: Naukova Dumka.
5. Lurie, A.I. (1970) *Theory of elasticity*. Moscow: Nauka.
6. Timoshenko, S.P., Goodier, J.N. (1975) *Theory of elasticity*. Moscow: Nauka.
7. Kochergin, K.A. (1952) *Selection of technology of resistance welding*. Leningrad: Sudpromgiz.

Received 25.08.2013

PROPERTIES OF FUSION-WELDED JOINTS ON HIGH-STRENGTH TITANIUM ALLOY T110

S.V. AKHONIN¹, V.Yu. BELOUS¹, S.L. ANTONYUK², I.K. PETRICHENKO¹ and R.V. SELIN¹

¹E.O. Paton Electric Welding Institute, NASU

11 Bozhenko Str., 03680, Kiev, Ukraine. E-mail: office@paton.kiev.ua

²SE «Antonov»

1 Akademik Tupolev Str., 03062, Kiev, Ukraine. E-mail:lavrenko@antonov.com

At present time, welding of high-strength titanium alloys can be performed using arc, electron beam in vacuum (EBW) and laser beam. There are successful examples of application of combined laser-arc process for performance of welded joints of titanium alloys. Negative effect of thermal cycle of EBW and laser welding on properties of series of alloyed titanium alloys is indicated in some cases. Aim of the present work lied in investigation of effect of different methods of welding and filler metal on mechanical properties and structure of welded joints by the example of titanium alloy T110. It is shown that high-strength titanium alloy T110 differs in good weldability in performance welded joints by EBW, full penetration argon-arc tungsten-electrode welding, argon-arc tungsten-electrode welding over the flux layer and laser-arc welding. SP-15 grade wire is reasonable for application as filler for argon-arc welding of T110 alloy. If welding without filler material is used, argon-arc tungsten-electrode welding over the flux layer provides the highest values of impact toughness of weld and HAZ metal. 8 Ref., 2 Tables, 3 Figures.

Keywords: titanium alloys, T110, argon-arc welding, properties, laser welding, flux

Titanium alloys are characterized by high strength, heat resistance at moderate temperatures and corrosion resistance in the most aggressive media. Due to such properties they find application during manufacture of critical structures in aircraft and engine construction, chemical and other branches of industry. Today more and more attention is focused on expansion of application of welded structures and assemblies from high-strength titanium ($\sigma_t \geq 1100$ MPa).

Welding is one of the most widespread technological processes at development of complex parts and assemblies. Therefore, weldability of titanium alloy is an important factor determining relevance of its application.

However, weldability of current high-strength titanium alloys, application of which could provide the maximum reduction of structure weight, is significantly worse than of low-alloyed alloys. Some high-strength steels are even inferior to them in this index.

The E.O. Paton Electric Welding Institute together with SE «Antonov» developed new high-strength titanium alloy T110 of Ti–Al–Mo–V–Nb–Fe–Zr system, containing the following alloying elements, wt.%: 5.0–6.0 Al, 3.5–4.8 Nb, 0.8–1.8 Mo, 0.8–2.0 V, 1.5–2.5 Fe and 0.3–

0.8 Zr [1, 2]. Developed alloy exceeds VT22 and VT23 alloys on its service characteristics.

At present time, welding of high-strength titanium alloys can be performed by arc, electron beam in vacuum and laser beam. Arc welding allows changing chemical composition of weld metal and has such advantages as cheap and simple equipment. EBW and laser welding differ in high energy concentration in a heating spot and, respectively, high penetrability and efficiency. However, feeding of filler metal at that is complicated.

Negative effect of thermal cycle of EBW and laser welding on properties of series of alloyed titanium alloys VT23 and VT22 [3] is marked in some cases. It is concerned with high rates of heating and cooling of weld and HAZ metal. There are successful examples of application of combined laser-arc process in performance of welded joints from titanium alloys [4]. Therefore, study of effect of different methods of welding on mechanical properties and structure of welded joints from high-strength titanium alloy T110 seems to be reasonable.

Aim of the present work lied in study of effect of different methods of welding and filler metals on mechanical properties and structure of welded joints by the example of alloy T110.

Properties of T110 welded joints 7 and 13 mm thick made by different methods were investi-

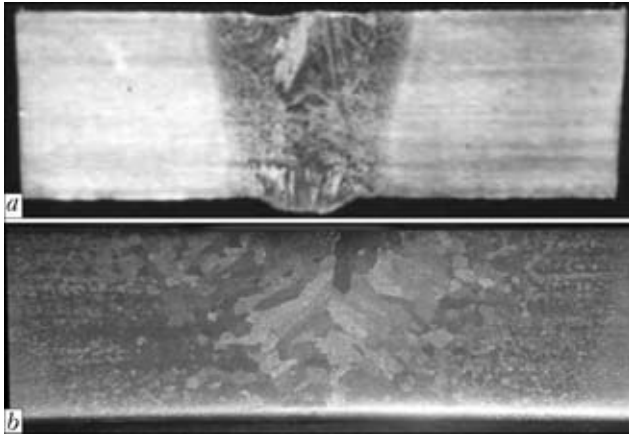


Figure 1. Transverse macrosections of EB- (a) and TIG-welded (b) joint from titanium alloy T110 of 7 mm thickness

gated in course of works. Mechanical properties of the base metal are given in Table 1.

Plates of T110 alloy of 7 mm thickness were welded by EBW, full penetration argon-arc tungsten-electrode (TIG), argon-arc tungsten-electrode welding over the flux layer (A-TIG) [5] and groove argon-arc tungsten-electrode welding (groove TIG). In the latter case alloyed wire of SP-15 grade (Ti-4.5Al-2.5Mo-2.5V-3.5Nb-1.5Zr) [6] was used as a filler. It can be used for welding of high-strength titanium alloys VT23 and VT22 [7].

TIG welding of plate 7 mm thick was carried out in automatic mode by laboratory welding head applying power source the ESAB ARISTO-500. EBW was performed using UL-144 unit, equipped with ELA 60/60 power source. Weld-

Table 1. Mechanical properties of titanium alloy T110

BM thickness, mm	σ_t , MPa	$\sigma_{0.2}$, MPa	KCV, J/cm ²
7	1190	1150	31
13	1130	999	38

ing of metal by A-TIG method was made using flux of ANT-25A grade [8]. T110 titanium plates 13 mm thick were welded by laser-arc method. Laser welding was used for surfacing of T110 alloy plates of 13 mm thickness. Laser and laser-arc welding were carried out using laser unit DY 044 (Nd:YAG laser, wave length 1.06 μm) on scheme, according to which tungsten electrode is positioned before laser beam and the laser beam itself comes into tail part of the weld pool [4]. At that, welding rectifier VDU-601 was used as welding arc power source.

The examples of performed joints are shown in Figures 1 and 2.

Metal of welds, made by EBW, consists of transformed equiaxed β -grains, inside which uniform decomposition of solid solution with precipitation of disperse colonies of particles of secondary α -phase is observed. The grains of former β -phase is finer in the near-weld zone, that indicates lower heat input in accumulative re-crystallization. Size of the polyhedral equiaxed grains reduces with increase of distance from the fusion zone to the base metal. EB-welded joints of T110 alloy, as well as welded joint of commercial titanium alloys of similar type, have high strength, insufficient ductility and impact toughness. Therefore, in order to increase these characteristics the welded joints of T110 alloy, made by EBW, should be annealed.

Dendrite structure (Figure 3, a) is well-observed in the weld of T110 alloy, made by laser welding. Primary β -grains, elongated in a heat sink direction, are observed on its background. Metastable β - and α'/α'' -phases are registered in the metal of weld, made by laser welding, and substructure is present in the weld grains.

Study of microstructure of welded joints from titanium alloy allowed making a conclusion that the weld metal, obtained only using laser welding, has higher internal stresses. It is indirectly indicated by presence of multiple etching pits along the fusion line on transverse microsections, which are etched in the places of emergence of dislocation accumulations on the surface. Area of coarse grain is absent in HAZ metal of the welded joints, made by laser welding, whereas it is present in HAZ metal of the welded joints, performed by laser-arc welding. No substructure

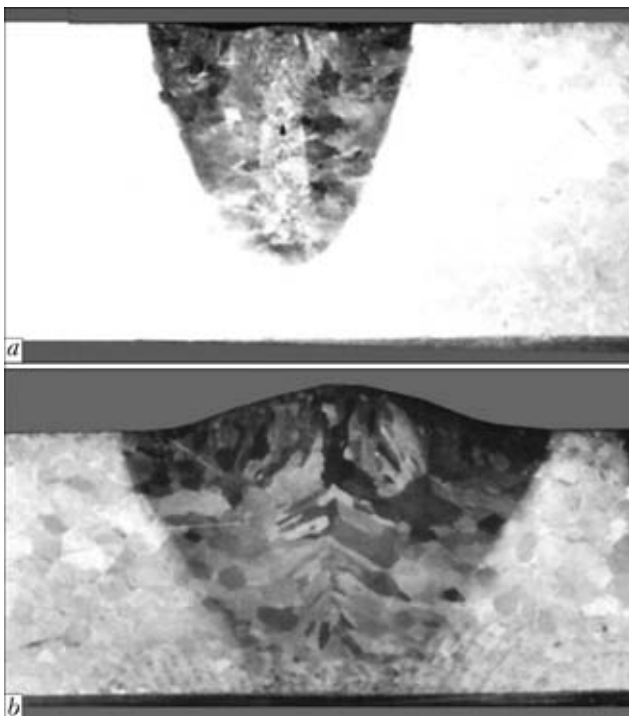


Figure 2. Transverse macrosections of welded joint from titanium alloy T110 of 13 mm thickness made by laser (a) and laser-arc (b) welding with equal laser beam power

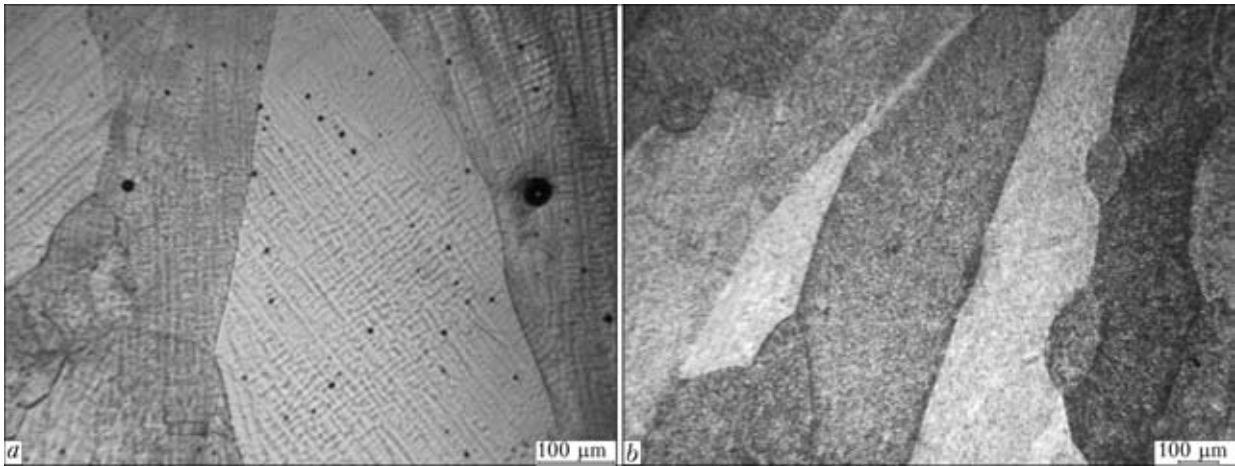


Figure 3. Microstructure of metal of T110 alloy weld, made by laser (a) and laser-arc (b) welding

was observed neither in weld nor in HAZ metal of the welded joint, made by laser-arc welding, in contrast to the welded joint from T110 alloy, performed by laser welding. The microstructure was more uniform and homogeneous (Figure 3, b). Etching of section of the welded joint, made by laser-arc welding, in the same agent and during the same time as the section of the welded joint, performed by laser welding, promoted no etching pits. Probably, it can be related with lower level of welding stresses in laser-arc welding than in laser welding.

Microstructure of the arc-welded joints has virtual no difference from microstructure of the EB-welded joints. Thus, metal of single-pass welds and near-weld zones of the joints, made by full penetration TIG method, has typical lamellar structure of β -transformed grains, where finer precipitates of tertiary α -phase are noticed between coarser α -phase plates. Areas with partially transformed β -phase and α -fringe on the β -grain boundaries are observed in separate grains as in the welds, made by EBW. Primary globular α -phase is observed inside the grains in spite of indicated structural elements in HAZ metal areas adjacent to the base metal. Size of structural elements is a common distinction of microstructure of the joints, made by arc welding. They, as a rule, coarser and that, probably, explains a relatively low level of strength of the arc welds (Table 2).

The EB- and laser-welded joints have the zone (fusion and heat-affected) with significantly less structural changes in comparisons with the joints, made by tungsten electrode. Such structural difference should have positive effect on conditions of plastic strain in process of loading. It is indicated by analysis of places of fracture of welded specimens after the mechanical tests. Typical place of fracture of EB-welded joints is the base

metal and in TIG welding it is the weld. The joints, made by laser-arc welding, typically fracture in the weld, and joints, performed by laser, failure in the base metal.

Comparison of the penetration depth during laser-arc and laser welding, received using the mode with similar laser beam parameters, showed double increase in penetration depth (see Figure 2) at constant laser beam power. Welded joints from T110 alloy, made by EBW and laser welding, have higher strength and insufficient impact toughness (see Table 2).

High impact toughness of HAZ metal should be noted in the A-TIG-welded joints and in laser-arc welding. The highest impact toughness is in the joints, performed by multi-pass groove TIG welding using filler wire SP-15, including lower content of alloying elements in comparison with the base metal. The weld metal, made by laser welding, has the lowest impact toughness. Strength of the welded joints of T110 alloy, made by laser and laser-arc welding, is 2–4 % higher than the strength of the base metal, that is explained by presence in the weld metal of dendrite structure, typical for cast weld metal.

Table 2. Mechanical properties of as-welded joints from titanium alloy T110 made by different methods

Welding method	Metal thickness, mm	σ_t , MPa	Impact toughness KCV, J/cm ²	
			Weld metal	HAZ
EBW	7	1140	10	10
Full penetration TIG	7	1118	11	10
Groove TIG	7	1030	20	12
A-TIG	7	1120	18	20
Laser	13	1131	6	13
Laser-arc	13	1180	15	23



Thus, the results of performed investigations indicate a good weldability of alloy T110 independent on method of welding.

Conclusions

1. High-strength titanium alloy T110 differs in good weldability during performance of welded joints using EBW, full penetration TIG, A-TIG and laser-arc welding.

2. As-welded joints, made by EBW, have the strength equal the base metal, and strength of the welded joints, performed by arc welding, makes not less than 90 % of strength of alloy itself. Heat treatment can be used in order to increase the level of mechanical properties of T110 alloy welded joints.

3. Application of SP-15 grade wire as a filler material is reasonable for TIG welding of T110 alloy.

4. Laser-arc welding allows receiving the welded joints from high-strength titanium alloy T110 with wider complex of mechanical characteristics and lower internal stresses in comparison with laser welding. HAZ of the welded joints, made only by laser welding, has no coarse grain area, that can result in reduction of HAZ metal impact toughness. Coarse grain area is present in HAZ of the welded joints, made by laser-arc welding.

5. A-TIG welding provides for the maximum values of impact toughness of weld and HAZ metal on T110 alloy without filler material application.

1. Zamkov, V.N., Topolsky, V.P., Trygub, M.P. et al. *High-strength titanium alloy*. Pat. 40087 Ukraine. Publ. 16.06.2003.
2. Antonyuk, S.L., Zamkov, V.N., Topolsky, V.F. et al. (2003) Investigation of mechanical properties of cast semi-products of experimental titanium alloy T110. *Advances in Electrometallurgy*, **3**, 27–30.
3. Paton, B.E., Shelyagin, V.D., Akhonin, S.V. (2009) Laser welding of titanium alloys. *The Paton Welding J.*, **7**, 30–34.
4. Shelyagin, V.D., Khaskin, V.Yu., Akhonin, S.V. et al. (2012) Peculiarities of laser-arc welding of titanium alloys. *Ibid.*, **12**, 32–36.
5. Gurevich, S.M., Zamkov, V.N., Blashchuk, V.E. et al. (1986) *Metallurgy and technology of welding of titanium and its alloys*. Kiev: Naukova Dumka.
6. Gurevich, S.M., Zamkov, V.N., Kushnirenko, N.A. et al. (1980) Selection of filler material for welding of ($\alpha + \beta$)-titanium alloys. In: *Actual problems of welding of non-ferrous metals*. Kiev: Naukova Dumka, 314–320.
7. Zamkov, V.N., Topolsky, V.F., Tyapko, I.K. et al. (1993) Influence of heat treatment on serviceability of VT23 alloy welded joints. *Avtomatich. Svarka*, **4**, 25–27.
8. Gurevich, S.M., Zamkov, V.N., Prilutsky, V.P. et al. *Welding flux*. USSR author's cert. 439363. Publ. 15.08.74.

Received 28.10.2013

ELECTRODE AND FILLER MATERIALS FOR SURFACING AND WELDING OF CAST TIN BRONZES (Review)

T.B. MAJDANCHUK

E.O. Paton Electric Welding Institute, NASU
11 Bozhenko Str., 03680, Kiev, Ukraine. E-mail: office@paton.kiev.ua

Tin bronzes find wide application in machine-building, metallurgy and other branches of industry. They are used for manufacture of parts operating under conditions of increased wear resistance by casting method. Welding and surfacing processes are used for production, as well as elimination of pouring spoilage and repair of parts from tin bronzes. This review gives an analysis of existing developments in area of current technological processes of welding and surfacing of tin bronzes, as well as new electrode and filler materials for these purposes. The main difficulties were considered appearing during application of welding processes, namely high porosity susceptibility (copper alloys are more susceptible), formation of solidification cracks in welds and HAZ, tin liquation, that results in structure inhomogeneity, as well as high susceptibility to hot crack formation in deposited bronze metal or steel during bronze on steel surfacing. Described are the methods of welding and surfacing of cast tin bronzes, among which argon-arc welding, submerged-arc welding and manual coated-electrode arc welding are the most widespread. It is shown that wires and strips from wrought alloys used as electrode and filler materials do not provide the necessary chemical composition of the deposited metal. Development of special flux-cored wires and coated electrodes, providing optimized metal alloying and receiving of necessary properties, is preferable. For example, welding consumables, chemical composition and properties of which would correspond to the base metal, are necessary for welding and surfacing of cast tin bronzes (BrO10F1, BrO5Ts5S5). A conclusion was made based on performed analysis about necessity of development of new consumables (coated electrodes, flux-cored wires) for welding and surfacing of bronzes of critical designation. 40 Ref., 4 Tables. 1 Figure.

Keywords: tin bronzes, electrode materials, methods of welding and surfacing, metallurgical peculiarities

Today copper-based alloys such as tin bronzes find wide application in assemblies and friction pairs of machines and mechanisms operating under conditions of increased wear resistance at different operation modes. This to significant extent is promoted by favorable combination of their physical and technological properties.

Melting of parts from tin bronzes using new casting methods [1] increases every year. However, at that complete elimination of spoilage is impossible (1–10 % depending on production standards and technical level of casthouses, and 50–70 % at manufacture of complex castings) [2]. The problem of sporing application of these metals is relevant since tin bronzes refer to scarce and expensive alloys, the demand and price on which constantly grow [3, 4].

Partially, elimination of cast spoilage is solved through application of different welding processes (surfacing, welding and welding-up). Also these processes are used for:

- repair of worn bronze parts, increasing in such a way their service life;
- manufacture of bimetal parts instead of all-cast ones for economy of expensive metal, as well as reduction of total weight of part;
- production of cast-welded parts of complex configuration instead of cast ones.

The aim of present review is the analysis of properties of existing grades of tin bronzes, determination of main difficulties, appearing in welding and surfacing of given alloys, as well as generalizing of data on welding processes and filler materials used for welding and surfacing of tin bronzes.

Commercial grades of cast tin bronzes. Tin bronzes containing together with tin such alloying elements as zinc, lead, phosphorous and nickel [5–7] (Table 1) are used in industry as a rule.

Zinc is added for increase of corrosion resistance of bronze in the salt water as well as for uniform distribution of high-density lead in the alloy. Besides, zinc is cheaper than tin and copper.

Lead is virtually insoluble in tin bronze in solid state. It rises antifriction properties, density of castings as well as improves machinability, but, at that, reduces their mechanical properties.

Table 1. Grades of cast tin bronzes [5]

Alloy	CIS	USA	Germany	Japan
	GOST 613-79	ASTM B30, B427, B0505, B584	DIN 17656	JIS H5111, H5113, H5115
Copper-tin	–	C91000	SnBz14 (2.1057)	
Tin-nickel	– – –	C96000 C91700 C96800	– – –	– – –
Tin-phosphorous	BrO10F1 – – – –	– C90700 C90800 C91100 C91300	– – – – –	– H5113/class 2 H5113/class 2b – –
Tin-zinc	BrO8Ts4 BrO10Ts2	C90300 C90500 –	– – Rg10 (2.1087)	– – –
Tin-zinc-nickel	–	C94700	–	–
Tin-lead	– – – – BrO10S10 – – – – BrO5S25 –	C92700 C92800 C93400 C93600 C93700 – C93800 C93900 C94000 C94100 C94300 C94500	– – – – – SnPbBz10 (2.1177) SnPbBz10 (2.1183) – – SnPbBz10 (2.1189) – –	– – – – H5115/class 3.3c – H5115/class 4.4c – – – H5115/class 5
Tin-lead-nickel	– –	C92500 C92900	– –	– –
Tin-lead-zinc	BrO6Ts6S3 BrO5Ts5S5 – BrO4Ts7S5 – BrO3Ts12S5 BrO4Ts4S17 – – – – –	– C83800 – C83900 C84200 C84800 – C92200 C92300 C92600 C93200 C93500	– – Rg5 (2.1097) – – – – – – Rg7 (2.1091) – –	– H5111/class 6.6c – – – H5111/class 1.1c – H5111/class 7.7c H5111/class 2.2c H5111/class 3.3c – –
Tin-zinc-nickel	BrO3Ts7S5N1 – – – – –	– C83450 C94800 C94900 C97300 C97600	– – – – – –	– – – – – –

Tin bronzes in order to increase the mechanical properties and fluidity are alloyed by phosphorous which is also a deoxidizing agent.

Nickel (up to 0.25 %) has positive effect on tin-phosphorous bronzes somewhat increasing the mechanical properties and refining the grain. It also provides significant grain refinement in tin-lead bronzes that promotes more uniform distribution of lead in the castings. Nickel (0.5–1.0 %) has no observable effect on tin-zinc bronzes.

Small additions of zirconium, boron, titanium and niobium to tin bronzes improve their mechanical properties and pressure processibility in cold and hot state.

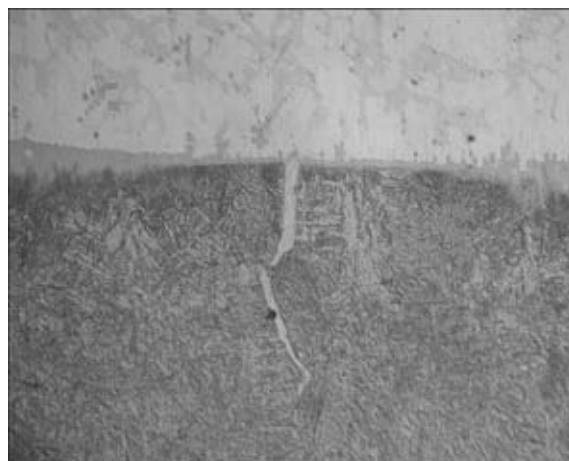
CIS countries produce bronzes, which have no analogues in other countries (namely BrO10F1, BrO6Ts6S3, BrO4Ts4S17, and BrO3Ts7S5N1).

Main difficulties in welding and surfacing of tin bronzes. Welding and surfacing of tin bronzes are connected with specific difficulties, namely high porosity susceptibility (copper al-

loys are the most susceptible among all), formation of solidification cracks in welds and HAZ, liquation of tin and, respectively, structure inhomogeneity, as well as penetration of tin bronze in steel during surfacing.

Porosity of welds is promoted by emission of hydrogen and water vapors from the weld pool metal during the solidification process [8, 9]. Consumables, which provide dilution of gas phase and, thus, reduction of hydrogen partial pressure in arc atmosphere (due to introduction of gas-forming constituents in a composition of electrode coating), as well as application of active agents deoxidizing the weld pool metal (electrode rods and wires, alloyed by phosphorous, silicon, manganese and aluminum) [10], are used for porosity prevention.

Great problem in welding and surfacing of cast tin bronzes is initiation of solidification cracks [11, 12]. Intercrystalline cracks are initiated in a fusion line and can have an appearance of separate penetrations between the grains or mesh on a grain boundary. The main reason of crack formation is the liquid interlayers between the crystalline particles at the moment of tensile stress effect. Presence of the liquid interlayers depends on a content of impurities, which form fusible eutectics, in the metal. These are bismuth, sulfur and phosphorous for most of tin bronzes. Crack initiation is also related with formation of large quantity of tin-riched brittle δ -phase. Susceptibility of BrO10Ts2 bronze to initiation of cracks in the welded joints increases with rise of



Microstructure ($\times 100$) of fusion zone of tin bronze to steel (bronze filled crack)

tin content in the alloy and in presence of more than 0.004 % Pb [13] in it. Crack is also effected by different physical-chemical properties of tin bronzes and steels and modes of surfacing on steel. Sizes of cracks are different, namely from several microns to several (and even tens) of millimeters (Figure). The measures on prevention of crack initiation in steel should be taken during surfacing of tin bronzes (perform surfacing without steel melting at minimum temperature of heating of its surface, apply intermediate surfacing by silicon bronze or yellow metal, use technological processes, at which minimum tensile stresses will be developed in steel) [14–16].

It should be noted that process of crack initiation in welding and surfacing of tin bronzes is not enough studied.

Table 2. Pressure-treat grades of tin bronzes [5]

Alloy	CIS	USA	Germany	Japan
	GOST 5017–74	ASTM B103, B122, B139, B740	DIN 17662, 17664	JIS H3110, H3130
Tin-phosphorous	BrOF2-0.25	–	–	–
	BrOF4-0.25	C51100	CuSn4 (2.1016)	C5111
	–	C53400	–	–
	BrOF6.5-0.15	–	CuSn6 (2.1020)	C5191
	–	C51000	–	–
	–	C53200	–	–
	BrOF6.5-0.4	–	–	–
	BrOF7-0.2	–	CuSn6 (2.1020)	C5210
Tin-zinc	–	–	CuSn8 (2.1030)	–
	BrOF8-0.3	C52100	CuSn8 (2.1030)	C5212
	–	C52400	–	–
	–	–	–	–
Tin-zinc	BrOTs4-3	–	CuSn6Zn6 (2.1080)	–
	–	–	–	–
Tin-nickel	–	C72500	CuNi9Sn2 (2.0875)	–
	–	C72650	–	–
	–	C72700	–	–
	–	C72900	–	–
Tin-zinc-lead	BrOTsS4-4-2.5	–	–	–
	–	C54400	–	–
	BrOTsS4-4-4	–	–	–

Liquation of tin related with big temperature interval of solidification is possible in welding and surfacing of tin bronzes, due to what chemical inhomogeneity along the section and, respectively, heterogeneity of the mechanical properties take place in the metal. Welding at minimum heat input and with intervals for temperature adjustment, application of intermediate and final annealing and, as a rule, usage of consumables with reduced content of tin in comparison with welded bronze [17, 18] should be plasticized for liquation decrease.

Welding processes and consumables for surfacing and welding of tin bronzes. Many of welding processes, namely gas-shielded consumable or non-consumable electrode welding or automatic submerged-arc and manual coated-electrode arc welding have found application in industry, regardless all difficulties in welding and surfacing of tin bronzes. Plasma-arc, gas, electroslag, vibrating-electrode arc and other methods of welding and surfacing are rarely used.

Gas-shielded welding using consumable and non-consumable electrodes received the widest distribution. It differs by versatility and simplicity of shielding of weld pool metal from effect of environment. Inert gases, namely argon, helium as well as their mixtures (Ar + 30 % He) are mainly used as shielding atmosphere. Nitrogen is more rarely used.

Wires from wrought bronzes which are manufactured in CIS countries and abroad (Table 2) are used depending on grade of bronze to be welded and media of part operation.

Minimizing of base metal penetration and ingress into cladding layer of iron, significantly deteriorating service properties of the deposited metal, requires application of argon-arc surfacing using consumable and non-consumable electrodes at small current densities. The most dense metal is obtained in consumable-electrode surfacing using solid wires.

Wide application of gas-shielded arc welding and surfacing of tin bronzes is prevented by low strain properties of cast tin alloys, since manufacture of welding wires from them is complicated. Necessity in small diameter wires is, in particular, high. This problem can be solved through application as filler material of flux-cored and composite wires, which allow relatively easy receiving of the metal of necessary composition and satisfactory quality.

Surfacing using split and strip electrodes [19–21] should be referred to advanced methods of electric arc surfacing, allowing regulation of steel penetration in a wide range and providing high

efficiency. Investigation of peculiarities of arcing and base metal penetration using such electrodes allowed determining that the minimum steel penetration at that is achieved due to intensive «erratic» arc and more favorable distribution of heat input over pool width caused by that. Rate of surfacing and current density have significant effect on the base metal penetration and iron content in the deposited layer in strip electrode surfacing. Regulation of the base metal penetration in strip electrode surfacing can be performed by 60–45° angle of strip turning relatively to surfacing direction (bead axis).

Fluxes of OSTs-45, AN-20, AN-26, AN-348-A and AN-M2 grades can be used in automatic submerged-arc welding and surfacing for greater efficiency of the process. They provide the necessary level of welding-technological properties and metallurgical treatment of the weld pool. Welding wire with the same composition as in the deposited metal is preferable in surfacing and welding of tin bronzes. Production of flux-cored wires is one of the most simple and economical methods for receiving of the deposited metal of specific chemical composition in the absence of necessary welding wires. Developed are the flux-cored wires for surfacing of BrO6Ts6S3 [11] and BrO8S21 [20, 22] bronze as well as for welding of BrO10Ts2 [23].

Manual coated-electrode arc welding is widely used in industry together with automatic methods of welding and surfacing of cast tin bronzes. This process is constantly improved in order to rise the quality of deposited metal and fulfill increased service requirements.

Electrodes with different coating compositions [24] are used in arc surfacing and welding of tin bronzes. Mainly, these are coatings consisting of halogenides as well as deoxidizing, stabilizing and slag-forming materials. Overwhelming majority of coating mixtures are manufactured using sodium silicate water solution as a binding component, providing good adaptability to fabrication and application of such electrodes [17].

Drawn wires (GOST 16130–90) and cast bars of diameter not less than 6–8 mm are used as rods for manufacture of coated electrodes for welding and surfacing of tin bronzes. Specified standard provides for only two grades of welding wire, namely BrOF6.5-0.15 and BrOTs4-3 (Table 3). Besides, cold-roll bars are produced on GOST 10025–78 from tin-phosphor bronze of BrOF6.5-0.15 grade, and tin-zinc bronzes are used for drawn ones on GOST 6511–60. Bars on these standards are produced in diameter from 5 to 10 mm [24].

Table 3. Chemical composition of welding wire and rods for manual arc welding and surfacing of tin bronzes

Grade of wire and rod	GOST on rolled-metal wire/rod	GOST on chemical composition	Main elements, wt.%			
			Sn	P	Zn	Cu
BrOF6.5-0.15	16130-90/10025-78	5017-74	6.0-7.0	0.10-0.25	–	Rest
BrOTs4-3	16130-90/6511-60	5017-74	3.5-4.0	–	2.7-3.3	

Cast bars provide lower quality of the deposited metal than wrought ones; therefore, they are used only in extreme case.

Table 4 shows the data on coated electrodes, which have the widest application for welding and surfacing of tin bronzes, as well as welding-up of defects of bronze casting. It can be seen that content of tin is on the level of 5.0–7.5 % (except UTP-320) and values of mechanical properties differ in several times when using of the mentioned above electrodes. For example, elongation of OZB-2M deposited metal equals 10 % and that of Phosphor Bronze C Electrode makes 45–50 %; tensile strength of AS Bronz equals 260 MPa and that of Phosphor Bronze C Electrode makes 450 MPa. In addition, given electrodes not always have good welding-technological characteristics.

Plasma method [25] received wide distribution for tin bronze surfacing. At that, wire, rods, fixed filler (stowed or in other way fixed on the surface) and powder can be used as filler material. Surfacing with solid wire filler is the most often used. The grades of these wires are given above. Specific modification of tin bronze surfacing is plasma-powder method allowing significantly ex-

panding the list of alloys for mechanized surfacing. Minimum penetration of the base metal with good bead formation [25, 26] is provided in plasma surfacing. Expensive equipment and low process efficiency can be referred to method disadvantages.

Vibrating-electrode arc surfacing of copper alloys [36] finds its application in repair of small diameter cylinder parts and for surfacing of thin layers. It allows surfacing small diameter parts. The surfacing is carried out in a jet of coolant fluid or foam, having also the function of shielding media.

Electroslag surfacing of tin bronze on steel [37] can be used for one pass surfacing of large thickness layer of metal (≥ 20 mm). As a rule, plates or chips from bronze, which are preliminary stowed on ferrous metal, are used as filler. Advantage of electroslag surfacing is possibility of application of cast electrodes. Its disadvantage is laboriousness of preliminary operations as well as necessity of application of high currents in surfacing of large surfaces. The electroslag process is reasonable when it is necessary to surface large quantity of metal.

Other methods, namely gas surfacing and welding [38], gas-shielded pulse-arc and sub-

Table 4. Electrodes for welding (welding-up) and surfacing of tin bronzes

Grade of electrode	Chemical composition of deposited metal, wt.%							Hardness HB	δ , %	σ_t , MPa	Reference
	Sn	P	Mn	Ni	Fe	Si	Cu				
OZB-2M	6.0	0.35	1.0	0.80	0.5	–	Rest	115	10	340	[24]
OK 94.25	7.0	0.15	0.5	–	<0.2	–	92	95	25–35	330–390	[33]
UTP-32	7.0	–	–	–	–	–	93	100	34	295–345	[32]
UTP-320	13.0	–	–	–	–	–	87	150	34	245–295	[32]
AS Bronz	7.0	0.10	0.5	–	–	–	Rest	90	20	260	[35]
SP-33	5.3	0.09	–	–	–	–	Same	–	27	400	[34]
SV 082	8.0	0.10	0.01	0.05	0.1	0.05	»	105	18	340	[31]
Capilla 48	6.0–8.0	–	–	–	–	–	»	100–110	–	280	[30]
E-CuSn-C	7.0–9.0	<0.30	Si + Mn + Fe + Al + Ni + Zn \leq 0.5				»	–	–	–	[27]
Phosphor Bronze C Electrode	7.0–9.0	<0.35	–	–	0.25	–	»	85–100	45–50	450	[28]
Nihonweld N-CuSn-C	7.8	0.11	–	–	0.17	–	»	90–100	30	390	[29]
Nihonweld N-CuSn-A	5.15	0.18	–	–	0.52	–	»	65–75	24	424	[29]

merged-arc welding [39] and spark surfacing [40] are used for welding and surfacing of tin bronze, but they have not found wide application. If these methods are used, the same consumables as considered above are applied.

Conclusions

1. The following welding processes, namely welding-up of cast defects, surfacing with the purpose of repair of worn bronze parts, welding during manufacture of welded-cast parts as well as surfacing on steel for production of bimetal parts, are successfully used for economy of expensive tin bronzes. At that, welding and surfacing metallurgical peculiarities of these alloys, i.e. increased porosity susceptibility, initiation of solidification cracks in welds and HAZ, tin liquation and, respectively, structure inhomogeneity and initiation of bronze-filled cracks in steel (during surfacing on steel) should be considered.

2. It is not always possible to produce the welding wire, which can be used for automatic welding as well as for manufacture of coated electrode rods, due to low ductility of tin bronzes.

3. There are virtually no domestic consumables, including coated electrodes which can be used for welding, surfacing and welding-up of cast defect of bronzes with more than 8 % Sn.

4. Development and mastering of production of special flux-cored wires, providing welds and deposited metal of necessary compositions and properties, is perspective for application of mechanized processes of welding and surfacing of tin bronzes in industry.

1. Ponomarenko, O.I., Shinsky, I.O., Morgun, N.N. (2004) Casting on gasified models of bronze alloys. *Litejn. Proizvodstvo*, **11**, 30.
2. Ponomarenko, O.I., Lysenko, T.V., Stanovsky, A.L. et al. (2012) *Control of casting systems and processes*: Monography. Kharkov: KhPI.
3. www.non-ferrous@metalresearch.ru
4. Makarevich, O.P., Fedorov, G.E., Platonov, E.O. (2005) *Production of special steel casts*. Kyiv: KPI.
5. Osintsev, O.E., Fedorov, V.N. (2004) *Copper and copper alloys. National and foreign grades*: Refer. Book. Moscow: Mashinostroenie.
6. Smiryagin, A.P., Smiryagina, N.A., Belova, A.V. (1974) *Commercial non-ferrous metals and alloys*: Refer. Book. Moscow: Metallurgiya.
7. Lebedev, K.P., Rajnes, L.S., Shemtov, G.S. et al. (1973) *Cast bronzes*. Leningrad: Mashinostroenie.
8. Dzhevaga, I.I. (1961) *Electric arc welding of non-ferrous metals and alloys*. Leningrad: Sudpromgiz.
9. Khmel, G.P., Krasnenko, E.G., Ilyushenko, V.M. et al. (1966) Surfacing of worn bronze parts of metallurgical equipment. *Avtomatich. Svarka*, **3**, 68–71.
10. Redchits, V.V. (1991) Pore prevention in fusion welding of non-ferrous metals. *Ibid.*, **6**, 31–34.
11. Ilyushenko, V.M., Opanasenko, S.I., Fishkis, M.M. et al. (1966) Mechanized welding-up of cast defects in tin bronze. *Ibid.*, **2**, 64–66.

12. Dzhevaga, I.I., Zhuravlyov, Yu.A. (1965) Relation between structure and resistance of welds on bronze to solidification cracks. *Ibid.*, **11**, 14–19.
13. Simanenkov, L.N. (1981) *Study and development of electric arc welding technology of tin bronze of Br.OTs10-2 grade*: Syn. of Thesis for Cand. of Techn. Sci. Degree. Moscow.
14. Vajnerman, A.E., Osetkin, A.A. (1968) To problem of crack formation in surfacing of copper alloys on steel. *Avtomatich. Svarka*, **6**, 23–25.
15. Timofeev, V.N., Isaev, N.I. (1965) Surfacing of copper alloys on steel surfaces. *Ibid.*, **4**, 34–37.
16. Ardentov, V.V., Vajnerman, A.E., Gajdaj, P.I. et al. *Method of surfacing*. USSR author's cert. 548391. Int. Cl. B23k 9/04. Fil. 05.08.1974. Publ. 28.02.1977.
17. Abramovich, V.R., Demyantsevich, V.P., Efimov, L.A. (1988) *Fusion welding of copper and copper-based alloys*. Leningrad: Mashinostroenie.
18. Hanke, H., Retzlaff, O., Schultz, H.-W. (1968) Schweissen von Gusszinbronze. *Schweisstechnik*, **2**, 1–12.
19. Timofeev, A.I., Potakhin, V.P. (1967) Automatic surfacing of Br.AMts9-2 bronze with strip electrode on coating. *Svarochn. Proizvodstvo*, **10**, 14–16.
20. Ilyushenko, V.M., Sedov, V.E. (1969) Surfacing of tin-lead bronze on steel with split electrode. *Avtomatich. Svarka*, **6**, 52–54.
21. Ilyushenko, V.M. (1978) Advanced methods of arc surfacing copper alloys on steel. In: *Welding and surfacing of heavy non-ferrous metals*. Kiev: PWI, 30–32.
22. Ilyushenko, V.M., Sedov, V.E., Opanasenko, S.I. et al. *Flux-cored wire for surfacing*. USSR author's certificate 202391. Int. Cl. B23k. Fil. 03.01.1966. Publ. 14.09.1967.
23. Dzhevaga, I.I., Simanenkov, L.N. *Composition of welding wire*. USSR author's cert. 593868. Int. Cl. B23k 35/30. Fil. 18.10.1976. Publ. 25.02.1978.
24. Zaks, I.A. (1999) *Electrodes for arc welding of non-ferrous metals and alloys*: Refer. Book. St.-Petersburg: Strojizdat.
25. Gladky, P.V., Pereplyotchikov, E.F., Ryabtsev, I.A. (2007) *Plasma surfacing*. Kiev: Ekotekhnologiya.
26. Ilyushenko, V.M. (1977) *Welding and surfacing of heavy non-ferrous metals*. Kiev: Znanie.
27. www.hzdayang.com/aws-ecusn-c.html
28. www.brazing.com/MSDS_PhosBronze_E.pdf
29. www.nihonweld.com/products.do?item_id=15402
30. www.rs-nt.ru/capilla-gmbh-germany/376/2687
31. www.stlg-sd.ru/sb_082
32. (2004) *UTP Schweissmaterial GmbH*. Bad Krozingen.
33. (2005) *Filler materials for manual and automatic welding*: ESAB Welding Handbook. 4 ed. Goeteborg.
34. (2006) *Kobe steel welding consumables*: Catalog. Tokyo.
35. (2005) *ASKANYAK welding electrodes and wire*: Catalog of products. Istanbul.
36. Patskevich, I.R., Bautina, V.A. (1962) Vibrating electrode arc surfacing of bronze on steel. *Svarochn. Proizvodstvo*, **11**, 43–45.
37. Dudko, D.A., Shcherbina, N.Ya., Podsatsky, V.V. (1979) Electroslag surfacing of copper and its alloys on steel using boiling fluxes. *Avtomatich. Svarka*, **2**, 34–37.
38. Gvozdem, M.S. (1963) Welding-up of defects in casts of non-ferrous metals. *Litejn. Proizvodstvo*, **9**, 42.
39. Potapievsky, A.G., Agarkov, L.A., Osadchenko, A.E. (1967) Mechanized pulsed-arc surfacing of bronze on steel items. *Sudostroenie*, **8**, 46–50.
40. Pushkin, I.A. (2001) Some peculiarities of recovery of worn bronze bushings by spark surfacing. In: *Abstr. of Ural Welding Conf*. Nizhny Tagil: NTTI, 127–129.

Received 16.10.2013



INTERNATIONAL CONFERENCE «WELDING AND RELATED TECHNOLOGIES — PRESENT AND FUTURE»

On November 25–26, 2013 in Kiev at the E.O. Paton Electric Welding Institute the International Conference «Welding and Related Technologies — Present and Future», organized by the National Academy of Sciences of Ukraine and E.O. Paton Electric Welding Institute, took place. More than 200 representatives of academic institutes, branch research institutes, research-design and engineering centers, industrial enterprises and education universities, chiefs and managers of business structures, etc. took part there. Among the participants of the Conference there were about 70 representatives from Austria, Bulgaria, Great Britain, Germany, India, Canada, China, Poland, Slovakia, USA, France, Japan, Belarus, Georgia, Kazakhstan, Russia, etc.

Among the honorary guests of the Conference Correspondent Member of the RAS M.P. Lebedev, the President of the Sakha Academy of Sciences (Yakutia); Prof. O.I. Steklov, the President of the Russian Scientific and Technical



Welding Society; Dr. V.G. Fartushny, the President of the Society of Ukrainian Welders; Prof. L.S. Denisov, the President of the Belarus Welding Society, were present.

At the Conference, 22 invited papers of scientists from many countries about the most impor-





tant scientific achievements, obtained in the recent time in the field of welding, surfacing, brazing, strength, new materials, non-destructive testing and technical diagnostics, evaluation of residual life of welded structures, surface engineering, special electrometallurgy, and also prospects for development of these directions, were listened and discussed at the plenary sessions.

Among the speakers, the famous scientists, such as I.V. Gorynin, Guan Qiao, J. Pilarczyk, U. Reisgen, Yu.M. Pleskachevsky, Y. Okamoto, S. Keitel, V. Lysak, M. Beloiev, B.S. Lomborg, A.V. Dub, P. Mudge, A. De, T. Mochizuki, Yu. Saraev, K. Alaluss, took the floor. The papers were of great interest among the participants of the Conference and were accompanied by questions to the speakers.

On November 26 in the reading hall of the PWI Library, 195 poster papers were presented for familiarization. The exposition included the following chapters:

- Technologies, materials and equipment for welding and related technologies (76 papers);
- Strength of welded joints and structures, theoretical and experimental investigations of stress-strain states and their control (44 papers);

- Non-destructive testing and technical diagnostics (16 papers);
- Surface engineering (36 papers);
- Special electrometallurgy (13 papers);
- Problems of welding in medicine, ecology, certification and standardization of welding production (10 papers).

The active exchange of scientific information about the investigation results had a mutual benefit.

In the period of work of the Conference a series of bilateral negotiations took place directed to cooperation and strengthening of collaboration, the Agreement about cooperation between the Society of Ukrainian Welders and the Russian Scientific and Technical Welding Society was signed.

Before the beginning of the Conference the plenary papers as the single issues of the journals «Аvtomaticheskaya Svarka» and «The Paton Welding Journal» (№ 10/11, 2013) and also abstracts of poster papers were published (see www.patonpublishinghouse.com).

By the end of the Conference the friendly reception for its participants was held.

V.N. Lipodaev, A.T. Zelnichenko



20 YEARS IN THE WORLD OF FLUX-CORED WIRES



Decomposition of the USSR and emergence of independent republics in the post-Soviet space at the start of 1990s was accompanied by upsetting of industry operation, breaking up and loss of production links, mass stoppage of production. In 1993 in Kiev a joint Russian-Ukrainian Company «TM VeldTek Ltd.» was set up by the initiative of PWI staff. The Company was successfully developing in the direction of flux-cored wire manufacture. This was promoted by the support of «Dnepropetrovsk Hardware Production Association», where the management appreciated the idea of restoring flux-cored wire manufacturing in Ukraine.

In 2001 flux-cored wire manufacturing was moved to a separate subdivision — «TM.VELTEK Ltd.».

Over 20 years of operation the Company implemented a number of important engineering measures on repair and upgrading of the main equipment, in particular, flux-cored wire production lines, charge section improvement, has mastered modern forms of product supply, has optimized technologies of manufacturing wires of 1.0–6.0 mm diameter. Series of modern welding and surfacing flux-cored wires have been developed and are manufactured at present. Such results have been achieved owing to dedicated efforts of highly qualified engineering and technical staff and workers.

Positive result of cooperation with enterprises is achieved owing to application of comprehensive approaches to order fulfillment, including, if required consultative assistance on selection of

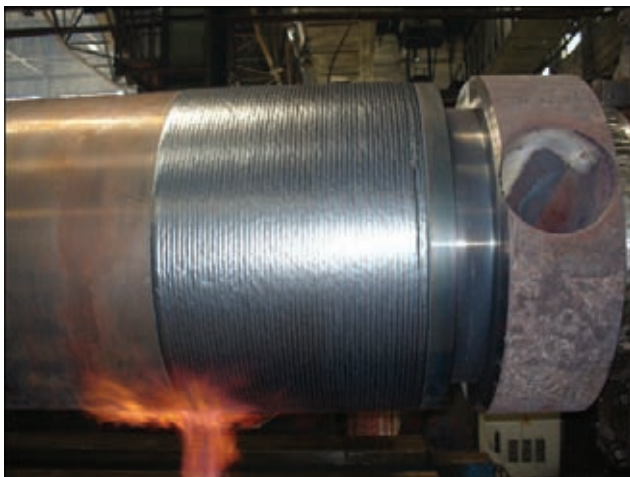
material, optimum technology and equipment for its application and engineering support.

High scientific and technical potential of the Company, irrespective of the range and volume of batches, allows fulfilling the orders in the shortest time, taking into account customer requirements. Such an approach allowed occupying a quite large market segment in Ukraine, ensuring stable foreign contacts and becoming a firm partner for many enterprises. Experience of interaction and cooperation with research institutes and universities of Ukraine and Russia is to the company's credit.

By their applications and performance VELTEK wires now are not inferior to the products of leading foreign companies, that is confirmed by their high evaluation in the local and foreign exhibitions and independent ratings, company's recognition as a reliable supplier by leading enterprises of Ukraine and CIS, continuous widening of consumption regions and growth of sales.

«TM.VELTEK» developed a number of new flux-cored wires for building-up by surfacing.

VELTEK-N470 flux-cored wire of 2.0–4.0 mm diameter in combination with fluxes AN-20 and AN-26 and VELTEK-N470S self-shielded wire of 2.0–2.4 mm diameter are manufactured for building-up by welding of CCM rolls. These wires ensure self-separation of slag crust, absence of pores or cracks in the deposited metal in case of following the technological recommendations. Comparative testing of VELTEK-N470 and VELTEK-N470S wires showed that they are on the level of those of leading foreign companies.





Built-up rolls have the service life of not less than 1.5 mln t.

«TM.VELTEK» together with metallurgical plants «Krivorozhstal», «Dneprovsky F.E. Dzerzhinsky» and «Zaporozhstal» performed a package of work aimed at improvement of surfacing consumables, technology and equipment for mill roll surfacing. Standard flux-cored wires of PP-Np-35V9Kh3SF and PP-Np-25Kh5FMS grades were used to optimize the alloying systems and develop new flux-cored wires VELTEK, allowing for mill roll operating conditions, namely N370-RM, N460, N500-RM, N505-RM, N550-RM. Surfacing by these wires is performed using AN-20, AN-26 and AN-348-A fluxes. Application of the proposed wires improved the effectiveness of mill roll operation.

In cooperation with Nikopol Plant of Seamless Pipes «Niko Tube» performed work on introduction of hardsurfacing of continuous mill rolls by VELTEK-N480NT flux-cored wire with C-Si-Mn-Cr-V-Mo-W alloying system. The wire provides a stable process of DCRP surfacing using AN-20S and AN-26P fluxes, easy separation of slag crust, absence of cracks and pores in the deposited metal. Deposited metal hardness is *HRC* 50–56.

Self-shielded flux-cored wire VELTEK-N250RM of 1.6–3.0 mm diameter is successfully applied at reconditioning of mill stand and shear pads, spindels and couplings of roll drives, sprockets, bushings, shafts, hubs, etc.

Surfacing of dogging crane cores and striper crane jaws, exposed to impact and compressive loads at high temperatures in service, was implemented. For this purpose, 2.0 mm self-shielded flux-cored wire of VELTEK-N480S grade with C-Cr-W-Mo-V-Ti alloying system was applied, which ensures deposited metal hardness after surfacing equal to *HRC* 50–54, and hot hardness of *HRC* 40–44 at 600 °C. Application of mechanized surfacing with VELTEK-N480S wire instead of T-590 and T-620 electrodes allowed extending core service life 4–5 times. The problem of core reconditioning was solved in a comprehensive manner (equipment–material–technology).

Flux-cored wires of VELTEK-N300-RM and VELTEK-N350-RM grades of 1.6–4.0 mm diameter are proposed for crane wheel surfacing. Surfacing is performed with AN-348 and AN-60 fluxes or in CO₂. Over the recent years VELTEK-N300-RM wire has been successfully applied instead of solid wire Np-30KhGSA. Technology of surfacing using AN-348 flux and 3.6 mm flux-cored wire of VELTEK-N285 grade has been developed for heavy-duty crane wheels. Chromium-manganese deposited metal with the structure of metastable austenite ensures high wear resistance of the wheels through development of the process of self-strengthening at cold working.

The Company is taking an active social stand, providing financial support to local sports, medicine and science.